

University of Alberta

Cell-electronic Sensing of Cellular Responses and Toxicity Induced by
Nanoparticles and Arsenic Species

by

Birget Krystine Moe

A thesis submitted to the Faculty of Graduate Studies and Research
in partial fulfillment of the requirements for the degree of

Doctor of Philosophy

Medical Sciences – Laboratory Medicine and Pathology

©Birget Krystine Moe

Fall 2013

Edmonton, Alberta

Permission is hereby granted to the University of Alberta Libraries to reproduce single copies of this thesis and to lend or sell such copies for private, scholarly or scientific research purposes only. Where the thesis is converted to, or otherwise made available in digital form, the University of Alberta will advise potential users of the thesis of these terms.

The author reserves all other publication and other rights in association with the copyright in the thesis and, except as herein before provided, neither the thesis nor any substantial portion thereof may be printed or otherwise reproduced in any material form whatsoever without the author's prior written permission.

Abstract

We demonstrate the development of a real-time cell analysis (RTCA) platform for studying nanoparticle- and arsenic-induced cytotoxicity with potential applications to risk assessment, environmental toxicity monitoring, and drug development. RTCA is an impedance-based *in vitro* detection system capable of simultaneously performing 96 cytotoxicity tests. To develop a RTCA method for nanoparticle-mediated cytotoxicity testing, we examined two well-characterized nanoparticles, titanium dioxide and silver nanoparticles, and used three cell lines, A549, SK-MES-1, and CHO-K1. Continuous real-time sensing provided qualitative and quantitative data, revealing concentration-, particle-, time-, and cell-dependent toxicological relationships. We further applied our RTCA method to evaluate cytotoxicity of air particulate matter (PM), including coal fly ash (CFA) and PM_{2.5} collected on air monitoring filters, using two human lung cell lines, A549 and SK-MES-1. The RTCA method was able to overcome the interference commonly encountered in colorimetric toxicity assays, making the RTCA approach potentially useful in air quality monitoring.

Real-time cell sensing also enabled toxicity ranking of thirteen arsenic species in two human cancer cell lines, A549 and T24, and revealed unique kinetic information about cellular responses to the various arsenic species. Testing of a newly synthesized arsenical, Arsenicin A, showed that it was more toxic than the inorganic arsenic species. Analysis of cell accumulation of arsenic species suggests that a higher intracellular accumulation of Arsenicin A compared to inorganic arsenic is a major contributor to its higher toxicity. Determination of the

chemical conversion of arsenic species in cell culture media over time provided insights into understanding the unique RTCA profiles of cells responding to some arsenic species.

Co-treatment of a human cancer cell line, A549, with arsenic species and oxidized single-walled carbon nanotubes (SWCNT) showed that the SWCNT altered the toxicity of the arsenic species to the cancer cells. SWCNT reduced the cytotoxicity of a highly toxic trivalent phenylarsenical, but enhanced the cytotoxicity of a less toxic pentavalent phenylarsenical. The changes in arsenic toxicity were dependent on the dose of SWCNT in combination with the dose of arsenic species. These results suggest a potential application of RTCA to research on drug development.

Acknowledgment

First and foremost I'd like to thank my supervisor, Dr. Xing-Fang Li, for providing the support, guidance, and encouragement necessary for me to complete my PhD program. Even though we may not have always seen eye-to-eye during many discussions, I know you have always had my best interests at heart, and I truly appreciate the role you played in my development as a researcher.

I'd also like to thank my committee members, Drs. Chris Le, Elaine Leslie, and Jason Acker, for their insightful criticisms and suggestions over the years, in addition to opening my eyes to a world of arsenic and to Ohm's Law. I also thank Drs. Stephan Gabos and Weiping Zhang from Alberta Health for their continued support and for providing opportunities for me to interact with other RTCA users.

My thesis research required collaborations with many of my fellow AET graduate students, post-docs, and research associates, and I was very thankful to work with people I not only considered colleagues, but also friends. These included my cell culture labmates: Li Xie, Claire McGuigan, Jinhua Li, and Dr. Haiying Du, and my mass spec operators: Xiufen Lu, Dr. Baowei Chen, Dr. Lydia Chen, and Hanyong Peng. Your help was very much appreciated.

I am also particularly indebted to our divisional and departmental administrative staff, Katerina Carastathis, Dianne Sergy, and Cheryl Titus, who never failed to provide assistance even if it was something left to the eleventh hour. In addition to your assistance, I am also grateful for your friendship and the many laughs we shared over the past six years.

Thanks also go out to the many friends I have made in the AET division over the course of my program. I credit all of you with helping to maintain my sanity, sense of humor, and survival within the student room. But particularly to J-boyd, Megan, Emily, Chamula, Kim Maconkalonkey, Tony, Feng, Nena, Yuli, Qi, Wei, Yichao, and Brittany: my time spent in the lab would not have been nearly as enjoyable without all of you there to share and commiserate with.

Finally, to my family back in the States and to my 'adopted' family here in Edmonton, I thank all of you for being who you are, for accepting me even at my worst, and for providing me with a life outside of the lab. I would especially like to thank Betty and Robbin for supporting me throughout my time here in Edmonton. You opened up both your homes and your hearts to me, and I am very fortunate to have both of you in my life.

Table of Contents

Chapter 1: Introduction	1
1.1 Cell-Based Biosensors	1
1.2 Impedance-based Cell-electronic Sensing	3
1.2.1 <i>Monitoring Cellular Responses in Impedance-based CBBs</i>	7
1.2.2 <i>Qualitative and Quantitative Analysis</i>	8
1.2.3 <i>Advantages of Impedance-based CBBs</i>	13
1.2.3.1 <i>Real-time Analysis</i>	14
1.2.3.2 <i>Sensitivity</i>	17
1.2.3.3 <i>Dye- and Label-free Data Processing</i>	22
1.2.4 <i>Limitations of Impedance-based CBBs</i>	23
1.3 Particle Toxicology	25
1.4 Arsenic Toxicity	31
1.5 Rationale and Scope of Thesis	35
1.6 References	36
Chapter 2: Development of a Real-Time Cell-electronic Sensing Method for Analysis of Nanoparticle-Induced Cytotoxicity	43
2.1 Introduction	43
2.2 Materials and Methods	46
2.2.1 <i>Cell Culture Conditions</i>	46
2.2.2 <i>Nanoparticles and Characterization</i>	46
2.2.3 <i>RTCA Analysis</i>	47
2.2.4 <i>Neutral Red Uptake (NRU) Assay and Cell Cycle Analysis</i>	50
2.2.5 <i>Data Analysis</i>	52
2.3 Results and Discussion	52
2.3.1 <i>Characterization of nAg and nTiO₂</i>	52
2.3.2 <i>RTCA Method Development</i>	55
2.3.3 <i>RTCA Screening of nTiO₂ and nAg on Three Cell Lines</i>	59
2.3.4 <i>IC₅₀ Validation using the Neutral Red Uptake (NRU) Assay</i>	63
2.4 Conclusions	65

2.5 References.....	67
---------------------	----

Chapter 3: Application of Developed RTCA Method for Environmental Air

Quality Monitoring.....	70
3.1 Introduction.....	70
3.2 Materials and Methods.....	74
3.2.1 <i>Cell Culture Conditions</i>	74
3.2.2 <i>Particulate Matter (PM) Preparation</i>	75
3.2.2.1 <i>Coal Fly Ash (CFA)</i>	75
3.2.2.2 <i>Concentrated Air Particulates (CAPs)</i>	75
3.2.3 <i>RTCA Analysis</i>	76
3.2.4 <i>Neutral Red Uptake (NRU) Assay</i>	77
3.2.5 <i>Data Analysis</i>	78
3.3 Results and Discussion.....	78
3.3.1 <i>RTCA Analysis of Size-fractionated Coal Fly Ash (CFA)</i>	78
3.3.2 <i>NRU Analysis of Size-fractionated CFA</i>	86
3.3.3 <i>RTCA Analysis of Filter-collected Particulate Matter</i>	87
3.4 Conclusions.....	90
3.5 References.....	92

Chapter 4: Profiling Cytotoxicity of Thirteen Arsenic Species for Toxicity

Ranking.....	94
4.1 Introduction.....	94
4.2 Materials and Methods.....	97
4.2.1 <i>Cell Culture Conditions</i>	97
4.2.2 <i>Arsenic Solution Preparation</i>	98
4.2.3 <i>RTCA Analysis</i>	101
4.2.4 <i>Data Analysis</i>	101
4.3 Results and Discussion.....	102
4.3.1 <i>Inorganic Arsenicals</i>	102
4.3.2 <i>Arsenic Metabolites</i>	107

4.3.3 Thiolated Arsenic Metabolites	110
4.3.4 Non-metabolite Organoarsenicals	115
4.4 Conclusions	122
4.5 References	123

**Chapter 5: Cellular Accumulation of Arsenic Species in Human Cell Lines
and Conversion of Arsenic Species in Culture Media 125**

5.1 Introduction	125
5.2 Materials and Methods	127
5.2.1 Cell Culture Conditions	127
5.2.2 Arsenic Solution Preparation	128
5.2.3 Cellular Accumulation of Arsenic	129
5.2.4 Conversion of Arsenic over Time in Culture Media	131
5.3 Results and Discussion	132
5.3.1 Cellular Accumulation of Arsenic	132
5.3.1.1 Arsenicin A and As(III) in A549 Cells	132
5.3.1.2 As(III), MMA(III), and DMA(III) in A549 and T24 Cells	136
5.3.2 Conversion of Arsenic over Time in Culture Media	139
5.4 Conclusions	152
5.5 References	154

**Chapter 6: Altered Cytotoxicity of Arsenic Species by Carbon Nanotubes in
Human Cancer Cell Lines 156**

6.1 Introduction	156
6.2 Materials and Methods	159
6.2.1 Cell Culture Conditions	159
6.2.2 Arsenic Solution Preparation	159
6.2.3 o-SWCNT Preparation	160
6.2.4 RTCA Analysis	161
6.2.5 ICP-MS	162
6.3 Results and Discussion	162

6.3.1 PAO(III)	162
6.3.2 PAPA0(III)	166
6.3.3 Roxarsona	169
6.4 Conclusions.....	172
6.5 References.....	174
Chapter 7: Conclusions and Future Prospects.....	176
7.1 Introduction.....	176
7.2 Chapter Summaries	177
7.2.1 Chapter 2: Development of a Real-Time Cell-electronic Sensing Method for Analysis of Nanoparticle-Induced Cytotoxicity	177
7.2.2 Chapter 3: Application of Developed RTCA Method for Environmental Air Quality Monitoring	178
7.2.3 Chapter 4: Profiling Cytotoxicity of Thirteen Arsenic Species for Toxicity Ranking	179
7.2.4 Chapter 5: Accumulation of Arsenic Species in Human Cell Lines and Conversion of Arsenic Species in Culture Media	181
7.2.5 Chapter 6: Altered Cytotoxicity of Arsenic Species by Carbon Nanotubes in Human Cancer Cell Lines	183
7.3 Significance of Thesis Research	184
7.4 Future Trends and Studies	186
7.4.1 Future Trends.....	186
7.4.2 Future Work.....	187
7.5 References.....	189

List of Tables

Table 1.1: Comparative IC ₅₀ Values Between Impedance-based CBBs and Traditional Cytotoxicity Assays	19
Table 1.2: Estimated and Measured Concentrations of Nanomaterials in the Environment.....	28
Table 2.1: Agglomeration of nAg and nTiO ₂ in Water and Cell Culture Media.	54
Table 2.2: IC ₅₀ Values at 24 h and 48 h Post-exposure Determined Using the RTCA and NRU Assays for nAg and nTiO ₂ in Three Cell Lines	64
Table 3.1: Ambient Air Quality Standards for PM in North America.....	72
Table 4.1: Structures of Thirteen Arsenic Species Profiled.....	100
Table 4.2: IC ₅₀ Values (μM ± SEM) for all Arsenic Species on A549	106
Table 4.3: IC ₅₀ Values (μM ± SEM) for all Arsenic Species on T24.....	106
Table 5.1: Structures of Arsenic Species Studied in this Chapter	129
Table 5.2: IC ₅₀ Values for Human Cell Lines Exposed to As(III) and Arsenicin A	133
Table 5.3: Concentrations of Total Arsenic in A549 Cells after 24 h Arsenicin A (AA) Exposure	134
Table 5.4: Concentrations of Total Arsenic in A549 Cells after 24 h As(III) Exposure	134
Table 5.5: Concentrations of Total Arsenic in A549 cells after 24 h Exposure	135
Table 6.1: Structures of Arsenic Species Studied in this Chapter	160
Table 6.2: o-SWCNT-PAO(III) Complex Formation in 0.8 μM PAO(III)	166

List of Figures

- Figure 1.1:** Examples of electrode arrangements found in various impedace-based CBB arrays. (a) The electrode arrangement of a single well found in the monopolar system available in some 8-well and 96-well ECIS arrays. The arrow points to the small sensing electrode, while the bracket indicates the large reference (counter) electrode. (b) This electrode arrangement represents the ‘circle-on-line’ IDE system available in the 16-well or 96-well RTCA arrays. The electrode arrangements in (c) and (d) represent interdigitated electrode (IDE) systems available in some 8-well and 96-well ECIS arrays. Drawings are not to scale. **6**
- Figure 1.2:** Cell index (CI) over time (normalized at time of cell treatment) for CHO-K1 cells exposed to silver nanoparticles determined using RTCA. Digital imaging microscopy images correspond to the marked time points on the cytotoxicity profile and show (a) untreated CHO-K1 control cells and CHO-K1 cells exposed to (b) $10 \mu\text{g mL}^{-1}$, (c) $20 \mu\text{g mL}^{-1}$, and (d) $40 \mu\text{g mL}^{-1}$ silver nanoparticles. **11**
- Figure 1.3:** Cytotoxicity profile of the cell index (CI) over time (normalized at time of cell treatment) for an introduced toxicant generated using data from the RTCA system. Hourly dose-response data from the cytotoxicity profile was used to produce a temporal IC_{50} histogram, representing the hourly concentrations causing a 50% reduction in normalized CI compared to the untreated controls. **13**
- Figure 1.4:** Proposed pathways of inorganic arsenic methylation in humans. The top pathway is that of oxidative methylation proposed by Challenger (1945). The boxed pathway below is that of non-oxidative methylation proposed by Hayakawa et al. (2005). **32**

- Figure 2.1:** Transmission electron microscopy (TEM) images of A) nAg and B) nTiO₂ magnified 20,000 times with a 2.85 enlargement factor. The scale bar is composed of five 100 nm segments (500 nm total). **53**
- Figure 2.2:** Determination of nTiO₂ cytotoxicity in CHO-K1 cells using RTCA: A) RTCA sensing profile of the normalized cell index (CI) over time for CHO-K1 cells exposed to nTiO₂; B) Temporal IC₅₀ histogram of the IC₅₀ values determined at each hour over the exposure period; C) RTCA sensing profile of CHO-K1 cells exposed to the solvent control, DMSO; D) RTCA sensing profile of nTiO₂ suspensions in culture media without CHO-K1 cells present. **56**
- Figure 2.3:** Percentage of CHO-K1 cells in each phase of the cell cycle after 24 h exposure to 40 µg mL⁻¹ nTiO₂. Statistical analysis was performed using a two-tailed Mann-Whitney test with 95% confidence (**p*<0.01, ***p*<0.05). Values are the mean ± SEM (n=9)..... **58**
- Figure 2.4:** RTCA sensing profiles of nAg in A) A549 (x2), B) CHO-K1 (x1), and C) SK-MES-1 (x1.43) cells and nTiO₂ in D) A549 (x1.25), E) CHO-K1 (x1.67), and F) SK-MES-1 (x2.5). The cell index (CI) scales were normalized using the corresponding multiplication factor (in parentheses) to allow for easier visual analysis. **60**
- Figure 2.5:** Temporal IC₅₀ histograms for nAg and nTiO₂ in A) A549, B) CHO-K1, and C) SK-MES-1 cells. Values are the mean ± SEM (n=3)..... **62**
- Figure 3.1:** Production of coal combustion residues (CCRs) in a coal-powered plant. The CCRs are depicted in gray boxes. Adapted from the USGS Fact Sheet 076-01 (2001)..... **80**
- Figure 3.2:** RTCA cytotoxicity profiles of the normalized cell index (CI) over time for A549 cells exposed to A) PM₁₀, B) PM_{10-2.5} (x1.5), and C) PM_{2.5} (x1.5) coal fly ash (CFA). The CI scales were normalized using the multiplication factor (in parentheses) for easier visual analysis. **81**

- Figure 3.3:** RTCA cytotoxicity profiles of the normalized cell index (CI) over time for SK-MES-1 cells exposed to A) PM10 (x1.2), B) PM10-2.5, and C) PM2.5 coal fly ash (CFA). The CI scales were normalized using the multiplication factor (in parentheses) for easier visual analysis. **82**
- Figure 3.4:** RTCA profiles of the cell index over time showing the interference of high concentrations of A) PM10 and B) PM10-2.5 and PM2.5 coal fly ash (CFA) on the RTCA electrodes in the absence of cells. **84**
- Figure 3.5:** Temporal IC₅₀ histograms of the hourly IC₅₀ values ($\mu\text{g mL}^{-1} \pm \text{SEM}$) over the exposure period for A) A549 and B) SK-MES-1 cells exposed to the three size fractions of CFA: PM10, PM10-2.5, and PM2.5..... **85**
- Figure 3.6:** Temporal IC₅₀ histograms of the hourly IC₅₀ values ($\mu\text{g mL}^{-1} \pm \text{SEM}$) over the entire exposure period for A) A549 and B) SK-MES-1 cells exposed to the two smaller size fractions of CFA: PM10-2.5 and PM2.5..... **86**
- Figure 3.7:** RTCA cytotoxicity profiles of the normalized cell index over time for SK-MES-1 cells exposed to A) concentrated air particulates (CAPs) extracted from a PM2.5 air quality monitoring filter (a 100% mass recovery was assumed), B) quartz standard reference material, Q66, and C) urban dust standard reference material, SRM 1649a..... **89**
- Figure 3.8:** Temporal IC₅₀ histograms of the hourly IC₅₀ values (in $\mu\text{g mL}^{-1}$) over the exposure period for SK-MES-1 cells exposed to CAPs, quartz standard reference material, Q66, and an urban dust standard reference material, SRM1649a. Values are the mean \pm SEM. The tabulated 24, 48, and 72 h IC₅₀ values for all three PM are included. **90**
- Figure 4.1:** RTCA cytotoxicity profiles of the normalized cell index (CI) over time for A) A549 and B) T24 (x1.67) cells exposed to As(V). The CI scales were normalized using the multiplication factor (in parentheses) for easier visual analysis. **102**

Figure 4.2: RTCA cytotoxicity profiles of the normalized cell index (CI) over time for A) A549, B) T24 (x1.11), and C) HepG2 (x2) cells exposed to As(III). The CI scales were normalized using the multiplication factor (in parentheses) for easier visual analysis. 104

Figure 4.3: Temporal IC₅₀ histograms of the hourly IC₅₀ values ($\mu\text{M} \pm \text{SEM}$) for A) A549 and B) T24 cells exposed to the inorganic arsenicals, As(V) and As(III). 105

Figure 4.4: RTCA cytotoxicity profiles of the normalized cell index over time for A549 cells exposed to A) MAO(III), B) MMA(III), and C) DMA(III), and T24 cells exposed to D) MAO(III) (x1.56), E) MMA(III) (x2.33), and F) DMA(III) (x1.56). The CI scales were normalized using the multiplication factor (in parentheses) for easier visual analysis. 108

Figure 4.5: Temporal IC₅₀ histograms of the hourly IC₅₀ values ($\mu\text{M} \pm \text{SEM}$) for A) A549 and B) T24 cells exposed to the inorganic arsenicals, As(V) and As(III), in comparison to the trivalent arsenic metabolites, MAO(III), MMA(III), and DMA(III). 110

Figure 4.6: RTCA cytotoxicity profiles of the normalized cell index over time for A) A549 (x1.5) and B) T24 cells exposed to the trivalent thiolated arsenic species, DMAG (III). The CI scales were normalized using the multiplication factor (in parentheses) for easier visual analysis. 111

Figure 4.7: Temporal IC₅₀ histograms showing the hourly IC₅₀ values ($\mu\text{M} \pm \text{SEM}$) over the exposure period for A) A549 and B) T24 cells exposed to the trivalent inorganic arsenical, As(III), in comparison to the dimethylated trivalent arsenic species, DMA(III) and DMAG(III)..... 112

Figure 4.8: RTCA cytotoxicity profiles of the normalized cell index over time for A549 cells exposed to A) MMTTA(V), B) DMMTA(V), and C) DMDTA(V) (x1.43) and T24 cells exposed to D) MMTTA(V) (x1.33), E) DMMTA(V)

(x2), and F)DMDTA(V) (x2.5). The CI scales were normalized using the multiplication factor (in parentheses) for easier visual analysis. 113

Figure 4.9: Temporal IC₅₀ histograms of the hourly IC₅₀ values (μM ± SEM) for A) A549 and B) T24 cells exposed to the pentavalent inorganic arsenical, As(V), in comparison to the pentavalent arsenic metabolites, MMTA(V), DMMTA(V), and DMDTA(V). 115

Figure 4.10: RTCA cytotoxicity profiles of the normalized cell index over time for A) A549, B) T24, and C) HepG2 cells exposed to Arsenicin A. 116

Figure 4.11: Temporal IC₅₀ histograms showing the hourly IC₅₀ values (μM ± SEM) over the exposure period for A549, T24, and HepG2 cells exposed to A) Arsenicin A and B) the trivalent inorganic arsenical, As(III). 117

Figure 4.12: RTCA cytotoxicity profiles of the normalized cell index over time for A549 cells exposed to A) roxarsone (x1.5) and B) p-arsanilic acid (x1.2) and T24 cells exposed to C) roxarsone and D) p-arsanilic acid. The CI scales were normalized using the multiplication factor (in parentheses) for easier visual analysis. 119

Figure 4.13: RTCA cytotoxicity profiles of the normalized cell index over time for A) A549 and B) T24 (x1.43) cells exposed to the trivalent organoarsenical, PAO(III). The CI scales were normalized using the multiplication factor (in parentheses) for easier visual analysis. 120

Figure 4.14: Temporal IC₅₀ histograms of the hourly IC₅₀ values (μM ± SEM) for A) A549 and B) T24 cells exposed to PAO(III), inorganic As(III), and roxarsone. 121

Figure 5.1: Proposed modes of action for arsenic. Adapted from Hughes et al. (2011). 125

Figure 5.2: Chromatograms showing the speciation analysis for the As(III) samples collected at all nine timepoints. By 24 h, there is a small As(V) peak present, indicating some conversion of As(III) to As(V) in culture media. **140**

Figure 5.3: A) Concentrations of As(III) and As(V) detected in cell culture media over time by HPLC-ICP-MS analyses. B) RTCA profile of the normalized CI over time for A549 cells treated with As(III). **141**

Figure 5.4: Chromatograms showing the speciation analysis for the MMA(III) samples collected at all nine timepoints. By 3 h, there is a small MMA(V) peak present, indicating conversion of MMA(III) to MMA(V) in culture media. The MMA(V) peak continues to increase in area over the exposure period, as the peak area for MMA(III) decreases. **142**

Figure 5.5: A) Concentrations of MMA(III) and MMA(V) detected in cell culture media over time by HPLC-ICP-MS analyses. B) RTCA profile of the normalized CI over time for A549 cells treated with MMA(III). **143**

Figure 5.6: Chromatograms showing the speciation analysis for the DMA(III) samples collected at the first five timepoints. There is clear, rapid conversion of DMA(III) to DMA(V) in culture media, as the DMA(III) peak is not visible by 9 h. **144**

Figure 5.7: A) Concentrations of DMA(III) and DMA(V) detected in cell culture media over time by HPLC-ICP-MS analyses. B) RTCA profile of the normalized CI over time for A549 cells treated with DMA(III). **145**

Figure 5.8: Chromatograms showing the speciation analysis for the DMAG(III) samples collected at all nine timepoints. At 0 h, there is a small DMA(V) peak present, indicating conversion of DMAG(III) to DMA(V) in culture media. The DMA(V) peak continues to increase in area over the exposure period, as the peak area for DMAG(III) decreases. **146**

- Figure 5.9:** A) Concentrations of DMAG(III) and DMA(V) detected in cell culture media over time by HPLC-ICP-MS analyses. B) RTCA profile of the normalized CI over time for A549 cells treated with DMAG(III)..... **147**
- Figure 5.10:** HPLC-ICP-MS chromatogram showing the speciation analysis for the As(V) samples collected at the final timepoint, 48 h, indicating that As(V) is highly stable in cell culture media..... **148**
- Figure 5.11:** A) Concentration of As(V) detected in cell culture media over time by HPLC-ICP-MS analyses. B) RTCA profile of the normalized CI over time for A549 cells treated with As(V)..... **149**
- Figure 5.12:** HPLC-ICP-MS chromatograms showing the speciation analysis for the DMMTA(V) samples collected at eight timepoints. The impurity of the DMMTA(V) standard as well as the lack of an HPLC-ICP-MS standard for retention time comparison made analysis of this data difficult. **150**
- Figure 5.13:** A) Concentrations of four arsenicals detected in cell culture media treated with DMMTA(V) over time by HPLC-ICP-MS analyses. B) RTCA profile of the normalized CI over time for A549 cells treated with DMMTA(V)..... **151**
- Figure 5.14:** HPLC-ICP-MS chromatogram showing the speciation analysis for DMDTA(V) samples collected at the last of eight timepoints at 48 h. DMDTA(V) is highly stable in cell culture media. **152**
- Figure 6.1:** A) RTCA profile of the CI over time for A549 cells treated with 1 μM PAO(III) and 0-50 $\mu\text{g mL}^{-1}$ o-SWCNT. B) RTCA profile of the CI over time for A549 cells treated with 0-50 $\mu\text{g mL}^{-1}$ o-SWCNT (as in Fig. 6.1A) and the CI over time for wells without cells present to show the effects of o-SWCNT on the RTCA electrodes (CI = 0). **164**
- Figure 6.2:** Change in pH during various stages of clathrin-dependent endocytosis..... **167**

Figure 6.3: A) RTCA profile of the CI over time for A549 cells treated with 12 μM PAPA(III) and 0-50 $\mu\text{g mL}^{-1}$ o-SWCNT. B) RTCA profile of the CI over time for A549 cells treated with 0-50 $\mu\text{g mL}^{-1}$ o-SWCNT (as in Fig. 6.3A) and the CI over time for wells without cells present to show the effects of o-SWCNT on the RTCA electrodes (CI = 0). **169**

Figure 6.4: RTCA profile of the CI over time for A549 cells treated with A) 7.5mM Roxarsone and 0-400 $\mu\text{g mL}^{-1}$ o-SWCNT and B) 5mM Roxarsone and 0-400 $\mu\text{g mL}^{-1}$ o-SWCNT. **171**

Figure 6.5: A) RTCA profile of the CI over time for A549 cells treated with 0-400 $\mu\text{g mL}^{-1}$ o-SWCNT (as in Fig. 6.4) and the CI over time for wells without cells present to show the effects of o-SWCNT on the RTCA electrodes (CI = 0). B) RTCA profile of the CI over time for A549 cells treated with the solvent controls present in 7.5 mM (0.62% DMSO, 15.5% H₂O) and 5 mM (0.46% DMSO, 11.6% H₂O) roxarsone. **172**

List of Abbreviations

AA	Arsenicin A
AC	Alternating current
AK	Adenylate kinase
ANOVA	Analysis of variance
AP	Acid phosphatase
APL	Acute promyelocytic leukemia
AQP	Aquaporin
As(III)	Arsenite
As(V)	Arsenate
ATCC	American Type Culture Collection
ATG(III)	Arsenic Triglutathione
CAAQS	Canada Ambient Air Quality Standard
CAPs	Concentrated air particulates
CBB	Cell-based biosensor
CCR	Coal combustion residue
CFA	Coal fly ash
CFE	Colony forming efficiency
CI	Cell Index
CNT	Carbon nanotube
CPS	Counts per second
CSC	Cigarette smoke condensate
CV	Coefficient of variation
CWS	Canada-wide Standard
DC	Direct current

DEP	Diesel exhaust particles
DI	Deionized
DMA(III)	Dimethylarsinous acid
DMA(V)	Dimethylarsinic acid
DMAG(III)	Dimethylarsenic glutathione
DMDTA(V)	Dimethyldithioarsinate
DMMTA(V)	Dimethylmonothioarsinate
DMSO	Dimethyl-sulfoxide
EC	Environment Canada
ECIS	Electrical cell-substrate impedance sensing
EDTA	Ethylenediaminetetraacetic acid
FBS	Fetal bovine serum
GEM	Genetically-engineered microbe
GSAO	4-(<i>N</i> -(<i>s</i> -glutathionylacetyl)amino)phenylarsonous acid
HPLC	High performance liquid chromatography
HTS	High-throughput screening
IC ₅₀	<i>In vitro</i> cytotoxicity at 50%
ICP-MS	Inductively-coupled plasma mass spectrometry
IDE	Interdigitated electrode
IL-8	Interleukin 8
ISFET	Ion-sensitive field-effect transistors
LC	Liquid chromatography
LD ₅₀	Lethal dose at 50%
LDH	Lactate dehydrogenase
MADG(III)	Monomethylarsonic diglutathione

MAO(III)	Methylarsine oxide
MBB	Molecular-based biosensor
MMA(III)	Monomethylarsonous acid
MMA(V)	Monomethylarsonic acid
MMMTA(V)	Monomethylmonothioarsonate
MMTTA(V)	Monomethyltrithioarsonate
MTS	Tetrazolium salt (dye)
MTT	Tetrazolium salt (dye)
NAAQS	National Ambient Air Quality Standard
nAg	Silver nanoparticles
NCGC	National Institutes of Health Chemical Genomics Center
NIEHS	National Institutes of Environmental Health Sciences
NIH	National Institutes of Health
NP	Nanoparticle
NRU	Neutral red uptake
nTiO ₂	Titanium dioxide nanoparticles
NTP	National Toxicology Program
o-SWCNT	Oxidized single-walled carbon nanotubes
PAH	Polycyclic aromatic hydrocarbon
PAO(III)	Phenylarsine oxide
PAPAO(III)	p-Amino-phenylarsine oxide
PBS	Phosphate buffered saline
PCB	Polychlorinated biphenyl
PDI	Polydispersity index
PEG	Polyethylene glycol

PI	Propidium iodide
PM	Particulate matter
PM0.1	Ultrafine fraction of air particulates
PM2.5	Fine fraction of air particulates
PM10	Coarse fraction of air particulates
Q66	Quartz standard reference material (diameter: 0.35-3.5 μm)
Q70	Quartz standard reference material (diameter: 1.2-20 μm)
QCM	Quartz crystal microbalance
QDs	Quantum dots
ROS	Reactive oxygen species
RT	Room temperature
RTCA	Real-time cell analysis
SEM	Standard error
SPR	Surface plasmon resonance
SRM	Standard reference material
SRM1649a	Urban dust standard reference material
SRM2795	Diesel exhaust particles standard reference material
SWCNT	Single-walled carbon nanotubes
TEM	Transmission electron microscopy
TER	Transendothelial electrical resistance
US EPA	United States Environmental Protection Agency
US FDA	United States Food and Drug Administration
WST-1	Water-soluble tetrazolium salt (dye)
XPS	X-ray photoelectron spectroscopy

Chapter 1: Introduction*

1.1 Cell-Based Biosensors

An important class of bioassays for detection, identification, and toxicity analysis of chemicals and particulates are cell-based biosensors (CBBs). CBBs are special analytical devices that utilize living cells as sensing elements combined with a detector to convert cellular responses and other parameters into qualitative and/or quantitative signals. In other words, CBBs can detect chemical or physical changes that are a direct result of the biological response of the cells due to the presence of an introduced substance. CBBs have been utilized in a variety of environmental and pharmaceutical applications, including identification of chemical and biological toxins, environmental monitoring of pollution, pharmaceutical drug screening, cell physiology analysis, and various other commercial applications [1-3].

CBBs are distinguished from other types of biosensors in that whole cells are used as the sensing element. For example, molecular-based biosensors (MBBs) use the specificity of interaction between biological molecules, such as purified antibodies, nucleic acids, or enzymes, which serve as the primary sensing component, and the analyte of interest. Readily recognized “household” MBBs include pregnancy test strips (antibody-based) and glucose meters (enzyme-based) [4]. MBBs have also been proven extremely valuable in environmental monitoring, particularly when identifying a specific contaminant or class of

* A version of this chapter has been accepted for publication. Moe et al. July 15, 2013. *Encyclopedia of Analytical Chemistry*.

contaminants or when a specific biological response is examined [5-10].

However, while the specificity of MBBs make them an excellent choice for the detection of a specific analyte of interest, this limits their effectiveness in general toxicity screening of environmental samples, which can contain a number of unknown toxic compounds. In addition, MBBs also require that the sensing biomolecules be purified prior to use, a process that is often extensive and costly. The use of whole cells by CBBs overcomes these limitations. Whole cells express and maintain a diverse number of native biomolecules on their cell membrane which can respond to a number of different, physiologically-active substances in a mixture. This allows for the determination of the bioavailability of chemicals in the mixture, which is essential to understanding the potential exposure risk [1, 11].

CBBs are most often categorized based on the cell types used for sensing and/or the detector used to convert the cellular responses into detectable signals. Both prokaryotic (bacteria and archaea) and eukaryotic cells (all other single and multicellular organisms) have been used [12]. CBBs incorporating prokaryotic cells are well established in the field of environmental monitoring [13]. A recent trend has been the incorporation of genetically-engineered microbes (GEMs) into CBBs, which, like MBBs, demonstrate high specificity and simple detection when identifying a known analyte in a sample or when a specific biological response is examined [5, 10, 14, 15]. While these CBBs may be beneficial for environmental detection, the specificity of these sensors may not be applicable to complex mixtures, and they are not as physiologically-relevant to human health effects as

eukaryotic cell biosensors. Hence, there has been renewed interest in incorporating eukaryotic cells (mammalian, fish, insect, plant, and yeast) into CBBs [16, 17].

Similar to the incorporation of different types of whole cells as sensing elements, CBBs also incorporate various types of methods to convert the physiologic signals or other parameters of the cell to detectable signals. The most commonly used techniques are optical and electrochemical transduction [1, 2]. Optically-based systems often measure fluorescence, absorbance, chemiluminescence, surface plasmon resonance (SPR), or changes in light reflectivity [2]. Electrochemical systems measure the transfer of electrons between the electrodes and molecules or ions present in the solution in which the electrodes are immersed. Based on the means of detection to measure those electron transfers, these CBBs are classified as amperometric (changes in current flow), potentiometric (changes in potential or the measured voltage between a sensing electrode and a reference electrode), conductometric (changes in ability to conduct an electric charge), or impedimetric (changes in the opposition to current flow). While electrochemical and optical methods are most commonly used, piezoelectric, thermal, and mechanical methods have also been reported [18].

1.2 Impedance-based Cell-electronic Sensing

Initial development of an impedance-based cell monitoring system was conducted by Giaever and Keese (1984) [19]. In this seminal work, the authors described the continuous detection of the behaviour of fibroblast cells adhered to gold planar electrodes after the application of an externally applied alternating

electric field (0.1V; 4000 Hz). This study demonstrated that the measured changes in impedance over time reflected changes in cell: 1) morphology, 2) density (number of cells adhered to the electrodes), and 3) motion (cell movement on the electrodes). Hence, Giaever and Keese (1984) pioneered a non-invasive monitoring technique for examining cell behaviour *in vitro* based on the measurement of impedance resulting from the capacitive nature of the cell membrane of adherent cell lines on gold-plated electrodes. The basic concept of the technology, as described by Atienza and colleagues, is as follows: adherent cells are cultured into specialized multi-well plates with electrodes embedded on the bottom surface of each culture well [20, 21]. The cells attach to the surface of the embedded electrodes. The plates are interfaced with a system capable of generating a low voltage alternating current (AC) and measuring any electrical impedance across the electrodes. The electric field is applied at user-defined intervals over the entire course of the experiment both before and after the testing substance is applied, allowing for continuous measurement of changes in impedance. Increases in impedance are associated with increased cell proliferation and cell surface binding to the electrodes, as these phenomena increase the number of cells and the degree of cell contact with the electrodes. Conversely, cell death, reduced proliferation, and detachment will result in decreased impedance due to the decreased cell-electrode contact.

Giaever and Keese's device has been trademarked and commercialized by the company they founded, Applied Biophysics Inc., and is widely known as electrical cell-substrate impedance sensing (ECIS). In the first device that Giaever

and Keese developed in 1984, the array consisted of a single 60 mm culture dish containing four small gold working electrodes ($\approx 3 \times 10^{-4} \text{ cm}^2$ in size) and one large gold reference (counter) electrode ($\approx 2 \text{ cm}^2$) (1984) [19]. Modifications over time have resulted in the most well-known ECIS array which consists of 8-wells (now also available in 96-wells) with one small 250 μm gold working electrode and a common large reference electrode per well. Figure 1.1A illustrates a single well from this array, where the small working electrode and reference electrode are marked with an arrow and bracket, respectively. This type of arrangement of electrodes is referred to as a monopolar system [22]. Because the ratio of the reference to the sensing electrode area is $< 1/100$, the total measured impedance of the well is dominated by the impedance at the interface of the small sensing electrode and the cell culture media. The advantage of this simple design makes fabrication of these arrays less technically challenging, and as such, this monopolar array is still available from Applied BioPhysics. However, because the sensing electrodes only cover a small portion of the surface of the plate ($< 0.1\%$) [23], this specific ECIS array measures a limited number of the cells attached to the surface of the plate, only about 50-100 cells [24]. This can lead to potentially large inter-experiment variability and limits sensitivity [25].

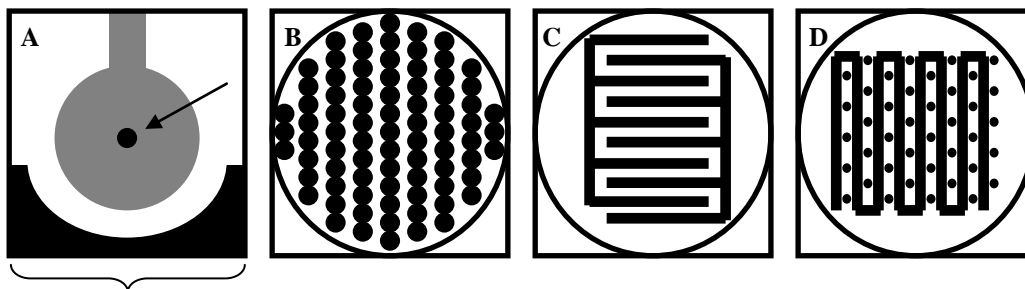


Figure 1.1: Examples of electrode arrangements found in various impedance-based CBB arrays. (a) The electrode arrangement of a single well found in the monopolar system available in some 8-well and 96-well ECIS arrays. The arrow points to the small sensing electrode, while the bracket indicates the large reference (counter) electrode. (b) This electrode arrangement represents the ‘circle-on-line’ IDE system available in the 16-well or 96-well RTCA arrays. The electrode arrangements in (c) and (d) represent interdigitated electrode (IDE) systems available in some 8-well and 96-well ECIS arrays. Drawings are not to scale.

To increase sensitivity and reproducibility, another electrode design for use in impedance-based CBBs, composed of interdigitated electrodes (IDEs), was developed [26]. IDEs are branched, formed by independently operating IDE units connected to a terminal strip [22]. The use of IDEs in commercially available impedance-based CBBs was developed by ACEA Biosciences Inc. for implementation into their real-time cell analyzer (RTCA) system. The RTCA system has also been known as real-time cell electronic sensing (RT-CES) or the xCELLigence™ system marketed by Roche Applied Science between 2009-2011. The IDE arrangement employed in each well of the 16-well and 96-well RTCA arrays is made up of approximately 2000 gold microelectrodes arranged in a ‘circle-on-line’ configuration that covers about 80% of the well surface area (Figure 1.1B) [20]. Because the IDEs cover a greater surface area than the electrode arrangement of monopolar systems, inter-well signal variability is reduced, and the RTCA system has an approximately two-log linear dynamic

range [25]. While the use of either the monopolar or IDE systems has distinct advantages, as each system has specific applications for which they are more suited, IDEs are being implemented more often into commercially available impedance-based CBBs. Both the CellKey™ platform from Molecular Devices, LLC (96-well and 384-well arrays) and the Bionas Discovery™ adcon reader system from Bionas GmbH (96-well array) use IDEs. Applied BioPhysics has also developed several 8-well and 96-well ECIS arrays with various designs of interdigitated finger electrodes (Figures 1.1C,D) [24]. This increase in popularity of IDE arrays is largely a result of the pharmaceutical industry's demand for high-throughput screening (HTS) of compounds for potential pharmaceutical application [27-29].

1.2.1 Monitoring Cellular Responses in Impedance-based CBBs

As mentioned briefly above (Section 1.2), monitoring cellular responses via impedance is based on monitoring current as ions diffuse down their concentration gradient from the electrode into the surrounding electrolyte-filled cell culture medium after the application of an electric field. Due to the capacitive nature of the cell membrane, cells that attach to an electrode change the local ionic environment at the interface of the electrode and culture medium, resulting in increased impedance [21, 30]. Impedance is therefore dictated by the ion environment in both the bulk solution (culture medium) and at the electrode/solution interface. An adhered cell will cause the current to travel in one of two paths in order to reach the bulk electrolyte, either around the cell (through the substrate-cell spaces) or through the cell membrane. That path is largely

determined by the applied frequency, with high frequencies causing the current to penetrate cell membranes, and low frequencies (or DC current) causing current to flow beneath and between cells [28, 31]. Hence, different cellular responses can be analyzed by changing the frequency of the current in order to monitor cell-to-cell separation, cell-to-substrate separation, and cell membrane capacitance. Cell adhesion, spreading, proliferation, wounding and healing, invasion and extravasation, barrier function, and signal transduction are only some of the many cellular responses that have successfully been examined using impedance-based CBBs, demonstrating the versatility of this technique [24, 32-34].

1.2.2 Qualitative and Quantitative Analysis

Most impedance-based CBBs report resistance and impedance as the functional values for measuring cellular responses. The only exception is the RTCA system, which uses a unitless parameter termed “cell index” (CI) to describe the interaction of the cells with the electrodes. CI is calculated based on equation (1.1), built-in to the RTCA software:

$$CI = \max_{i = 1, \dots, N} \left[\frac{R_{cell}(f_i)}{R_b(f_i)} - 1 \right] \quad (1.1)$$

where N refers to the number of frequencies at which impedance is measured (N=3, representing 10, 25, and 50 kHz), $R_{cell}(f_i)$ is the resistance of the electrodes at a given frequency when cells are present in the well, and $R_b(f_i)$ is the resistance of the electrodes at a given frequency when no cells are present [23]. As with measurements of impedance used in other systems, an increased CI indicates greater cell-electrode contact via cell adhesion, spreading, and proliferation; a

decreased CI indicates reduced cell-electrode contact via cell death, detachment, or induction of a cytostatic state [25].

Data from impedance-based CBBs are represented as resistance/impedance/CI over time, producing unique cellular kinetic response profiles. Data can be generated during both the cells' logarithmic growth phase and after a confluent monolayer has formed (stationary growth phase), although the data collected during the different phases may be analyzed and interpreted differently. This corresponds to the different cellular responses that are monitored during these distinct cellular growth phases. For either phase, when cells are seeded into the CBBs and allowed to proliferate (prior to treatment), different cell lines have distinct growth profiles (i.e. the rate in change of impedance over time), showing cell-specific growth profiles [35]. Hence impedance-based CBBs not only monitor cellular responses caused by a toxicant after treatment, but they also allow for the *quantitative* assessment of the overall health of the cell population tested both before (all cells) and after treatment (non-treated control cells). This provides an internal control that is not available in traditional dye-based assays, where a *qualitative* inspection of cell health using microscopy techniques is the only means to monitor cell status. This highlights the benefit of dynamic monitoring as a means of regularly checking cell status throughout an experiment [36, 37].

Figure 1.2 presents an example of a kinetic cellular response profile, or cytotoxicity profile, generated using data from RTCA testing. The profile shows the normalized CI values over time of CHO-K1 cells in their logarithmic growth

phase (i.e. prior to reaching confluency) after treatment with silver nanoparticles (nAg). The normalized CI values correlate to cell density on the electrodes, which is supported by the images taken using traditional microscopy techniques (Fig. 1.2A-D). It has been proposed that the shape of these cellular response profiles may indicate the specific mechanism of toxicity caused by the introduced compound [21]. A similar observation was made by Xia et al. (2008) who found that known DNA-damaging agents had similar “kinetic signatures” (i.e. similarly-shaped cell index curves), and that this property could be used to generate rationale hypotheses for further studies into the mechanism of toxicity [38].

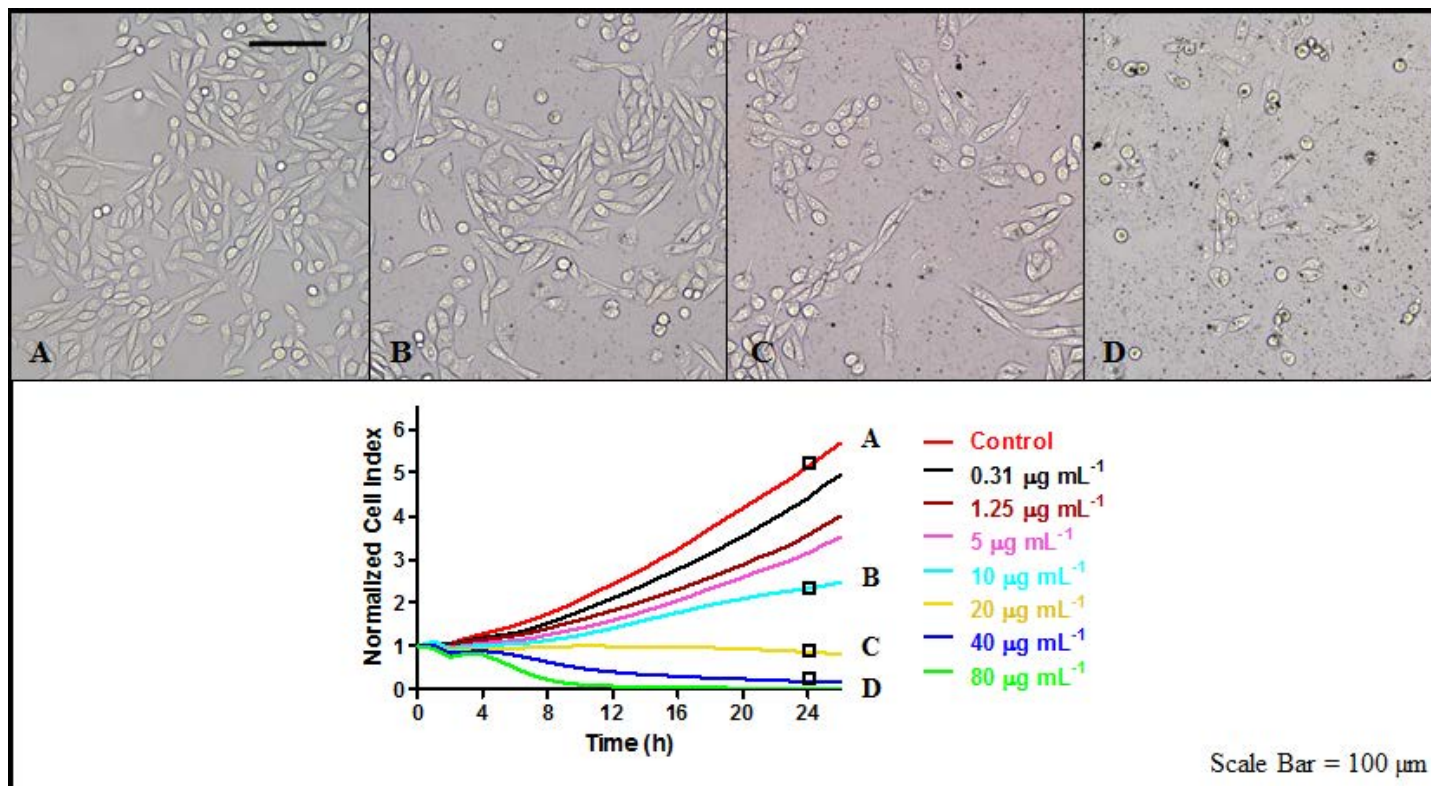


Figure 1.2: Cell index (CI) over time (normalized at time of cell treatment) for CHO-K1 cells exposed to silver nanoparticles determined using RTCA. Digital imaging microscopy images correspond to the marked time points on the cytotoxicity profile and show (a) untreated CHO-K1 control cells and CHO-K1 cells exposed to (b) 10 $\mu\text{g mL}^{-1}$, (c) 20 $\mu\text{g mL}^{-1}$, and (d) 40 $\mu\text{g mL}^{-1}$ silver nanoparticles.

Quantitative analysis of data generated during the logarithmic growth phase of cells is most often used to determine IC_{50} values. In impedance-based CBBs, IC_{50} values are defined as the treatment concentration that results in a 50% reduction in the impedance/resistance/CI as compared to a non-treated control at a specific timepoint. For risk assessment purposes, IC_{50} values generated using *in vitro* assays have been found to be an accurate measure for ranking the cytotoxicity of a compound. In addition, *in vitro* IC_{50} values determined using some traditional colorimetric cytotoxicity assays have been found to correlate with *in vivo* LD_{50} values (the dose resulting in 50% lethality of the test population) determined from acute toxicity tests in mammals [39]. Acute toxicity is often defined as the adverse effects that result almost immediately from either a single exposure or multiple exposures over a short period of time (<24 h) to an introduced compound [40]. This is in contrast to chronic toxicity, which is defined as the adverse effects associated with multiple exposures over a long period of time (months, years) [41]. Chronic toxicity testing is often performed to evaluate the potential oncogenicity of an introduced compound [41]. Hence, data obtained *in vitro* using impedance-based CBBs is more closely associated with acute toxicity, which is an important data measure for the areas of hazard identification and risk management.

Because IC_{50} values are a standard quantitative value determined in traditional colorimetric assays, many impedance-based CBB cytotoxicity studies also report IC_{50} values as $ECIS_{50}$ or EC_{50} to avoid confusion. Figure 1.3 shows a cytotoxicity profile and the resulting IC_{50} histogram generated using the data

from the RTCA system. Here, hourly IC_{50} values were determined using the CI values over time for each concentration of toxicant. For each timepoint, CI values for each treatment concentration, as seen in the cytotoxicity profile in Figure 1.3, were first transformed to a percent response scale (0-100%) relative to the CI of the untreated controls, which was defined as 100%. A sigmoidal dose-response curve was then generated at each timepoint after exposure, presenting percent response as a function of the logarithm of the treatment concentration. From these dose-response curves, IC_{50} values were derived. These values were then plotted over the exposure period to generate IC_{50} histograms, as seen in Figure 1.3.

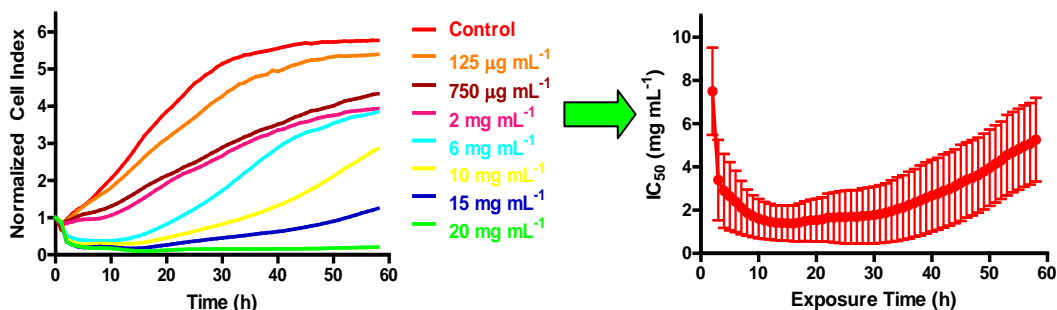


Figure 1.3: Cytotoxicity profile of the cell index (CI) over time (normalized at time of cell treatment) for an introduced toxicant generated using data from the RTCA system. Hourly dose-response data from the cytotoxicity profile was used to produce a temporal IC_{50} histogram, representing the hourly concentrations causing a 50% reduction in normalized CI compared to the untreated controls.

1.2.3 Advantages of Impedance-based CBBs

In vitro cytotoxicity is most commonly assessed using endpoint assays that rely on dye- or label-based detection of cellular responses. Most often, these assays measure changes in cell metabolism or cell membrane integrity through the addition of dyes or labels that interact with the cells or a cellular product. The

presence or absence of the dye or label is then quantified using colorimetric or fluorometric analysis. Impedance-based CBBs offer three distinct advantages over these traditional cytotoxicity assays, including real-time analysis, improved sensitivity, and dye- and label- free sample processing.

1.2.3.1 Real-time Analysis

Perhaps the greatest advantage of impedance-based CBBs over traditional cytotoxicity assays is the monitoring of cellular responses to an introduced toxicant in real-time. Impedance-based CBBs will monitor impedance as often as set by the user, on a scale of hours, minutes, or even seconds. Thus, real-time analysis generates far more data than traditional assays, which are limited to the number of pre-determined timepoints for analysis (which must be co-prepared for separate analysis). Furthermore, as discussed in Section 1.2.2, the real-time kinetic data generated is both qualitative and quantitative.

The utility of qualitative data generated with impedance-based CBBs is highlighted in two separate studies, one testing sodium arsenite [As(III)] and another studying metal oxide nanoparticles [25, 42]. In the first study, Xing et al. (2005) observed a unique RTCA cytotoxicity profile for NIH 3T3 cells treated with As(III) that was characterized by a rapid increase in CI in the first 5 h of exposure, followed by a decrease in CI. This produced a characteristic ‘bump’ in the treatment profiles that was higher than the CI of the untreated control cells. Further examination allowed the authors to conclude that the rapid increase in CI was due to individual cells fusing together to form multinuclear cell bodies. These cell bodies then dissociated, producing the decrease in CI observed after 5 h

exposure, consistent with the induction of apoptosis. Likewise, Seiffert et al. (2012) observed a similarly shaped RTCA cytotoxicity profile for A549 cells treated with either zinc oxide or copper oxide nanoparticles. They also observed a transient increase in impedance above the level of the untreated control cells, which was then followed by a dose-dependent decrease in impedance, producing a similar ‘bump’ that peaked at 3 h of exposure and returned to the control baseline by 5.5 h exposure. The authors speculated that the transient increase in CI was also due to membrane changes occurring as a result of the induction of apoptosis. Using a traditional assay that only provides a “snap-shot” of cytotoxicity at discrete timepoints, such a cellular response as described in these studies may have been easily missed, as it only occurred for a short period of time (<10 h) and at the very beginning of the exposure period. This highlights the advantages of real-time analysis due to the mechanistic information that can be ascertained from dynamic response profiles of impedance over time.

In addition to qualitative data generated from monitoring impedance over time, real-time quantitative data is also generated, as represented by the IC_{50} histograms produced by determining hourly IC_{50} values over the exposure period (Fig. 1.3). The production of IC_{50} histograms using the same cells throughout the exposure period is a unique benefit of impedance-based CBBs over traditional dye-based assays, and provides the user with information that is both quantitative (IC_{50} values) and kinetic (change in IC_{50} values over time). Unlike traditional dye-based assays, where a separate cell plate must be prepared and then most likely destroyed for analysis at each timepoint, hourly IC_{50} values can easily be

determined with impedance-based assays without the need to sacrifice the cell cultures. Not only does this reduce the variability of the quantitative data generated, but it also provides additional information to assist in prioritization of compounds, such as the time at which the greatest cytotoxicity is exerted (lowest IC_{50} value) to provide dynamic cytotoxicity information. Many authors have reported reduced variability amongst replicates generated with impedance-based CBBs over traditional dye-based assays. Chen et al. (2012) found a reduced coefficient of variation (CV) amongst six replicate IC_{50} values determined using the RTCA for five different cigarette smoke condensates compared to replicate values determined using the neutral red uptake (NRU) assay [37]. Huang et al. (2008) also reported smaller standard deviations for IC_{50} values determined using the RTCA compared to those values determined using the dye-based acid phosphatase assay for quartz microparticles [43].

Furthermore, quantitative IC_{50} histograms can also be used to infer qualitative information regarding cytotoxicity. For example, Tarantola et al. (2009) examined the effects of colloidal semiconductor quantum dots (QDs) with a multishell coating on epithelial MDCK (type II) cells using a custom-made ECIS platform [44]. IC_{50} histograms demonstrated the biphasic nature of QD cytotoxicity on this cell line, as the IC_{50} values decreased rapidly over the first 20 h of exposure and then plateaued for the remainder of the exposure period (20-50 h). The authors speculated this was due to the quick uptake of the QDs by the cells followed by the slow release of the toxic Cd ions from the multishell coating. This demonstrates that both qualitative kinetic response profiles and

quantitative IC₅₀ histograms generated through real-time cell analysis provide multiple benefits for *in vitro* cytotoxicity assessment.

1.2.3.2 Sensitivity

The sensitivity of a cytotoxicity assay is often defined as the ability of the assay to detect cellular responses at low treatment doses. Sensitivity is therefore greatly affected by the type of cellular response the assay detects. As mentioned in Section 1.2.3, traditional dye- or label-based cytotoxicity assays measure changes in cell metabolism or cell membrane integrity. For example, the MTT or MTS, NRU, and trypan blue assays are all measures of cell viability, but measure the activity of mitochondrial dehydrogenase, lysosomal function, and the integrity of the cell membrane, respectively [45-47]. Hence, quantitative analysis of different assays can produce differing cytotoxicity values, as they measure the impact of a toxicant on different cellular attributes [42]. Not only does this affect data comparability, but it also changes the sensitivity of an assay, as it is limited to the examination of only a specific cellular response that the toxicant under investigation may not even affect [48]. Therefore, an assay that can monitor a wide range of cellular responses will be more likely to produce a cytotoxic ‘hit,’ demonstrating higher sensitivity. This is extremely important when prioritizing chemicals or particulates for further toxicity testing. Impedance-based CBBs have the distinct advantage of measuring the integrated effects of several cellular processes at once, such as cell adhesion, spreading, and proliferation. In turn, these specific cellular processes can often be influenced by other cellular responses, such as a loss in cell viability reducing cell proliferation.

The sensitivity of different assays is often compared quantitatively with IC_{50} values, as lower IC_{50} values indicate that cytotoxic responses were observed at a lower range of toxicant concentrations. Several cytotoxicity studies using impedance-based assays have shown comparable, if not greater, sensitivity compared to traditional cytotoxicity assays, as determined by IC_{50} values recorded at the same timepoint after exposure. Table 1.1 shows IC_{50} values determined using impedance-based CBBs compared with traditional cytotoxicity assays for various toxicants, including nanoparticles and arsenicals, reported in the same studies. As seen here, the impedance-based CBBs produce comparable, if not lower, IC_{50} values for the toxicants tested using traditional cytotoxicity assays. Chen et al. (2012) reported a linear correlation coefficient of $R^2=0.9878$ between IC_{50} values determined using the RTCA and those determined using the NRU assay for five different cigarette smoke condensates [37]. Likewise, Tran et al. (2013) reported a coefficient of $R^2=0.905$ between the viability results they obtained using a custom-made ECIS platform and the MTS assay when examining silica nanoparticles and silica nanotubes [49]. In two separate studies, Tarantola and colleagues (2009, 2011) found the sensitivity of their custom-made ECIS platform to be either comparable to or more sensitive to the MTS assay when examining gold NPs and multishell coated QDs, with IC_{50} values 2- to 4-fold lower when determined using ECIS [44, 50]. In their examination of gold NPs, they also found ECIS to be more sensitive than another label-free sensing platform: the quartz crystal microbalance (QCM) [50].

Table 1.1: Comparative IC₅₀ Values Between Impedance-based CBBs and Traditional Cytotoxicity Assays

Cell Line	Toxicant	Time	System/Assay	IC ₅₀ Value	Reference
V79 (fibroblastic)	Yellow Quantum Dots	10-20 h	ECIS	5.1 μM	[51]
			NRU	1.7 μM	
	Green Quantum Dots	10-20 h	ECIS	6.0 μM	
			NRU	2.31 μM	
	Orange Quantum Dots	10-20 h	ECIS	3.2 μM	
			NRU	1 μM	
MDCK type II (epithelial)	Quantum Dots (dia = 5-6 nm) (CdSe/CdS/ZnCd/ZnS multishell)	24 h	ECIS	2x10 ¹⁴ particles mL ⁻¹	[44]
			MTS	Non-toxic to 4x10 ¹⁴ particles mL ⁻¹	
		48 h	ECIS	1x10 ¹⁴ particles mL ⁻¹	
			MTS	190x10 ¹⁴ particles mL ⁻¹	
	Au Nanorods (cetyl triammonium bromide-coated)	24 h	ECIS	1.20x10 ¹¹ particles mL ⁻¹	
			MTS	Non-toxic to 2.30x10 ¹¹ particles mL ⁻¹	
		48 h	ECIS	8.5x10 ¹⁰ particles mL ⁻¹	
			MTS	8.75x10 ¹⁰ particles mL ⁻¹	
MDCK type II	Rod-shaped Au Nanoparticles	24 h	ECIS	16.3 ± 0.15 μM (±SD)	[50]
			MTS	Non-toxic with tested dose-range	
			QCM	16.0 ± 0.5 μM (±SD)	
		48 h	ECIS	1.1 ± 0.15 μM (±SD)	
			MTS	1.8 ± 0.1 μM (±SD)	
			QCM	12.0 ± 0.5 μM (±SD)	

	Spherical Au Nanoparticles	24 h	ECIS	0.2 ± 0.15 μM (±SD)	
			MTS	0.3 ± 0.1 μM (±SD)	
			QCM	1.5 ± 0.5 μM (±SD)	
		48 h	ECIS	0.1 ± 0.15 μM (±SD)	
			MTS	0.3 ± 0.1 μM (±SD)	
			QCM	2.3 ± 0.5 μM (±SD)	
V79	CdCl₂	14-24 h	ECIS	3.9 ± 0.4 μM (±SD)	[52]
			NRU	3.0 ± 0.4 μM (±SD)	
	Na₂HAsO₄	14-24 h	ECIS	51.0 ± 6.7 μM (±SD)	
			NRU	52.2 ± 7.7 μM (±SD)	
	Benzalkonium chloride	14-24 h	ECIS	13.8 ± 0.5 μM (±SD)	
			NRU	15.3 ± 0.9 μM (±SD)	
SK-MES-1 (lung carcinoma)	Q66 (0.35-3.5 μm quartz SRM)	24 h	RTCA	0.06 ± 0.01 mg mL ⁻¹ (±SD)	[43]
			AP	0.08 ± 0.03 mg mL ⁻¹ (±SD)	
CHO-K1 (non-carcinoma)	Cigarette Smoke Condensate	24 h	RTCA	154.440 ± 6.641 μg mL ⁻¹ (±SD)	[37]
	A		NRU	157.875 ± 11.841 μg mL ⁻¹ (±SD)	
	B	24 h	RTCA	150.250 ± 8.114 μg mL ⁻¹ (±SD)	
			NRU	150.425 ± 11.131 μg mL ⁻¹ (±SD)	
	C	24 h	RTCA	110.630 ± 7.523 μg mL ⁻¹ (±SD)	
			NRU	120.273 ± 12.388 μg mL ⁻¹ (±SD)	
	D	24 h	RTCA	99.183 ± 6.050 μg mL ⁻¹ (±SD)	
			NRU	103.489 ± 11.384 μg mL ⁻¹ (±SD)	
	E	24 h	RTCA	91.016 ± 5.188 μg mL ⁻¹ (±SD)	
			NRU	90.746 ± 7.804 μg mL ⁻¹ (±SD)	

SMMC-7721 (human hepatocellular carcinoma)	CdTe Quantum Dots (cysteamine-capped)	24 h	RTCA	51.4 nM	[53]
			MTT	35.9 nM	
		48 h	RTCA	11.4 nM	
			MTT	17.9 nM	
		72 h	RTCA	5.5 nM	
			MTT	11.0 nM	
NIH 3T3 (mouse fibroblast)	Sodium Arsenite [As(III)]	24 h	RTCA	8.22 ± 0.43 μM (±SD)	[25]
			MTT	10.51 ± 0.72 μM (±SD)	
			NRU	8.96 ± 0.37 μM (±SD)	
BALB/c 3T3 (mouse fibroblast)	Sodium Arsenite [As(III)]	24 h	RTCA	7.71 ± 0.27 μM (±SD)	
			MTT	24.6 ± 0.63 μM (±SD)	
			LDH	38.66 ± 0.87 μM (±SD)	
			NRU	7.96 ± 0.54 μM (±SD)	
CHO-K1 (hamster ovary)	Sodium Arsenite [As(III)]	24 h	RTCA	9.19 ± 0.54 μM (±SD)	
			MTT	19.02 ± 0.58 μM (±SD)	
			LDH	56.9 ± 1.15 μM (±SD)	
			NRU	11.7 ± 0.43 μM (±SD)	
BALB/3T3 (clone A31-1-1)	Co-Micron	24 h	Adcon Reader	218 ± 18 μM (±SD)	[54]
			MTT	220 μM	
			CFE	7 μM	
	Co-Nano	24 h	Adcon Reader	303 ± 30 μM (±SD)	
			MTT	140 μM	
			CFE	8 μM	
CBBs = Cell-based Biosensors; ECIS = Electrical Cell-substrate Impedance Sensing; NRU = Neutral Red Uptake; MTS = Tetrazolium Salt Assay; QCM = Quartz Crystal Microbalance; SRM = Standard Reference Material; RTCA = Real-Time Cell Analysis; AP = Acid Phosphatase; MTT = Tetrazolium Salt Assay; LDH = Lactate Dehydrogenase; CFE = Colony Forming Efficiency					

1.2.3.3 Dye- and Label-free Data Processing

Dye- and label-free data processing is an important advantage over traditional cytotoxicity assays, as impedance-based detection is far less invasive to the cell itself. The addition of dyes or labels can affect the cell, possibly preventing accurate analysis. Furthermore, in the absence of labeling, assays also have the potential to be multiplexed. Once the impedance-based assay is complete, the cells can be further analyzed with another assay, as the cells are still intact with no additional chemicals present [55].

With respect to cytotoxicity testing of nanomaterials, the dye- and label-free analysis provided by impedance-based CBBs is particularly advantageous. Traditional colorimetric or fluorometric assays are often impaired by the optical properties of the nanomaterials, such as their ability to autofluoresce, or their light scattering or fluorescence quenching abilities [44]. This interference has been reported in several studies. Braydich-Stolle et al. (2005) found aluminum nanoparticles formed light-scattering cytoplasmic aggregates at low concentrations, preventing analysis using a spectrophotometer needed for the MTS assay [56]. Likewise, AshaRani et al. (2009) found that starch coated silver nanoparticles had high absorbance readings in the spectrophotometer even in the absence of cells, preventing the use of the MTS assay for cell viability analysis [57]. Some studies have also shown that nanomaterials can interact directly or indirectly with the dyes themselves, further complicating analysis. Single-walled carbon nanotubes have been shown to interact with dyes used in the MTT and WST-1 cytotoxicity assays [58, 59]. Fisichella et al. (2009) also reported that

mesoporous silica nanoparticles were able to accelerate the exocytosis of formazan crystals from HeLa cells and astrocytes, thereby interfering with the MTT assay [60].

While many studies have reported particle-interference with traditional dye-based cytotoxicity assays, to our knowledge, no interference with impedance-based CBBs caused by particles have been reported in the literature. Some studies have even shown that impedance-based CBBs have generated quantitative cytotoxicity data when dye-based assays failed to do so. Huang et al. (2008) reported that quartz microparticles interfered with the acid phosphatase (AP) cytotoxicity assay, particularly in the higher doses, while no interference was detected when using the 16-well RTCA system [43]. Likewise, Otero-Gonzalez et al. (2012) reported that cells had to be washed extra times prior to the addition of the MTT solution before an accurate spectrophotometric measurement could be made when analyzing ZnO nanoparticles. They reported no issues when using RTCA to examine cytotoxicity [61].

1.2.4 Limitations of Impedance-based CBBs

Although impedance-based CBBs present many advantages over traditional cytotoxicity assays, there are some notable limitations of these techniques for routine *in vitro* cytotoxicity analysis. One of the main limitations of these assays is the cost of the instrumentation itself, and particularly the cost of replacing the single-use electronic plates. For example, the cost of one 96-well E-plate purchased in a bulk package for RTCA testing is roughly 25 times the cost of a single standard 96-well plastic cell culture plate also purchased in bulk.

However, while a standard 96-well plastic cell culture plate can usually only be used for analysis at a single timepoint, numerous timepoints can be collected with a single 96-well E-plate depending on the user's requirements. Thus, impedance-based CBBs can be cost effective if the data collected at multiple timepoints is properly utilized.

Another significant limitation of impedance-based CBBs is the limitation of these assays to adherent monolayers of cells or cell lines. Although most vertebrate cells cultured *in vitro* grow as adherent monolayers, some cell types are nonadhesive [62]. These include many cells derived from hematopoietic stem cells, such as red and white blood cells, as well as leukemic, human small-cell lung cancer, and murine ascites tumor cells [62]. As many of these cell types represent important models for studying human disease, their incompatibility with most impedance-based CBB platforms is a significant drawback. In addition, some commonly used adherent cell lines, such as HepG2 cells, grow as clumps and rarely form a perfect monolayer [63]. Hence, not all of the cells present would be in direct contact with the electrodes, affecting the accurate quantitative analysis of the cellular response [23, 64].

An additional potential drawback of impedance-based CBBs is the blended measurement of cell adhesion, spreading, and proliferation. Although this combined measurement can also be an advantage, as discussed previously (Section 1.2.3.2), impedance-based CBBs cannot distinguish the individual effects of each of these cellular responses on the overall measured change in impedance/resistance/CI. Therefore, additional assays must be performed to

determine the contribution of an individual effect if a specific process is under examination. In other words, the exact changes in impedance/resistance/CI measured by impedance-based CBBs cannot be correlated to specific cellular changes unless supporting assays are performed to reveal the contributions of each of those responses.

1.3 Particle Toxicology

Particle toxicology examines the hazards associated with particle exposure. Particle contaminants are distinguished as physical contaminants, as they have distinct toxicological properties from the often more well-studied chemical contaminants. Historically, particle toxicology emerged through the gradual examination and identification of an association between industrial activities and adverse human health effects caused by exposure to commercially important materials such as coal, asbestos, silica, and other minerals [65]. Most often, the people examined were those exposed occupationally, particularly in the mining industries. More recently, however, as industrial exposure to particles has been reduced due to exposure control, particle toxicology has focused on the study of ambient particulate matter (PM). PM is a complex mixture of organic and inorganic matter that is ubiquitous in our environment due to formation from both natural and synthetic sources. PM is classified by regulatory agencies by size, which is one of the most significant factors in the determination of a particles' ability to penetrate the human respiratory system [66]. Epidemiological studies have shown a clear association between long-term and short-term exposures to

PM air pollution and increased mortality, with long-term exposures showing stronger association with mortality and greater relative risks [67].

Currently, interest in particle toxicology is undergoing a resurgence due to the increased use of nanoparticles. Nanotechnology is generally defined as the manipulation and application of structures, devices, or systems, on a scale ranging from 100 nm down to the atomic scale of approximately 0.2 nm [68].

Nanomaterials often exhibit novel properties compared to the same material on a larger scale, properties which are a direct result of their small size and/or unique surface chemistry. These novel properties are often what make them valuable for use in consumer products. The unintentional creation of nanosized particles has been a known by-product of anthropogenic thermo-degradation processes, such as combustion and automobile use, and until recently, has been the only significant source of human exposure to nanosized particles [69]. However, with the recent and rapid development of nanotechnology, nanoparticles have already been incorporated into thousands of consumer products [70], and have found applications in pharmaceuticals, personal care products, and electronics [71].

Furthermore, as nanomaterials are capable of being released into the environment throughout their lifecycle, from production to use to disposal, several studies have sought to not only model their release into different spheres of the environment, including water, soil, and air, but they have also directly measured engineered-nanoparticles in the environment. Table 1.2 shows the various studies that have either estimated or calculated known concentrations of engineered nanoparticles in the environment. Other studies have also shown the direct environmental

release of nanoparticles from consumer goods, including the leaching of titanium dioxide nanoparticles from exterior paint on building facades into surface waters [72], and the release of silver nanoparticles from socks into wash water during laundering [73].

Table 1.2: Estimated and Measured Concentrations of Nanomaterials in the Environment

Nanomaterial	Location of Study	Estimated/Measured Concentrations	Reference
Carbon Nanotubes	Switzerland	1.5x10 ⁻³ µg m ⁻³ air (<i>Estimated</i>) 5x10 ⁻⁴ µg L ⁻¹ water 1x10 ⁻² µg kg ⁻¹ soil	[74]
	United States^a	0.5 µg kg ⁻¹ sediments (<i>Estimated</i>) <0.5 µg kg ⁻¹ sludge treated soil	[75]
	Aquatic Sediments (varying parameters)	1.2-2000 µg kg ⁻¹ aquatic sediments (<i>Estimated</i>)	[76]
	Kitchens (US) (Exhaust from propane and natural gas cooking stoves)	10 ⁴ -10 ⁵ particles m ⁻³ (<i>Measured</i>)	[77]
Gold Nanoparticles	United Kingdom^b (from face cream)	0.14 µg L ⁻¹ water (<i>Estimated</i>) 4.07 mg kg ⁻¹ sludge 5.99 µg kg ⁻¹ soil	[78]
	Las Vegas, NV, USA (Surface water consisting of urban runoff)	10 particles mL ⁻¹ wash water (<i>Measured</i>)	[79]
Silver Nanoparticles	United Kingdom^b (from biocidal coatings, shampoo, soap, toothpaste)	0.010 µg L ⁻¹ water (<i>Estimated</i>) 0.29 mg kg ⁻¹ sludge 0.43 µg kg ⁻¹ soil	[78]
	Switzerland	1.7x10 ⁻³ µg m ⁻³ air (<i>Estimated</i>) 0.03 µg L ⁻¹ water 0.02 µg kg ⁻¹ soil	[74]
	United States^a	2.1 µg kg ⁻¹ sediments (<i>Estimated</i>) 7.5 µg kg ⁻¹ sludge treated soil	[75]

(50 nm diameter)	Las Vegas, NV (Surface water consisting of urban runoff)	200 particles mL ⁻¹ wash water (<i>Measured</i>)	[79]
Titanium Dioxide	United Kingdom^b (from paint and sunscreen)	24.5 µg L ⁻¹ water (<i>Estimated</i>) 701 mg kg ⁻¹ sludge 1030 µg kg ⁻¹ soil	[78]
	Switzerland	1.5x10 ⁻³ µg m ⁻³ air (<i>Estimated</i>) 0.7 µg L ⁻¹ water 0.4 µg kg ⁻¹ soil	[74]
	United States^a	0.6 mg kg ⁻¹ sediments (<i>Estimated</i>) 0.47 mg kg ⁻¹ sludge treated soil	[75]
	Rhine River (Switzerland and the Netherlands)	ng L ⁻¹ range in water (10 ⁸ particle m ⁻³) (<i>Estimated</i>) mg kg ⁻¹ range in sediment (10 ¹³ particles m ⁻³)	[80]
	Arizona (1 wastewater plant) CA, CO, IA, MY, NY (8 wastewater plants)	36 µg Ti L ⁻¹ wastewater effluent (<i>Measured</i>) 8 - 31 µg Ti L ⁻¹ wastewater effluent (average 16 ± 7 µg Ti L ⁻¹)	[81]
	(60 nm diameter) (< 400 nm)	Las Vegas, NV, USA (Surface water consisting of urban runoff)	400 particles mL ⁻¹ wash water (<i>Measured</i>)
Zinc Oxide	United Kingdom^b (from paint, scratch resistant coatings, sunscreen)	76 µg L ⁻¹ water (<i>Estimated</i>) 2172 mg kg ⁻¹ sludge 3194 µg kg ⁻¹ soil	[78]
	United States^a	5.7 µg kg ⁻¹ sediments (<i>Estimated</i>) 22 µg kg ⁻¹ sludge treated soil	[75]

a = predicted values for the year 2012; b = model assumes 10% market penetration

With such a variety of applications and a known environmental presence, exposure to these ultrafine particles (PM < 0.1 μm) may therefore occur via several routes, including inhalation, ingestion, dermal exposure, and injection [82]. Hence, human exposure to nanomaterials has the potential to increase rapidly in the near future, placing a priority on the development of high-throughput *in vitro* screening tools for the safe use and development of nanotechnology [83]. Cytotoxicity testing of particulates is currently done using the traditional colorimetric or fluorometric cytotoxicity assays described previously (Section 1.2.3) [84]. However, as many nanomaterials have been found to interfere with the dyes or absorbance measurements requisite for many of these traditional assays [56-60], they cannot provide reliable assessment of nanoparticle-mediated cytotoxicity, leading to recommendations that multiple assays be performed to overcome any erroneous results [85]. These recommendations limit the utility of these assays for high-throughput assessment, highlighting the need to develop new technology for more efficient and reliable measurement of nanomaterial-mediated toxicity.

Because of their demonstrated use in high-throughput chemical cytotoxicity screening to produce both qualitative and quantitative data, impedance-based CBBs show great promise to be implemented for *in vitro* cytotoxicity analysis of nanomaterials as well. The development of impedance-based CBBs for use in *in vitro* cytotoxicity analysis will not only provide tools for use in the risk assessment of nanomaterials developed for consumer use, but they will also provide tools in environmental toxicity monitoring to assess nanoparticle

exposure risks as well as in pharmaceutical research to examine the utility of nanomaterial-altered cytotoxicity.

1.4 Arsenic Toxicity

Arsenic is a metalloid that occurs naturally throughout the geosphere and is thus ubiquitous in the environment [86]. Arsenic contamination of groundwater that serves as human drinking water sources is a serious public health concern, as chronic consumption of inorganic arsenic has been associated with skin, bladder, and lung cancers [87, 88], as well as several non-carcinogenic ailments such as skin lesions and reproductive, cardiovascular, and neurological diseases [89]. In humans, inorganic arsenic is enzymatically oxidized and reduced to promote elimination, resulting in the formation of several methylated intermediates and metabolites. The metabolism of inorganic arsenic is generally accepted to follow the pathway of $\text{As(V)} \rightarrow \text{As(III)} \rightarrow \text{MMA(V)} \rightarrow \text{MMA(III)} \rightarrow \text{DMA(V)} \rightarrow \text{DMA(III)}$ [89-91], although alternative pathways have been proposed [92]. Figure 1.4 shows the pathway of oxidative methylation proposed by Challenger in 1945 [93], in comparison to the alternative pathway of non-oxidative methylation proposed by Hayakawa et al. in 2005 that includes the formation of glutathione-conjugated intermediates [92].

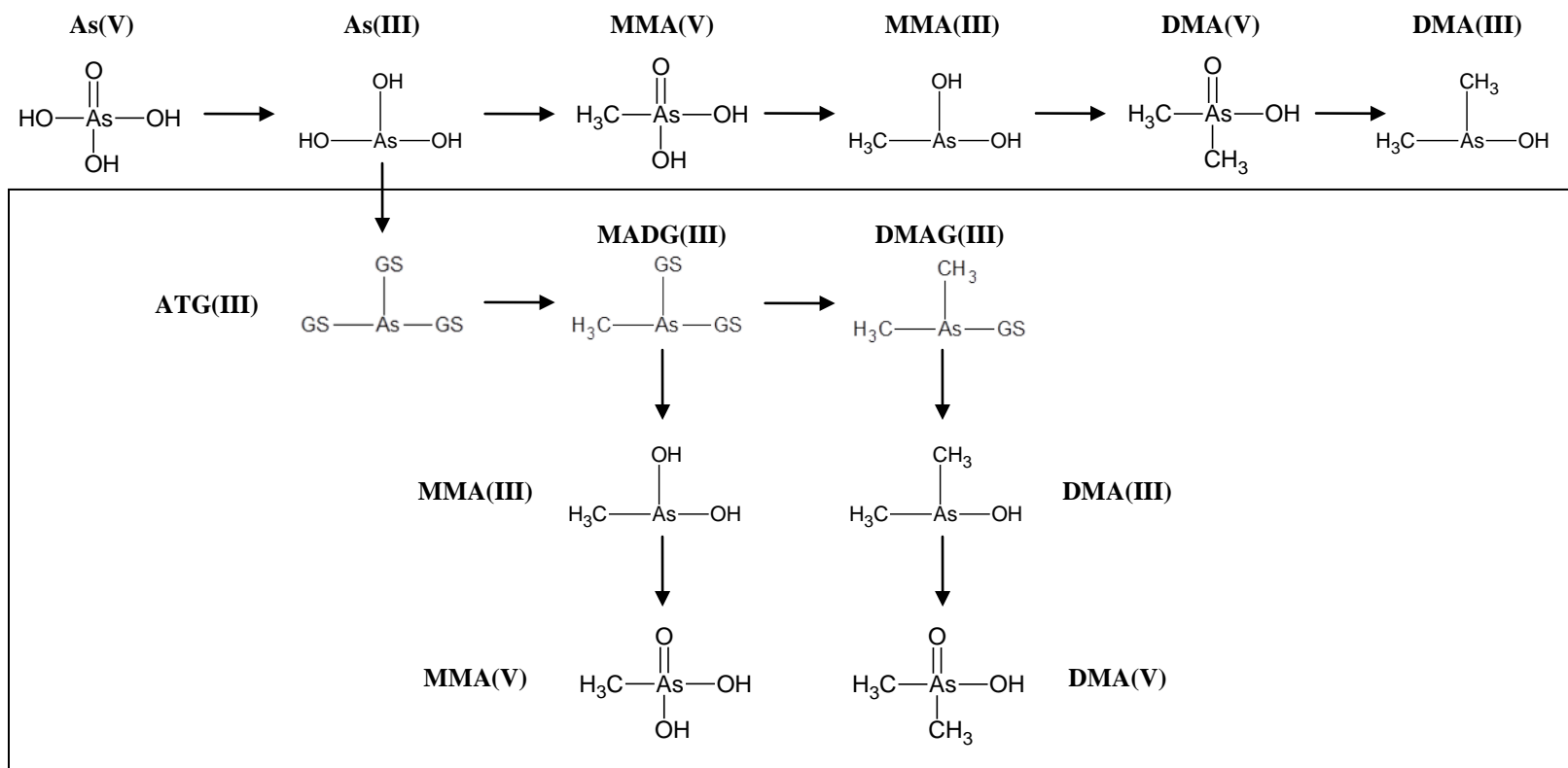


Figure 1.4: Proposed pathways of inorganic arsenic methylation in humans. The top pathway is that of oxidative methylation proposed by Challenger (1945) [88]. The boxed pathway below is that of non-oxidative methylation proposed by Hayakawa et al. (2005) [92].

While it is known that the toxicity of arsenic is dependent upon the specific chemical species, the roles of those species in the mechanisms underlying observed arsenic-induced cytotoxic effects are not well understood. Several studies have sought to understand the cytotoxicity-induced by different species of arsenic. In general, MMA(III) and DMA(III) have been found to be more cytotoxic than the inorganic arsenicals, As(III) and As(V), which in turn are more cytotoxic than DMA(V) and MMA(V) [94-98]. Hence, toxicity is dependent on the oxidation state (trivalent vs. pentavalent) and on the degree of methylation (inorganic vs. monomethyl- vs. dimethyl-). Although many studies have shown that trivalent arsenicals are generally much more toxic than the pentavalent species, cytotoxicity analysis of pentavalent thiolated arsenicals has suggested the importance of thiol conjugation to arsenic toxicity. DMMTA(V) is a pentavalent thiolated arsenical that has been demonstrated to be as toxic as the trivalent species, As(III) and DMA(III), in human cancer cell lines [99, 100]. The trivalent glutathione conjugated arsenical, DMAG(III) (Fig. 1.4), has also been shown to be a potent cytotoxicant, with IC_{50} values equal to or less than those of As(III) [95, 101]. Hence, in addition to oxidation state and degree of methylation, recent research has also revealed another factor influencing arsenic cytotoxicity: thiol conjugation.

Even though there is much data surrounding the cytotoxicity of individual arsenicals, these data were generated throughout a number of studies. These studies not only tested different sets of arsenic species on different cell lines, but

also used different assays for cytotoxicity assessment. This makes the comparison of the relative cytotoxicity of arsenicals very difficult. However, the application of new methods for analysis of arsenic-induced cytotoxicity may provide a more comprehensive study of and toxicity ranking for biologically significant arsenicals.

Impedance-based CBBs have had demonstrated use in high-throughput screening of chemical cytotoxicity. As mentioned in Section 1.2, these techniques are popular in the pharmaceutical industry for rapid cytotoxicity analysis of compounds with potential pharmacologic activity [102]. Furthermore, these techniques are also being utilized by government regulatory agencies. For example, RTCA is one of the cell-based *in vitro* assay technologies currently being implemented in Tox21, a joint collaboration between US government agencies: the National Toxicology Program (NTP), National Institutes of Health Chemical Genomics Center (NCGC), and the United States Environmental Protection Agency (USEPA), to prioritize the vast number of environmental chemicals, many of which are already under heavy commercial use, for further toxicological testing through the development of predictive *in vitro* assays [38, 103]. Hence, with their demonstrated use in HTS of chemicals within the pharmaceutical industry and regulatory agencies, impedance-based CBBs may be useful techniques for more accurate cytotoxicity ranking of biologically significant arsenicals.

1.5 Rationale and Scope of Thesis

With the demonstrated need to develop analytical methods for use in *in vitro* cytotoxicity analysis of nanomaterials and arsenic species, my research objectives for this thesis were:

1. To develop and validate a RTCA method to examine the cytotoxicity of nanomaterials using two well-characterized engineered nanoparticles, nano-silver and nano-titanium dioxide (Chapter 2);
2. To demonstrate the application of the developed RTCA method toward environmental air quality monitoring by screening environmentally-sampled air particulates (Chapter 3);
3. To rank the cytotoxicity of thirteen arsenic species in two human carcinoma cell lines using RTCA testing for a comprehensive study of species- and cell-dependent cytotoxicity (Chapter 4);
4. To examine cellular uptake and arsenic conversion over time to identify mechanisms responsible for the observed cytotoxicity of the tested arsenic species (Chapter 5); and
5. To demonstrate the application of the developed RTCA method toward the investigation of nanoparticle-altered cytotoxicity by testing the cytotoxicity of the tested arsenic species in the presence of oxidized single-walled carbon nanotubes (Chapter 6).

In the final chapter of this thesis (Chapter 7), I will summarize all findings and discuss their significance. Future research objectives and studies will also be proposed.

1.6 References

- [1] F. Asphahani, M. Zhang, *Analyst* 132 (2007) 835-841.
- [2] J.H. Luong, K.B. Male, J.D. Glennon, *Biotechnol. Adv.* 26 (2008) 492-500.
- [3] P. Wang, in: P. Wang, Q. Liu, and D. Schutzer (Eds.), *Cell-Based Biosensors: Principles and Applications*, Artech House Publishers, 2009, p. 1-11.
- [4] P. McFadden, *Science* 297 (2002) 2075-2076.
- [5] J.J. Pancrazio, J.P. Whelan, D.A. Borkholder, W. Ma, D.A. Stenger, *Ann. Biomed. Eng.* 27 (1999) 697-711.
- [6] S. Sole, S. Alegret, *Environ. Sci. Pollut. Res. Int.* 8 (2001) 256-264.
- [7] A.J. Baeumner, *Anal. Bioanal. Chem.* 377 (2003) 434-445.
- [8] S. Rodriguez-Mozaz, M.J. Lopez de Alda, D. Barcelo, *Anal. Bioanal. Chem.* 386 (2006) 1025-1041.
- [9] M. Ornatska, M. Ganesana, S. Andreescu, in: M.C. Flickinger (Ed.), *Encyclopedia of Industrial Biotechnology*, John Wiley & Sons, Inc., 2009.
- [10] I. Palchetti, M. Mascini, in: M. Mascini and I. Palchetti (Eds.), *Nucleic Acid Biosensors for Environmental Pollution Monitoring*, The Royal Society of Chemistry, 2011, p. 1-16.
- [11] S. Prasad, X. Zhang, C.S. Ozkan, M. Ozkan, *Electrophoresis* 25 (2004) 3746-3760.
- [12] B. DeRennaux, in: S.E. Jorgensen and B. Fath (Eds.), *Encyclopedia of Ecology, Five-Volume Set*, Elsevier Science, 2008, p. 1428-1432.
- [13] X. Xu, Y. Ying, *Food Rev. Int.* 27 (2011) 300-329.
- [14] M.B. Gu, R.J. Mitchell, B.C. Kim, *Adv. Biochem. Eng. Biotechnol.* 87 (2004) 269-305.
- [15] F. Lagarde, N. Jaffrezic-Renault, *Anal. Bioanal. Chem.* 400 (2011) 947-964.
- [16] K.B. Male, Y.K. Rao, Y.M. Tzeng, J. Montes, A. Kamen, J.H. Luong, *Chem. Res. Toxicol.* 21 (2008) 2127-2133.
- [17] E. Hondroulis, C. Liu, C.Z. Li, *Nanotechnology* 21 (2010) 315103 (9pp).

- [18] A.S. Bassi, in: M.C. Flickinger (Ed.), *Encyclopedia of Industrial Biotechnology*, John Wiley & Sons, Inc., 2009.
- [19] I. Giaever, C.R. Keese, *Proc. Natl. Acad. Sci. U.S.A.* 81 (1984) 3761-3764.
- [20] J.M. Atienza, J. Zhu, X. Wang, X. Xu, Y. Abassi, *J. Biomol. Screen.* 10 (2005) 795-805.
- [21] J.M. Atienza, N. Yu, S.L. Kirstein, B. Xi, X. Wang, X. Xu, Y.A. Abassi, *Assay Drug Dev. Technol.* 4 (2006) 597-607.
- [22] Z. Hu, Q. Liu, P. Wang, in: P. Wang, Q. Liu, and D. Schutzer (Eds.), *Cell-Based Biosensors: Principles and Applications*, Artech House Publishers, 2009, p. 151-178.
- [23] K. Solly, X. Wang, X. Xu, B. Strulovici, W. Zheng, *Assay Drug Dev. Technol.* 2 (2004) 363-372.
- [24] Applied Biophysics, Applied Biophysics ECIS Cultureware™, <http://www.biophysics.com/cultureware.php> (accessed 01.06.2013).
- [25] J.Z. Xing, L. Zhu, J.A. Jackson, S. Gabos, X.J. Sun, X.B. Wang, X. Xu, *Chem. Res. Toxicol.* 18 (2005) 154-161.
- [26] R. Ehret, W. Baumann, M. Brischwein, A. Schwinde, K. Stegbauer, B. Wolf, *Biosens. Bioelectron.* 12 (1997) 29-41.
- [27] G. Leung, H.R. Tang, R. McGuinness, E. Verdonk, J.M. Michelotti, V.F. Liu, *J. Assoc. Lab. Autom.* 10 (2005) 258-269.
- [28] R. McGuinness, *Curr. Opin. Pharmacol.* 7 (2007) 535-540.
- [29] B. Xi, N. Yu, X. Wang, X. Xu, Y.A. Abassi, *Biotechnol. J.* 3 (2008) 484-495.
- [30] J.Z. Xing, L. Zhu, S. Gabos, L. Xie, *Toxicol. In Vitro* 20 (2006) 995-1004.
- [31] H. Cai, P. Wang, in: P. Wang, Q. Liu and D. Schutzer (Eds.), *Cell-Based Biosensors: Principles and Applications*, Artech House Publishers, 2009, p. 37-64.
- [32] ACEA Biosciences, Applications Webpage, <http://aceabio.com/case.aspx> (accessed 01.06.2013).
- [33] Molecular Devices, LLC, Label-Free Analysis Webpage, <http://www.moleculardevices.com/Products/Instruments/Label-Free-Analysis.html> (accessed 01.06.2013).

- [34] Bionas GmbH, Bionas Discovery™ Adcon Reader Webpage, <http://www.bionas-discovery.com/applications/adconreader/index.html> (accessed 01.06.2013).
- [35] S.L. Kirstein, J.M. Atienza, B. Xi, J. Zhu, N. Yu, X. Wang, X. Xu, Y.A. Abassi, *Assay Drug Dev. Technol.* 4 (2006) 545-553.
- [36] Q. Mu, S. Zhai, B. Yan, *Methods Mol. Biol.* 625 (2010) 85-94.
- [37] H. Chen, L. Cui, X.Y. Jiang, Y.Q. Pang, G.L. Tang, H.W. Hou, J.H. Jiang, Q.Y. Hu, *Food Chem. Toxicol.* 50 (2012) 612-618.
- [38] M. Xia, R. Huang, K.L. Witt, N. Southall, J. Fostel, M.H. Cho, A. Jadhav, C.S. Smith, J. Inglese, C.J. Portier, R.R. Tice, C.P. Austin, *Environ. Health Perspect.* 116 (2008) 284-291.
- [39] National Institute of Environmental Health Sciences, National Institutes of Health, US Public Health Service, Department of Health and Human Services, NIH Publication 01-4500 (2001).
- [40] E. Walum, *Environ. Health Perspect.* 106 Suppl 2 (1998) 497-503.
- [41] D.L. Eaton, C.D. Klaassen, in: C.D. Klaassen and J.B. Watkins (Eds.), *Casarett and Doull's Essentials of Toxicology*, McGraw-Hill/Medical Pub. Div., 2003, p. 6-20.
- [42] J.M. Seiffert, M.O. Baradez, V. Nischwitz, T. Lekishvili, H. Goenaga-Infante, D. Marshall, *Chem. Res. Toxicol.* 25 (2012) 140-152.
- [43] L. Huang, L. Xie, J.M. Boyd, X.F. Li, *Analyst* 133 (2008) 643-648.
- [44] M. Tarantola, D. Schneider, E. Sunnick, H. Adam, S. Pierrat, C. Rosman, V. Breus, C. Sonnichsen, T. Basche, J. Wegener, A. Janshoff, *ACS Nano* 3 (2009) 213-222.
- [45] E. Borenfreund, J.A. Puerner, *Toxicol. Lett.* 24 (1985) 119-124.
- [46] T. Mosmann, *J. Immunol. Methods* 65 (1983) 55-63.
- [47] J.R. Tennant, *Transplantation* 2 (1964) 685-694.
- [48] Y. Fang, *Int. J. Electrochem.* 2011 (2011) 1-16.
- [49] B. Tran Trong, D. Nguyen Phuong, H. Um Soong, J. Son Sang, J. Min, J. *Biomed. Nanotechnol.* 9 (2013) 286-290.

- [50] M. Tarantola, A. Pietuch, D. Schneider, J. Rother, E. Sunnick, C. Rosman, S. Pierrat, C. Sonnichsen, J. Wegener, A. Janshoff, *Nanotoxicology* 5 (2011) 254-268.
- [51] K.B. Male, B. Lachance, S. Hrapovic, G. Sunahara, J.H. Luong, *Anal. Chem.* 80 (2008) 5487-5493.
- [52] C. Xiao, B. Lachance, G. Sunahara, J.H. Luong, *Anal. Chem.* 74 (2002) 5748-5753.
- [53] C. Wu, L. Shi, Q. Li, H. Jiang, M. Selke, L. Ba, X. Wang, *Chem. Res. Toxicol.* 23 (2010) 82-88.
- [54] L. Ceriotti, J. Ponti, F. Broggi, A. Kob, S. Drechsler, E. Thedinga, P. Colpo, E. Sabbioni, R. Ehret, F. Rossi, *Sensors Actuators B: Chem.* 123 (2007) 769-778.
- [55] E. McAuley, B. Mohanraj, T. Phamduy, G.E. Plopper, D. Corr, D. Chrisey, *Int. J. Biomed. Nanosci. Nanotechnol.* 2 (2011) 136-151.
- [56] L. Braydich-Stolle, S. Hussain, J.J. Schlager, M.C. Hofmann, *Toxicol. Sci.* 88 (2005) 412-419.
- [57] P.V. AshaRani, G. Low Kah Mun, M.P. Hande, S. Valiyaveetil, *ACS Nano* 3 (2009) 279-290.
- [58] J.M. Worle-Knirsch, K. Pulskamp, H.F. Krug, *Nano Lett.* 6 (2006) 1261-1268.
- [59] M. Davoren, E. Herzog, A. Casey, B. Cottineau, G. Chambers, H.J. Byrne, F.M. Lyng, *Toxicol. In Vitro* 21 (2007) 438-448.
- [60] M. Fisichella, H. Dabboue, S. Bhattacharyya, M.L. Saboungi, J.P. Salvetat, T. Hevor, M. Guerin, *Toxicol. In Vitro* 23 (2009) 697-703.
- [61] L. Otero-Gonzalez, R. Sierra-Alvarez, S. Boitano, J.A. Field, *Environ. Sci. Technol.* 46 (2012) 10271-10278.
- [62] R.I. Freshney, *Culture of Animal Cells: a Manual of Basic Technique and Specialized Applications*, Sixth Edition, Wiley-Blackwell, Hoboken, 2010.
- [63] M.C.E. McFadyen, P.H. Rooney, W.T. Melvin, G.I. Murray, *Biochem. Pharmacol.* 65 (2003) 1663-1674.
- [64] J.M. Boyd, L. Huang, L. Xie, B. Moe, S. Gabos, X.F. Li, *Anal. Chim. Acta* 615 (2008) 80-87.

- [65] K. Donaldson, P. Borm (Eds.), *Particle Toxicology*, CRC Press/Taylor & Francis Group, Boca Raton, 2007, p. 1-12.
- [66] D.L. Swift, W.M. Foster (Eds.), *Air Pollutants and the Respiratory Tract*, Marcel Dekker, New York, 1999, p. 39-71.
- [67] D. Krewski, R. Burnett, M. Jerrett, C.A. Pope, D. Rainham, E. Calle, G. Thurston, M. Thun, *J. Toxicol. Environ. Health A* 68 (2005) 1093-1109.
- [68] The Royal Society & The Royal Academy of Engineering, *Nanoscience and Nanotechnologies: Opportunities and Uncertainties*, London, 2004.
- [69] K. BeruBe, D. Balharry, K. Sexton, L. Koshy, T. Jones, *Clin. Exp. Pharmacol. Physiol.* 34 (2007) 1044-1050.
- [70] Woodrow Wilson International Center for Scholars, *Project on Emerging Nanotechnologies, Consumer Product Inventory*, www.nanotechproject.org/inventories/consumer (accessed 4.12.2012).
- [71] J.R. Lead, E. Smith, *Environmental and Human Health Impacts of Nanotechnology*, Wiley, Chichester, 2009.
- [72] R. Kaegi, A. Ulrich, B. Sinnet, R. Vonbank, A. Wichser, S. Zuleeg, H. Simmler, S. Brunner, H. Vonmont, M. Burkhardt, M. Boller, *Environ. Pollut.* 156 (2008) 233-239.
- [73] T.M. Benn, P. Westerhoff, *Environ. Sci. Technol.* 42 (2008) 4133-4139.
- [74] N.C. Mueller, B. Nowack, *Environ. Sci. Technol.* 42 (2008) 4447-4453.
- [75] F. Gottschalk, T. Sonderer, R.W. Scholz, B. Nowack, *Environ. Sci. Technol.* 43 (2009) 9216-9222.
- [76] A.A. Koelmans, B. Nowack, M.R. Wiesner, *Environ. Pollut.* 157 (2009) 1110-1116.
- [77] L. Murr, K. Garza, K. Soto, A. Carrasco, T. Powell, D. Ramirez, P. Guerrero, D. Lopez, J. Venzor, *Int. J. Environ. Res. Public Health* 2 (2005) 31-42.
- [78] A. Boxall, Q. Chaudhry, C. Sinclair, A. Jones, R. Aitken, B. Jefferson, C. Watts, *Current and Future Predicted Environmental Exposure to Engineered Nanoparticles*, Central Science Laboratory, York, 2007.
- [79] E.M. Heithmar, S.A. Pergantis, *Characterizing Concentrations and Size Distributions of Metal-containing Nanoparticles in Wastewater*, US Environmental Protection Agency, Washington, D.C., 2010, EPA/600/R-10/117.

- [80] A. Praetorius, M. Scheringer, K. Hungerbuhler, *Environ. Sci. Technol.* 46 (2012) 6705-6713.
- [81] M.A. Kiser, P. Westerhoff, T. Benn, Y. Wang, J. Perez-Rivera, K. Hristovski, *Environ. Sci. Technol.* 43 (2009) 6757-6763.
- [82] G. Oberdorster, E. Oberdorster, J. Oberdorster, *Environ. Health Perspect.* 113 (2005) 823-839.
- [83] A.D. Maynard, R.J. Aitken, T. Butz, V. Colvin, K. Donaldson, G. Oberdorster, M.A. Philbert, J. Ryan, A. Seaton, V. Stone, S.S. Tinkle, L. Tran, N.J. Walker, D.B. Warheit, *Nature* 444 (2006) 267-269.
- [84] N. Lewinski, V. Colvin, R. Drezek, *Small* 4 (2008) 26-49.
- [85] N.A. Monteiro-Riviere, A.O. Inman, L.W. Zhang, *Toxicol. Appl. Pharmacol.* 234 (2009) 222-235.
- [86] W.R. Cullen, K.J. Reimer, *Chem. Rev.* 89 (1989) 713-764.
- [87] National Research Council, *Arsenic in Drinking Water*, The National Academies Press, 1999.
- [88] National Research Council, *Arsenic in Drinking Water: 2001 Update*, The National Academies Press, 2001.
- [89] U. Schuhmacher-Wolz, H.H. Dieter, D. Klein, K. Schneider, *Crit. Rev. Toxicol.* 39 (2009) 271-298.
- [90] X.C. Le, X. Lu, M. Ma, W.R. Cullen, H.V. Aposhian, B. Zheng, *Anal. Chem.* 72 (2000) 5172-5177.
- [91] M. Styblo, Z. Drobna, I. Jaspers, S. Lin, D.J. Thomas, *Environ. Health Perspect.* 110 Suppl 5 (2002) 767-771.
- [92] T. Hayakawa, Y. Kobayashi, X. Cui, S. Hirano, *Arch. Toxicol.* 79 (2005) 183-191.
- [93] F. Challenger, *Chem. Rev.* 36 (1945) 315-361.
- [94] J.S. Petrick, F. Ayala-Fierro, W.R. Cullen, D.E. Carter, H. Vasken Aposhian, *Toxicol. Appl. Pharmacol.* 163 (2000) 203-207.
- [95] M. Styblo, L.M. Del Razo, L. Vega, D.R. Germolec, E.L. LeCluyse, G.A. Hamilton, W. Reed, C. Wang, W.R. Cullen, D.J. Thomas, *Arch. Toxicol.* 74 (2000) 289-299.

- [96] S.M. Cohen, L.L. Arnold, E. Uzvolgyi, M. Cano, M. St. John, S. Yamamoto, X. Lu, X.C. Le, *Chem. Res. Toxicol.* 15 (2002) 1150-1157.
- [97] E. Dopp, L.M. Hartmann, A.M. Florea, U. von Recklinghausen, R. Pieper, B. Shokouhi, A.W. Rettenmeier, A.V. Hirner, G. Obe, *Toxicol. Appl. Pharmacol.* 201 (2004) 156-165.
- [98] V. Charoensuk, W.P. Gati, M. Weinfeld, X.C. Le, *Toxicol. Appl. Pharmacol.* 239 (2009) 64-70.
- [99] H. Naranmandura, K. Ibata, K.T. Suzuki, *Chem. Res. Toxicol.* 20 (2007) 1120-1125.
- [100] H. Naranmandura, Y. Ogra, K. Iwata, J. Lee, K.T. Suzuki, M. Weinfeld, X.C. Le, *Toxicol. Appl. Pharmacol.* 238 (2009) 133-140.
- [101] L. Vega, M. Styblo, R. Patterson, W. Cullen, C. Wang, D. Germolec, *Toxicol. Appl. Pharmacol.* 172 (2001) 225-232.
- [102] B. Xi, N. Yu, X. Wang, X. Xu, Y. Abassi, *Biotechnol. J.* 3 (2008) 484-495.
- [103] R.S. Judson, K.A. Houck, R.J. Kavlock, T.B. Knudsen, M.T. Martin, H.M. Mortensen, D.M. Reif, D.M. Rotroff, I. Shah, A.M. Richard, D.J. Dix, *Environ. Health Perspect.* 118 (2010) 485-492.

Chapter 2: Development of a Real-Time Cell-electronic Sensing Method for Analysis of Nanoparticle-Induced Cytotoxicity*

2.1 Introduction

There are currently over 1000 nanotechnology-based consumer products available on the market [1]. Within the next decade, yearly global production rates of nanomaterials are estimated to increase over 25 times to nearly 60,000 metric tonnes per year [2, 3]. This dramatic increase in production and application of nanomaterials raises concerns about human exposure and health risks. Hence, developing *in vitro* screening tools has become a priority for the safe use and development of nanotechnology [4]. Current methods for assessment of nanoparticle cytotoxicity are dominated by end-point colorimetric assays, such as the MTT (3-[4,5-dimethylthiazol-2-yl]-2,5-diphenyltetrazolium bromide) and LDH (lactate dehydrogenase) assays [5, 6]. Although these colorimetric assays have been extensively validated for use in traditional cytotoxicity studies and are often inexpensive to perform, they are also time-consuming, requiring the preparation of multiple replicates for repeated analysis at each time point under investigation. Not only does this extra preparation limit the number of time points that can be examined, but it also makes high-throughput screening of numerous emerging materials difficult. In addition, many nanoparticles have also been found to cause serious interference within traditional assays, ultimately limiting their use in nanotoxicity testing [7-10]. This has led to the recommendation that more than one assay be performed to compensate for any potential interference

* A version of this chapter has been published. Moe et al. 2013. *Analytica Chimica Acta*. 789: 83-90.

[11], further complicating the high-throughput screening potential of end-point, dye-based assays for nanomaterial cytotoxicity testing.

Cell-impedance sensing techniques, such as real-time cell analysis (RTCA), are one possible solution to the issues encountered with the use of colorimetric assays for nanoparticle cytotoxicity testing. These *in vitro* techniques are based on monitoring changes in impedance generated by the adherence of cell lines to microelectrodes covering the bottom of microelectronic wells. This enables real-time monitoring of changes in cellular status without the use of labels or dyes, as impedance changes represent a blended measurement of changes in cell adhesion, proliferation, or morphology caused by exposure to an introduced toxicant over time. RTCA has been shown to be highly effective in the determination of chemical cytotoxicity [12-14], and is also one of the cell-based *in vitro* assay technologies currently being implemented by several US government interagency programs, including the National Toxicology Program (NTP), the National Institutes of Health Chemical Genomics Center (NCGC), and the US Environmental Protection Agency (EPA), to assess the cytotoxicity of environmental chemicals [15, 16].

A few studies have used RTCA systems to test the effects of nanoparticles on the anti-proliferative efficiency of chemotherapeutics [17-19], the effects of microscale and nanoscale silica on a murine macrophage cell line [20], the effects of carbon nanotubes on a human kidney epithelial cell line [21], and the effects of quantum dots on the viability of a human hepatocarcinoma cell line [22]. These studies demonstrated the use of one cell line to test a single nanomaterial. In the

present study, we aim to develop a 96x-RTCA method to profile two nanoparticles on a panel of cell lines to demonstrate cell-specific and nanoparticle-specific cytotoxicity. These results will provide a better understanding of the differential cytotoxicity of nanoparticles, which can be used for comparative analysis and toxicity ranking. In addition, it is important to demonstrate the potential advantages of the 96x-RTCA technique over traditional assays for screening nanoparticle cytotoxicity.

To develop a 96x-RTCA method to quantitatively and qualitatively assess the cytotoxicity of nanoparticles, we used a panel of three continuous cell lines, including two human lung carcinoma cell lines (A549 and SK-MES-1) and a non-tumor derived Chinese hamster ovary cell line (CHO-K1). The use of continuous cell lines will reduce response variability between generations of cells used for testing [23]. Two well-characterized nanoparticles, nano-titanium dioxide (nTiO_2) and nano-silver (nAg) were used to assess the 96x-RTCA method. This study will demonstrate the potential of the 96x-RTCA platform for comprehensive testing of emerging nanomaterials through the determination of concentration-, time-, particle-, and cell-dependent toxicological relationships. Because of its real-time analysis capabilities, the RTCA platform provides dynamic results for the differentiation of cytotoxicity that traditional assays cannot provide. Taking advantage of the impedance-based detection of the 96x-RTCA system that requires limited user manipulations, we will also demonstrate its potential to overcome many of the difficulties encountered in nanotoxicity testing when using traditional dye-based assays. This developed 96x-RTCA method will assist in the

prioritization of nanomaterials for further toxicological testing, which is essential for the protection of human health.

2.2 Materials and Methods

2.2.1 Cell Culture Conditions

The A549 (CCL-185; American Type Culture Collection (ATCC), Manassas, VA) and SK-MES-1 (HTB-58; ATCC) cell lines were cultured in RPMI 1640 media (Gibco (Invitrogen), Burlington, ON, Canada). The CHO-K1 (CCL-61; ATCC) cell line was cultured in (1:1) DMEM:F12 media (Gibco). Both media were supplemented with 10% fetal bovine serum (Sigma-Aldrich, Oakville, ON, Canada) and 1% penicillin-streptomycin (Invitrogen, Burlington, ON, Canada). The incubation conditions were maintained at 37 °C, 5.5% CO₂, and 90% humidity. During the study, the cells were sub-cultured twice weekly into standard 10 cm x 20 mm cell culture dishes (Corning Incorporated, Corning, NY) containing fresh media, using 0.05% trypsin-EDTA (Invitrogen) for cell detachment.

2.2.2 Nanoparticles and Characterization

Rutile titanium dioxide nanoparticles (nTiO₂) were specified by the manufacturer as having a particle size of 10 nm x 40 nm, surface area of 130-190 m² g⁻¹, and containing up to 5% (by weight) silicon dioxide as a surface coating [Sigma-Aldrich (637262)]. The silver nanoparticles (nAg) used were specified as organically-coated with a particle size of less than 100 nm and a surface area of 5.0 m² g⁻¹ [Sigma-Aldrich (576832)]. The organic coating was reported to promote dispersion of the nAg in polar solvents.

To further characterize the nanoparticles, x-ray photoelectron spectroscopy (XPS) (Axis 165 XPS system, Kratos Analytical) was used to determine the elemental and functional surface composition of both nanoparticles. Transmission electron microscopy (TEM) was performed to confirm the shape and size of the nanoparticles. The nanoparticles were applied to formvar-coated copper TEM grids and negatively-stained with 1% phosphotungstic acid (Sigma-Aldrich) in distilled water (pH = 7). The samples were examined with a Philips 410 transmission electron microscope.

To characterize the agglomeration of the nanoparticles as administered to the cells, the Z-average size of the nanoparticle agglomerates, at the highest concentration used to treat the cells, were determined using a Zetasizer (Nano-S, Malvern Instruments Ltd., UK). The nanoparticles were prepared as described below for the RTCA experiments for both DMEM:F12 and RPMI 1640 media at a final concentration of $160 \mu\text{g mL}^{-1}$ nanoparticles and 1% (v/v) dimethylsulfoxide (DMSO) (Sigma-Aldrich) in media. Samples containing only 1% (v/v) DMSO in media were also examined to confirm there was no background interference caused by components within the media or solvent.

2.2.3 RTCA Analysis

The principles of the RTCA system (ACEA Biosciences, San Diego, CA) have been thoroughly described previously [12, 24]. Briefly, this platform consists of three main parts: the 96-well E-plate, the device station, and the system analyzer. The 96-well E-plate is electronically connected with the device station located in the CO₂ incubator, which in turn is connected to the system

analyzer outside of the incubator. A constant electric current is applied to the individual microwells on the E-plate, and the change in impedance of each microwell at the electrode-solution interface is individually monitored in real time by the system analyzer at three different frequencies: 10 kHz, 25 kHz, and 50 kHz. The measured impedance (Z) is automatically converted to its analogous parameter, resistance (R), via the following the equation:

$$Z = R + jX \quad (2.1)$$

where X is the reactance and j is the imaginary component. The resistance is then automatically converted by the RTCA software provided with the platform to the unitless parameter defined as Cell Index (CI), which is the signal directly measured using this platform. CI is calculated via the following equation:

$$CI = \max_{i=1, \dots, N} \left[\frac{R_{cell}(f_i)}{R_b(f_i)} - 1 \right] \quad (2.2)$$

where $R_{cell}(f_i)$ is the frequency-dependent resistance of the microelectrode when cells are bound and $R_b(f_i)$ is the same parameter with no cells bound, and N is the number of frequency points where impedance is measured ($N = 3$), selected by the instrument to maximize signal. Hence, $R_{cell}(f_i)$ and CI are positively correlated, so an increase in $R_{cell}(f_i)$ results in a higher CI, and a decrease in $R_{cell}(f_i)$ results in a lower CI. Increases in CI result from an increase in the number of cells adhered to the microelectrodes (via cell proliferation), an increase in cell adhesion, or an increase in cell spreading. Decreases in CI occur when the number of cells adhered to the microelectrodes decrease due to cell detachment, usually caused by cell death, or the cells adhere to the microelectrodes less fully due to

morphological changes. Therefore, changes in CI can represent multiple cytological responses to the introduced compound.

For the RTCA experiments, cells were sub-cultured after 24 h growth and seeded into the wells of the 96-well E-plate at concentrations that had previously been calibrated to allow the cells to reach a CI of 1, indicating a confluency of 50-60%, after 18-24 h growth. This provides a real-time control of cell status, as the rate of normal cell proliferation is distinct for all three cell lines. A549 cells were seeded at 5000 cells well⁻¹, CHO-K1 at 6000 cells well⁻¹, and SK-MES-1 at 12,500 cells well⁻¹. To determine the cytotoxicity of the nanoparticles, nTiO₂ and nAg were dispersed in DMSO and vortexed for 2 min using a Vortex Genie 2 (Scientific Industries, Bohemia, NY). The dispersions were then diluted with the respective cell culture media for each cell line to a range of nanoparticle concentrations between 0.078 – 160 µg mL⁻¹. The maximum concentration of DMSO used was 1% (v/v) in cell culture media. Each treatment concentration of nAg or nTiO₂ was added at a volume of 200 µL to triplicate wells after vortexing for 1 min. Solvent controls and non-treated controls (cell culture media) were run concurrently with the nanoparticle-treated cells and were also added at a volume of 200 µL to triplicate wells. The highest concentration of nanoparticle-treatment was also placed in duplicate wells with no cells present to ensure that there was no interference of the nanoparticles with CI measurements. After treatment, CI was measured at hourly intervals until the CI of non-treated control wells plateaued. The CI values over time of the untreated control cells were used to determine cell doubling times. The correlation between CI values and the number

of cells in a well has been reported previously, indicating its suitability for use in the quantitation of cell number and growth [12, 24, 25].

Three separate experimental runs with all corresponding negative, solvent, and blank controls were performed for each nanoparticle on each cell line (n = 3).

2.2.4 Neutral Red Uptake (NRU) Assay and Cell Cycle Analysis

To validate this RTCA method for use in IC₅₀ determinations and for the examination of cellular response kinetics, we examined cell viability using the neutral red uptake (NRU) assay and performed cell cycle analysis using flow cytometry with propidium iodide staining. For the NRU assay, all three cell lines were seeded, grown, and treated with nTiO₂ or nAg under the same conditions as those described above for the RTCA experiments. Cells were analyzed at 24 h and 48 h post-exposure using a previously described protocol [26]; however, modifications to this protocol were made to correspond to the same conditions used in the RTCA assays. Namely, cells were sub-cultured from standard 10 cm x 20 mm cell culture dishes instead of flasks before seeding into 96-well cell culture plates (Corning), and cells were seeded at a volume of 150 µL instead of 200 µL, with the same final concentrations of cells per well as seeded into the RTCA. In addition, a dual wavelength measurement was taken instead of a single wavelength measurement, with a reference wavelength of 690 nm subtracted from the 540 nm reference wavelength, using a microplate reader (Bio-Rad, Mississauga, ON, Canada).

Cell cycle analysis of CHO-K1 cells using propidium iodide staining and flow cytometry was performed to corroborate a brief cytostatic response observed

in the sensing profiles. CHO-K1 cells were seeded into standard 10 cm x 20 mm cell culture dishes at concentrations that allowed for the proper confluency to be reached in 24 h. At that time, cells were treated with $40 \mu\text{g mL}^{-1}$ nTiO₂ or its corresponding solvent control of 0.25% DMSO, so that triplicate plates were prepared for each treatment. After 24 h exposure, cells were washed twice with phosphate buffered saline (PBS; Gibco), detached using 0.05% trypsin-EDTA, and suspended in fresh media. Cells were twice pelleted by centrifugation at 1700 rpm for 3 min and washed with ice-cold PBS. After pelleting again, the cells were gently resuspended in 1 mL ice-cold PBS. An aliquot of 0.5 mL each was transferred into 4.5 mL of ice-cold 70% ethanol (Commercial Alcohols, Brampton, ON, Canada). These cells were stored at 4 °C overnight. The next day, cells were twice pelleted by centrifugation at 1000 rpm for 10 min to completely remove all ethanol and resuspended via gentle vortexing in ice-cold PBS. The cells were then counted using a hemocytometer, and $1 \times 10^6 - 2 \times 10^6$ cells were transferred to 12 mm x 75 mm vials (BD Biosciences; Mississauga, ON, Canada) containing 1 mL of propidium iodide (PI) staining solution. The PI staining solution was prepared fresh and consisted of 0.2 mg mL^{-1} RNase A (Sigma-Aldrich), 0.1% Triton X-100 (v/v) (VWR, Edmonton, AB, Canada), and 3.3% (v/v) of 1 mg mL^{-1} PI (Sigma-Aldrich) in water, all in PBS. The cells were kept in the dark at room temperature for at least 30 min prior to analysis and were analyzed using a Becton and Dickinson FACScan™ (Mountain View, CA) and its accompanying CellQuest™ software. Data analysis was performed using ModFit LT™ software (Verity Software House, Topsham, ME).

2.2.5 Data Analysis

Analysis of data to determine viability curves, IC₅₀ values, Mann-Whitney u-tests, t-tests, analysis of variance (ANOVA), and nonlinear regressions was performed using Prism 5.0 (Graph Pad Software Inc., San Diego, CA). IC₅₀ values were defined as the concentration of nanoparticle that resulted in a 50% reduction in normalized CI as compared to the normalized CI of non-treated control cells at a given time point. The nonlinear regressions of the CI values of the untreated control cells over time were determined by the exponential growth model provided by Prism 5.0, with the cell doubling time computed as the $\ln(2)$ over the rate constant.

2.3 Results and Discussion

2.3.1 Characterization of nAg and nTiO₂

Characterization of nanomaterials used for toxicity testing is essential as changes in size or surface characteristics can greatly affect toxicity, even for particles of the same chemical composition [27]. We characterized the elemental and functional surface composition, the shape and size, as well as agglomeration of nTiO₂ and nAg.

X-ray photoelectron spectroscopy (XPS) analysis of nTiO₂ revealed the elemental surface composition consisted of Ti, O, and Si, with small amounts of adventitious C and N. The peaks detected in the O1s region included a main peak at 530.1 eV, indicating surface O atoms, and a small peak at 531.8 eV, supporting the presence of chemisorbed –OH group. This observation is consistent with previous findings of surface –OH groups in laboratory-made and in commercially

available nTiO₂ samples [28-30]. Similarly, we used XPS to analyze the elemental surface composition of nAg. Our XPS analysis confirmed the elemental composition of the nAg as Ag, C, and O. We did not observe any signals in the O1s region of 528 – 530 eV, where distinct peaks are associated with silver oxides [31, 32]. Our analysis confirms that the surface of nAg has no detectable silver oxides. These results support that our sample preparation methods did not unintentionally oxidize the nAg surface. This protection is likely due to the organic surface coating of the nAg prepared by the manufacturer.

The shapes and sizes of nTiO₂ and nAg were imaged using transmission electron microscopy (TEM) (Figure 2.1). These images demonstrate that the nTiO₂ are spindle-shaped, consistent with the rutile crystal form, while the individual particles of nAg are round in shape. The particle sizes of both nanoparticles were confirmed to be less than 100 nm, consistent with the description of the manufacturer.

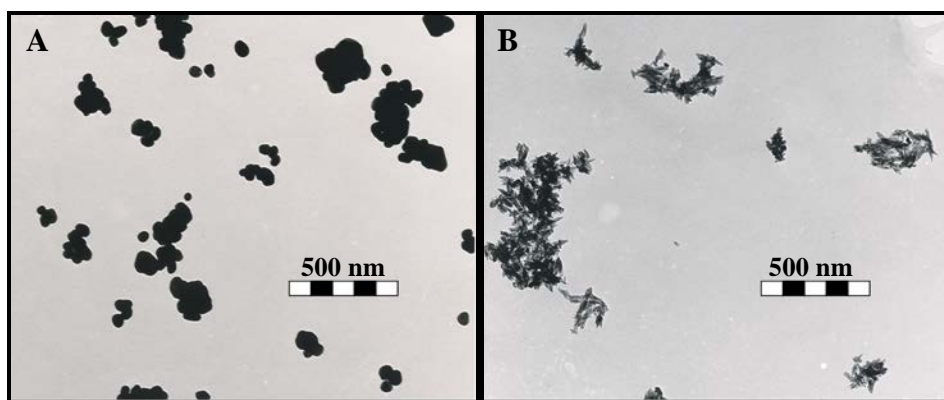


Figure 2.1: Transmission electron microscopy (TEM) images of A) nAg and B) nTiO₂ magnified 20,000 times with a 2.85 enlargement factor. The scale bar is composed of five 100 nm segments (500 nm total).

The agglomeration of nanoparticles in cell culture media is a common phenomenon and the size of the agglomerates is largely dependent on the specific media and dispersion conditions used. The Z-average size and polydispersity index (PDI) for nTiO₂ and nAg in the cell culture media used in our study was determined using a Zetasizer (Table 1.1). The Z-average size, or cumulants mean, is the intensity-weighted average size of particles in solution measured using dynamic light scattering (DLS). The PDI is a dimensionless value that quantifies the width of the particle size distribution and is measured on a scale of 0 (monodisperse) to 1 (polydisperse) [33, 34]. The results in Table 2.1 clearly show that both nAg and nTiO₂ can form agglomerates in water and in cell culture media with greater agglomeration in culture media than in water. These results also show nTiO₂ having greater agglomeration than nAg. Our measurements of the agglomeration of both nanoparticles are comparable to the reported values in other studies using similar nanoparticles and dispersion techniques [34, 35].

Table 2.1: Agglomeration of nAg and nTiO₂ in Water and Cell Culture Media

Dispersion	Z-Average size	PDI
nAg		
Distilled H ₂ O	160 nm	0.279
RPMI-1640 Media with 10% FBS	410 nm	0.433
DMEM/F12 Media with 10% FBS	370 nm	0.730
nTiO₂		
Distilled H ₂ O	240 nm	0.389
RPMI-1640 Media with 10% FBS	650 nm	0.364
DMEM/F12 Media with 10% FBS	700 nm	0.313

N.B. All samples contained 1% (v/v) DMSO.

PDI = Polydispersity Index. FBS = Fetal Bovine Serum

2.3.2 RTCA Method Development

Figure 2.2 illustrates a set of typical results obtained using the 96x-RTCA method with CHO-K1 cells exposed to nTiO₂ as an example. Figure 2.2A presents a real-time sensing profile representing the dynamic changes in CI (normalized at the time of cell treatment) for each concentration of nTiO₂. At any given time point, as the nTiO₂ concentration increases, the normalized CI decreases, demonstrating a concentration-dependent cytotoxic effect on CHO-K1 cells. To quantitatively present this concentration-response effect, IC₅₀ values were determined at each time point over the entire exposure period to generate a temporal IC₅₀ histogram (Figure 2.2B). Dynamic changes in the IC₅₀ values over time are clearly observed. During the first 12 h of exposure, the IC₅₀ values for nTiO₂ remain relatively high (IC₅₀ > 200 µg mL⁻¹) and are clearly outside of the tested concentration range. Although estimated, these values are included to show the trend of IC₅₀ values as the cells grow. We determined the cell doubling time of CHO-K1 cells to be 12.8±0.8 h. Therefore, the initial 12 h of exposure is within the first generation of CHO-K1 cells and the cells would likely generate limited responses during this period. The IC₅₀ values then decrease rapidly from 12-24 h, reaching a plateau for the remainder of the exposure period. This is where the maximal cytotoxicity (lowest IC₅₀ value) is observed. Hence, temporal IC₅₀ histograms can provide quantitative “fingerprinting” of dynamic changes in cell responses during exposure. This is an obvious advantage over traditional assays.

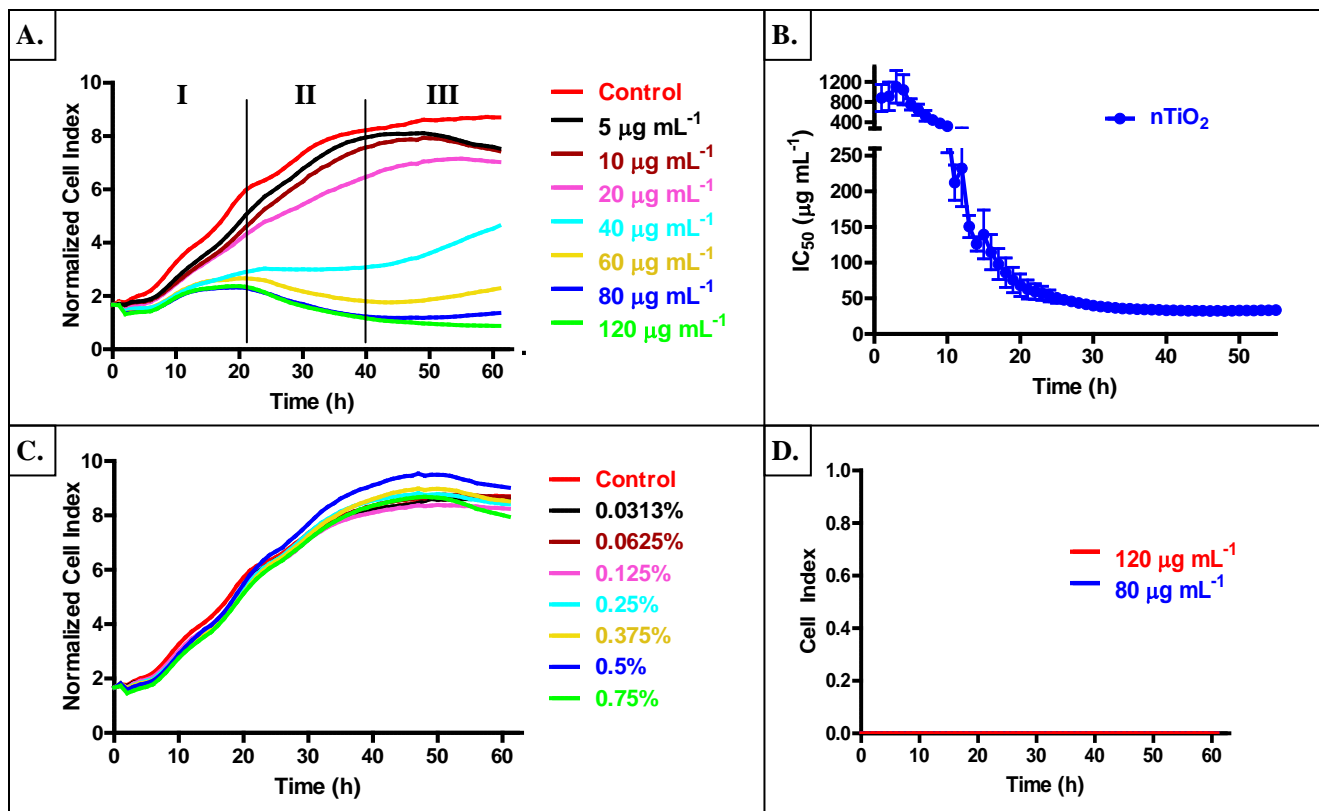


Figure 2.2: Determination of nTiO₂ cytotoxicity in CHO-K1 cells using RTCA: A) RTCA sensing profile of the normalized cell index (CI) over time for CHO-K1 cells exposed to nTiO₂; B) Temporal IC₅₀ histogram of the IC₅₀ values determined at each hour over the exposure period; C) RTCA sensing profile of CHO-K1 cells exposed to the solvent control, DMSO; D) RTCA sensing profile of nTiO₂ suspensions in culture media without CHO-K1 cells present.

In addition to quantitative IC_{50} values, the RTCA real-time sensing profiles can provide qualitative information about dynamic cell responses to $nTiO_2$. For example, during the first approximately 20 h of CHO-K1 treatment with $nTiO_2$, the cytotoxic effects appear to be delayed (Figure 2.2A, Section I). During this section of the exposure period, the normalized CI values of all concentrations of $nTiO_2$ continue to increase, albeit at different rates. However, after 20 h exposure (Figure 2.2A, section II), the normalized CI values begin to diverge, depending on the concentrations of $nTiO_2$. The cells treated with the higher $nTiO_2$ concentrations (60, 80, and $120 \mu\text{g mL}^{-1}$) have decreasing normalized CI values over time, while the cells treated with the lower concentrations (5, 10, and $20 \mu\text{g mL}^{-1}$) have increasing normalized CI values or normalized CI values that plateau ($40 \mu\text{g mL}^{-1}$) (Figure 2.2A, Section II). This pattern of delayed cytotoxicity is likely due to the fact that TiO_2 nanoparticles do not produce toxic metal ions in solution [36], and so may require uptake into the cell prior to initiating the observed cytotoxic response. Thus, the time period in Section I of Figure 2.2A likely reflects the period of time needed for the $nTiO_2$ to enter the cells through various endocytic pathways, which is consistent with previous observations [37, 38].

The plateau in normalized CI observed for the $40 \mu\text{g mL}^{-1}$ $nTiO_2$ concentration indicates a possible cytostatic response of the CHO-K1 cells (Figure 2.2A, Section II). A possible explanation of this effect may be the induction of cell cycle arrest by $nTiO_2$. To confirm this, we performed cell cycle analysis of CHO-K1 cells treated with $40 \mu\text{g mL}^{-1}$ $nTiO_2$ for 24 h. Cell cycle

analysis using flow cytometry showed a statistically significant increase ($p < 0.01$) in the number of cells in S-phase along with a statistically significant decrease ($p < 0.05$) in the number of cells in the G2/M-phase in comparison to control cells without nanoparticle treatment (Figure 2.3). This suggests that nTiO₂ induces S-phase cell cycle arrest in CHO-K1 cells, a non-carcinogenic mammalian cell line. Our cell cycle arrest findings correspond with those of Wang and colleagues that nano-titanium dioxide caused cell cycle arrest in human lymphoblastoid cells, although they did not determine which phase was arrested [39]. These results also correspond with those of Xia and colleagues, who reported that chemicals with different mechanisms of cytotoxicity produce distinct kinetic profiles in the RTCA system [15]. Our results and those of Xia and colleagues suggest that RTCA profiles may provide evidence for generating rational hypotheses to direct further investigation of cytotoxicity mechanisms of chemicals and nanoparticles [15]. This technique can be a powerful tool to generate useful information as part of comprehensive screening projects for the environmental and human health risk assessment of nanomaterials.

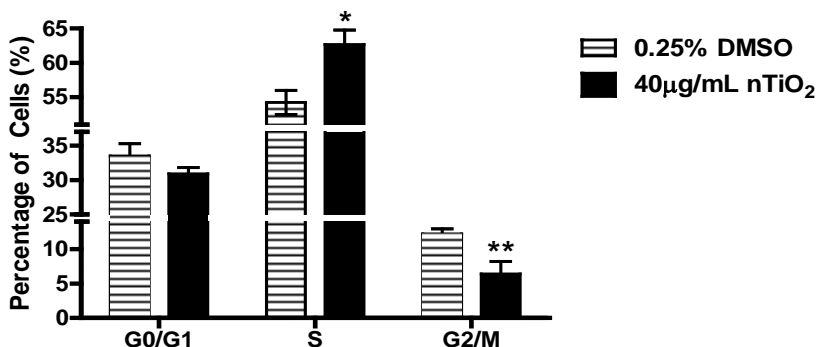


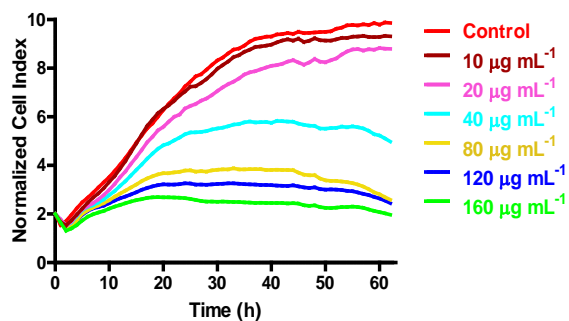
Figure 2.3: Percentage of CHO-K1 cells in each phase of the cell cycle after 24 h exposure to 40 µg mL⁻¹ nTiO₂. Statistical analysis was performed using a two-tailed Mann-Whitney test with 95% confidence (* $p < 0.01$, ** $p < 0.05$). Values are the mean ± SEM (n=9).

A set of controls were included in each experiment performed to support that the observed cytotoxic effects were nanoparticle-mediated. Because DMSO was used to disperse the nanoparticles in cell culture media, DMSO controls were included in each RTCA run. Figure 2.2C shows a typical RTCA sensing profile of CHO-K1 cells exposed to 0.031% to 0.75% (v/v) DMSO in cell culture media. The color of each DMSO concentration profile corresponds with the same color profile in Figure 2.2A, representing the concentration of nTiO₂ and DMSO used. No statistically significant cytotoxic effects were observed for any DMSO concentration, as was confirmed by comparing the normalized CI values of the solvent control cells and untreated control cells at 24 h and 48 h exposure using a one-way ANOVA with a Dunnett's post-test. Interactions between the particles and the microelectrodes (in the absence of cells) were also investigated (Figure 2.2D). Analysis of the two highest nTiO₂ concentrations did not generate a signal, as the CI readings of these wells remained at 0 throughout the exposure period. This confirms that nTiO₂ and DMSO do not interfere with RTCA measurements, and the effects observed in Figure 2.2A are indeed nanoparticle-mediated.

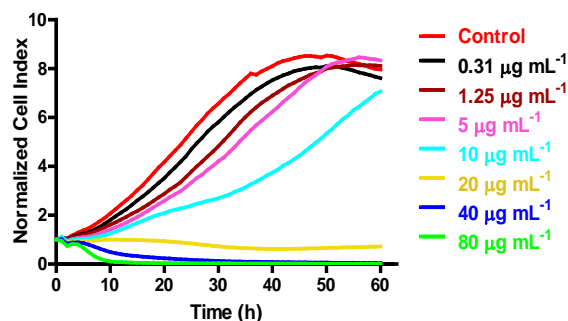
2.3.3 RTCA Screening of nTiO₂ and nAg on Three Cell Lines

Having demonstrated the application of our 96x-RTCA method toward the understanding of nTiO₂-mediated cytotoxicity in CHO-K1 cells, we expanded the method to include an additional nanoparticle (nAg) and two more cell lines (A549 and SK-MES-1). Figure 2.4 shows typical RTCA sensing profiles of nTiO₂ and nAg in all three cell lines. The profiles clearly show both nanoparticle-dependent and cell-dependent cytotoxicity.

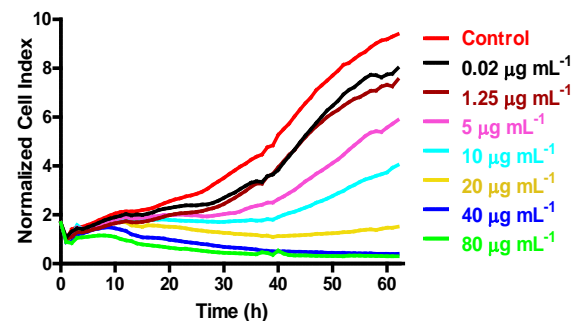
A. nAg on A549



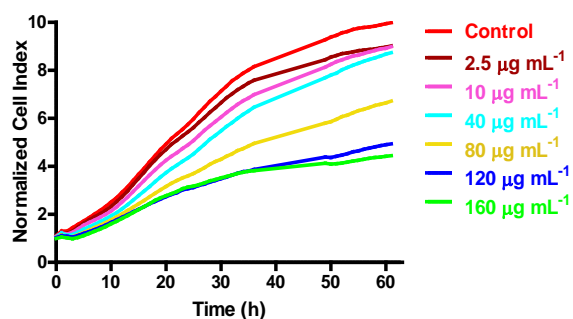
B. nAg on CHO-K1



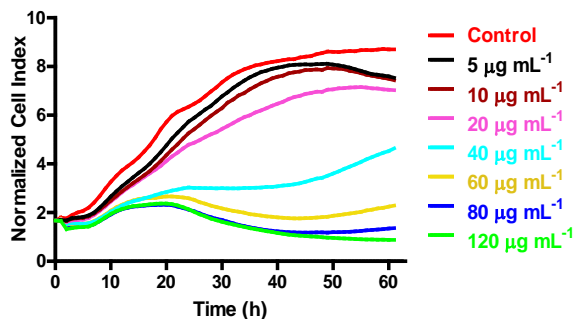
C. nAg on SK-MES-1



D. nTiO₂ on A549



E. nTiO₂ on CHO-K1



F. nTiO₂ on SK-MES-1

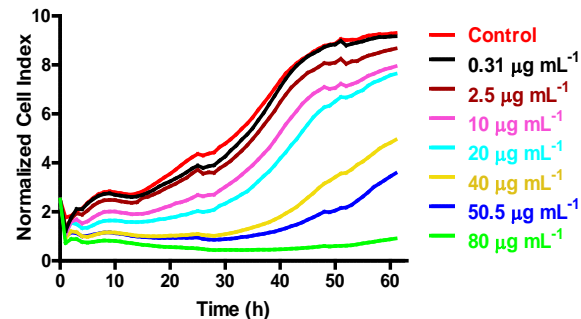


Figure 2.4: RTCA sensing profiles of nAg in A) A549 (x2), B) CHO-K1 (x1), and C) SK-MES-1 (x1.43) cells and nTiO₂ in D) A549 (x1.25), E) CHO-K1 (x1.67), and F) SK-MES-1 (x2.5). The cell index (CI) scales were normalized using the corresponding multiplication factor (in parentheses) to allow for easier visual analysis.

To quantitatively illustrate these relationships, we calculated the IC_{50} values over the exposure period for each nanoparticle on each cell line (Figure 2.5). Figure 2.5 clearly shows cell-dependent cytotoxicity for both nanoparticles. At all time points, Figures 2.5A and 2.5B show that the IC_{50} values for nAg are lower than those for nTiO₂ in both the CHO-K1 and A549 cell lines, indicating nAg is more cytotoxic than nTiO₂ to these two cell lines. This is consistent with previous studies, where lower IC_{50} values were reported for nAg than nTiO₂ in the A549 cell line [40], the murine alveolar macrophage cell lines RAW 267.9 [41] and RAW 267.4 [40], the human alveolar macrophage cell line THB-1 [40], and the rat liver cell line BRL3A [42]. Interestingly, Figure 2.5C shows that SK-MES-1 cells have a similar sensitivity to exposure to both nAg and nTiO₂, particularly during the first 30 h exposure. The IC_{50} values for SK-MES-1 cells exposed to nTiO₂ then begin to increase over time after 30 h exposure (Figure 2.5C), indicating that SK-MES-1 cells may be able to recover from the stress of nTiO₂ exposure compared to A549 and CHO-K1 cells. The recovery of SK-MES-1 cells exposed to nTiO₂ may be explained by the cell doubling times we determined for each cell line. During the first 1-30 h exposure, the cell doubling time for SK-MES-1 cells was 19.6 ± 2.4 h, while the doubling times for A549 and CHO-K1 cells were determined to be nearly twice as fast at 11.7 ± 0.6 h and 12.8 ± 0.8 h, respectively. However, for the exposure period from 31-50 h, while the doubling time for SK-MES-1 cells remained the same at 18.6 ± 1.6 h, the doubling times for A549 and CHO-K1 were dramatically reduced to 46.5 ± 3.8 h and 52.2 ± 2.7 h, respectively. While the SK-MES-1 cells are still in their

logarithmic growth phase after 30 h exposure, the A549 and CHO-K1 cells appear to be exiting their logarithmic growth phase and may not be able to recover from the exposure.

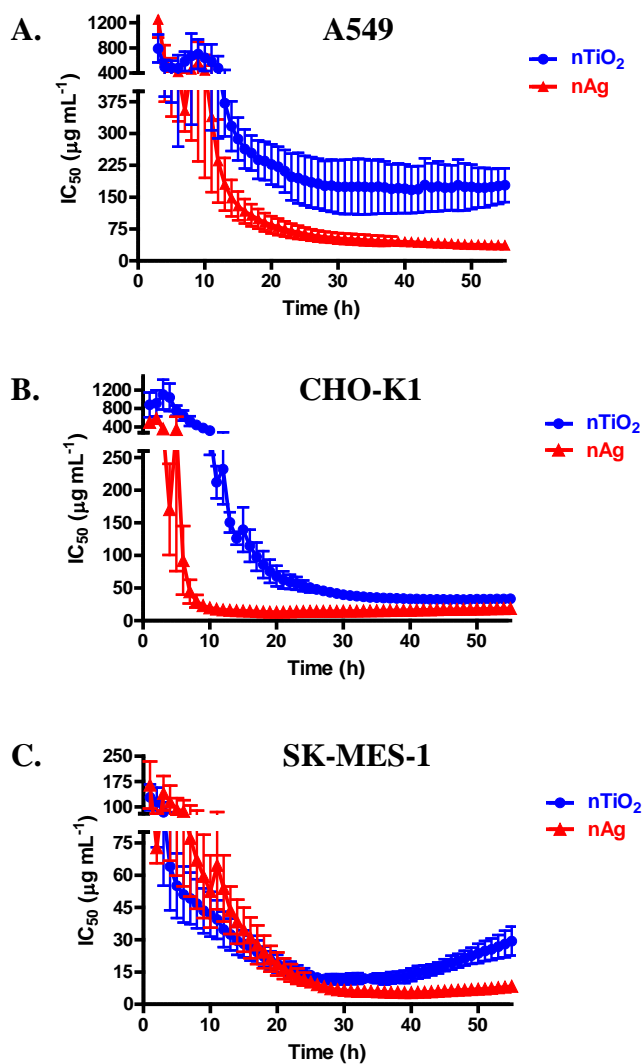


Figure 2.5: Temporal IC_{50} histograms for nAg and nTiO₂ in A) A549, B) CHO-K1, and C) SK-MES-1 cells. Values are the mean \pm SEM (n=3).

We also observed that SK-MES-1 cells are more sensitive to both nAg and nTiO₂ than A549 cells, as supported by the IC_{50} values we determined for each cell line. The results in Figure 2.5 demonstrate that our 96x-RTCA method can

sensitively differentiate cell-dependent responses, even amongst cell lines (A549 and SK-MES-1) derived from carcinomas of the same organ. This has implications for the safe use of nTiO₂ in different applications, as we have observed that different human lung cell lines can have different sensitivities to the same nanomaterials. In addition, the greater sensitivity of the SK-MES-1 cell line to nanoparticles may serve as a more sensitive model for screening nanomaterial cytotoxicity.

The establishment of concentration-, time-, particle-, and cell-dependent relationships using a single platform demonstrates the screening potential of RTCA toward the cytotoxicity evaluation of emerging nanomaterials. The identification of these relationships facilitates the determination of which nanomaterials pose the greater human health hazard and should be prioritized for further toxicological testing, particularly in *in vivo* systems.

2.3.4 IC₅₀ Validation using the Neutral Red Uptake (NRU) Assay

To validate the IC₅₀ values determined using our 96x-RTCA method, we also determined IC₅₀ values of nTiO₂ and nAg using the neutral red uptake (NRU) assay, as the NRU assay is one of the recommended assays by the National Institutes of Health (NIH) and the National Institute of Environmental Health Sciences (NIEHS) for determining the basal cytotoxicity of substances with unknown toxicity when used with the NIH:3T3 cell line [43]. The NRU assay has also been shown to achieve good correlation with IC₅₀ values determined using RTCA in chemical cytotoxicity studies [12, 13]. Table 2.2 presents the IC₅₀ values of nAg and nTiO₂ determined using both assays for the

three cell lines at 24 h and 48 h exposure. At the same time points, the IC₅₀ values of nAg obtained using the RTCA method were not statistically different from those obtained using the NRU assay, as determined using a two-tailed t-test with 95% confidence. The 24 h IC₅₀ value for nAg in the A549 cell line determined by RTCA ($67 \pm 16 \mu\text{g mL}^{-1}$ in Table 2.2) is also in agreement with a reported value of $106 \mu\text{g mL}^{-1}$ determined using a formazan dye assay with a similarly-sized silver nanoparticle [44].

Table 2.2: IC₅₀ Values at 24 h and 48 h Post-exposure Determined Using the RTCA and NRU Assays for nAg and nTiO₂ in Three Cell Lines

Cell line		nAg		nTiO ₂	
		RTCA*	NRU*	RTCA	NRU
A549	24 h	67 ± 16	67 ± 18	195 ± 60	AI
	48 h	39 ± 10	30 ± 7	179 ± 60	AI
CHO-K1	24 h	14 ± 5	5 ± 1	53 ± 8	AI
	48 h	18 ± 3	9 ± 2	32 ± 1	AI
SK-MES-1	24 h	12 ± 3	17 ± 2	15 ± 2	AI
	48 h	7 ± 1	10 ± 1	21 ± 3	AI

Values are the mean \pm SEM in $\mu\text{g mL}^{-1}$ (n=3)

* = values not statistically different (two-tailed t-test with 95% confidence)

AI = assay interference

This 96x-RTCA method easily determined IC₅₀ values for the three cell lines exposed to nTiO₂ at a given time (Figure 2.5). The NRU assay, however, could not determine IC₅₀ values for nTiO₂ (Table 2.2) because of interference with the absorbance measurements. We observed that suspensions of nTiO₂ in lysis buffer in the absence of cells had strong absorbance at 540 nm, regardless of whether neutral red dye was present or not (data not shown). Interference of nanoparticles with traditional dye-based assays is often observed. Studies have

reported interference caused by aluminum nanoparticles [7] and starch-coated silver nanoparticles [10]. Single-walled carbon nanotubes have been shown to interfere with the dyes requisite to the MTT, NRU, adenylate kinase (AK) release, and interleukin-8 (IL-8) measurement assays [8, 9]. These results further demonstrate the advantages of our 96x-RTCA method over traditional colorimetric assays in the examination of nanoparticle-mediated cytotoxicity.

2.4 Conclusions

This study has developed and demonstrated the application of a 96x-RTCA method for testing of nanoparticles on three cell lines, showing the promise of this technique for implementation in high-throughput screening of nanoparticle-mediated cytotoxicity. Real-time analysis provided multiple data showing concentration-, time-, particle-, and cell-dependent nanoparticle-mediated cytotoxicity, as represented qualitatively with RTCA sensing profiles and quantitatively with temporal IC_{50} histograms. The dynamic results differentiate the particle-dependent and cell-dependent sensitivity of nAg and nTiO₂. In the present study, the results clearly show that the CHO-K1 cell line is less sensitive to nTiO₂ than the SK-MES-1 cell line, but there is little difference in the sensitivity of the two cell lines to nAg. The A549 cell line was the least sensitive to either nanoparticle. The cytostatic response visible in the RTCA sensing profile of CHO-K1 cells was correlated with the effect of nTiO₂ on the cell cycle: nTiO₂-induced cell cycle arrest at S-phase in CHO-K1 cells. This indicates that RTCA profiles can reveal different cellular responses, directing further studies into mode of action of a nanoparticle using other cell biology tools.

The 96x-RTCA method does not suffer inferences from nTiO₂ and can determine IC₅₀ values for this nanoparticle, whereas the traditional NRU assay cannot measure these values due to severe interference from these nanoparticles. This is a unique advantage of RTCA over colorimetric assays. Although this study used a panel of three cell lines using nAg and nTiO₂ as examples, the method can be used for different adherent cell lines and other nanomaterials. This technique will be useful as a screening tool for initial assessment of the potential cytotoxic effects of nanomaterials to direct further toxicological testing.

2.5 References

- [1] Woodrow Wilson International Center for Scholars, Project on Emerging Nanotechnologies, Consumer Product Inventory, www.nanotechproject.org/inventories/consumer (accessed 4.12.2012).
- [2] The Royal Society & The Royal Academy of Engineering, Nanoscience and Nanotechnologies: Opportunities and Uncertainties, London, UK, 2004.
- [3] A.D. Maynard, Nanotechnology: A Research Strategy for Addressing Risk, PEN 3, Washington, D.C., 2006.
- [4] A.D. Maynard, R.J. Aitken, T. Butz, V. Colvin, K. Donaldson, G. Oberdorster, M.A. Philbert, J. Ryan, A. Seaton, V. Stone, S.S. Tinkle, L. Tran, N.J. Walker, D.B. Warheit, *Nature* 444 (2006) 267-269.
- [5] N. Lewinski, V. Colvin, R. Drezek, *Small* 4 (2008) 26-49.
- [6] J.M. Hillegass, A. Shukla, S.A. Lathrop, M.B. MacPherson, N.K. Fukagawa, B.T. Mossman, *Wiley Interdisc. Rev. Nanomed. Nanobiotech.* 2 (2010) 219-231.
- [7] L. Braydich-Stolle, S. Hussain, J.J. Schlager, M.C. Hofmann, *Toxicol. Sci.* 88 (2005) 412-419.
- [8] J.M. Worle-Knirsch, K. Pulskamp, H.F. Krug, *Nano Lett.* 6 (2006) 1261-1268.
- [9] M. Davoren, E. Herzog, A. Casey, B. Cottineau, G. Chambers, H.J. Byrne, F.M. Lyng, *Toxicol. In Vitro* 21 (2007) 438-448.
- [10] P.V. AshaRani, G. Low Kah Mun, M.P. Hande, S. Valiyaveetil, *ACS Nano* 3 (2009) 279-290.
- [11] N.A. Monteiro-Riviere, A.O. Inman, L.W. Zhang, *Toxicol. Appl. Pharmacol.* 234 (2009) 222-235.
- [12] J.Z. Xing, L. Zhu, J.A. Jackson, S. Gabos, X.J. Sun, X.B. Wang, X. Xu, *Chem. Res. Toxicol.* 18 (2005) 154-161.
- [13] J.Z. Xing, L. Zhu, S. Gabos, L. Xie, *Toxicol. In Vitro* 20 (2006) 995-1004.
- [14] J.M. Boyd, L. Huang, L. Xie, B. Moe, S. Gabos, X.F. Li, *Anal. Chim. Acta* 615 (2008) 80-87.
- [15] M. Xia, R. Huang, K.L. Witt, N. Southall, J. Fostel, M.H. Cho, A. Jadhav, C.S. Smith, J. Inglese, C.J. Portier, R.R. Tice, C.P. Austin, *Environ. Health Perspect.* 116 (2008) 284-291.

- [16] R.S. Judson, K.A. Houck, R.J. Kavlock, T.B. Knudsen, M.T. Martin, H.M. Mortensen, D.M. Reif, D.M. Rotroff, I. Shah, A.M. Richard, D.J. Dix, *Environ. Health Perspect.*, 118 (2010) 485-492.
- [17] K.T. Butterworth, J.A. Coulter, S. Jain, J. Forker, S.J. McMahon, G. Schettino, K.M. Prise, F.J. Currell, D.G. Hirst, *Nanotechnology* 21 (2010) 295101.
- [18] D. Guo, C. Wu, J. Li, A. Guo, Q. Li, H. Jiang, B. Chen, X. Wang, *Nanoscale Res. Lett.* 4 (2009) 1395-1402.
- [19] J. Li, D. Guo, X. Wang, H. Wang, H. Jiang, B. Chen, *Nanoscale Res. Lett.* 5 (2010) 1063-1071.
- [20] H. Yang, Q. Wu, M. Tang, X. Liu, H. Deng, L. Kong, Z. Lu, *J. Nanosci. Nanotechnol.* 10 (2010) 561-568.
- [21] Q. Mu, S. Zhai, B. Yan, *Methods Mol. Biol.* 625 (2010) 85-94.
- [22] C. Wu, L. Shi, Q. Li, H. Jiang, M. Selke, L. Ba, X. Wang, *Chem. Res. Toxicol.* 23 (2010) 82-88.
- [23] R.I. Freshney, *Culture of Animal Cells: a Manual of Basic Technique and Specialized Applications*, Sixth Edition, Wiley-Blackwell, Hoboken, 2010.
- [24] K. Solly, X. Wang, X. Xu, B. Strulovici, W. Zheng, *Assay Drug Dev. Technol.* 2 (2004) 363-372.
- [25] R. Limame, A. Wouters, B. Pauwels, E. Franssen, M. Peeters, F. Lardon, O. De Wever, P. Pauwels, *PLoS ONE* 7 (2012) e46536.
- [26] G. Repetto, A. del Peso, J.L. Zurita, *Nat. Protoc.* 3 (2008) 1125-1131.
- [27] D.B. Warheit, *Toxicol. Sci.* 101 (2008) 183-185.
- [28] L. Wu, J.C. Yu, X. Wang, L. Zhang, J. Yu, *J. Solid State Chem.* 178 (2005) 321-328.
- [29] V.H. Grassian, A. Adamcakova-Dodd, J.M. Pettibone, P.T. O'Shaughnessy, P.S. Thorne, *Nanotoxicology* 1 (2007) 211-226.
- [30] V.H. Grassian, P.T. O'Shaughnessy, A. Adamcakova-Dodd, J.M. Pettibone, P.S. Thorne, *Environ. Health Perspect.* 115 (2007) 397-402.

- [31] J.F. Moulder, J. Chastain, R.C. King, Handbook of X-ray Photoelectron Spectroscopy: A Reference Book of Standard Spectra for Identification and Interpretation of XPS Data, Physical Electronics, Eden Prairie, MN, 1995.
- [32] M.F. Al-Kuhaili, J. Phys. D: Appl. Phys. 40 (2007) 2847-2853.
- [33] H. Kato, in: S.C. Singh, H. Zeng, C. Guo, W. Cai (Eds.), Nanomaterials: Processing and Characterization with Lasers, Wiley-VCH Verlag GmbH & Co. KGaA, 2012, p. 535-554.
- [34] P. Bihari, M. Vippola, S. Schultes, M. Praetner, A.G. Khandoga, C.A. Reichel, C. Coester, T. Tuomi, M. Rehberg, F. Krombach, Part. Fibre Toxicol. 5 (2008) 14.
- [35] R.C. Murdock, L. Braydich-Stolle, A.M. Schrand, J.J. Schlager, S.M. Hussain, Toxicol. Sci. 101 (2008) 239-253.
- [36] A. Yamamoto, R. Honma, M. Sumita, T. Hanawa, J. Biomed. Mater. Res. A. 68 (2004) 244-256.
- [37] S. Singh, T. Shi, R. Duffin, C. Albrecht, D. van Berlo, D. Hohr, B. Fubini, G. Martra, I. Fenoglio, P.J. Borm, R.P. Schins, Toxicol. Appl. Pharmacol. 222 (2007) 141-151.
- [38] K.T. Thurn, H. Arora, T. Paunesku, A. Wu, E.M. Brown, C. Doty, J. Kremer, G. Woloschak, Nanomedicine 7 (2011) 123-130.
- [39] J.J. Wang, B.J.S. Sanderson, H. Wang, Mutat. Res. Gen. Toxicol. Environ. Mutagen. 628 (2007) 99-106.
- [40] K. Soto, K.M. Garza, L.E. Murr, Acta Biomater. 3 (2007) 351-358.
- [41] K.F. Soto, A. Carrasco, T.G. Powell, K.M. Garza, L.E. Murr, J. Nanopart. Res. 7 (2005) 145-169.
- [42] S.M. Hussain, K.L. Hess, J.M. Gearhart, K.T. Geiss, J.J. Schlager, Toxicol. In Vitro 19 (2005) 975-983.
- [43] National Institute of Environmental Health Sciences, National Institutes of Health, US Public Health Service, Department of Health and Human Services, NIH Publication 01-4500, 2001.
- [44] Y.S. Lee, D.W. Kim, Y.H. Lee, J.H. Oh, S. Yoon, M.S. Choi, S.K. Lee, J.W. Kim, K. Lee, C.W. Song, Arch. Toxicol. (2011) 1529-1540.

Chapter 3: Application of Developed RTCA Method for Environmental Air Quality Monitoring*

3.1 Introduction

While humans may be able to survive days without food or water, most humans would survive no longer than a few minutes without air. The average person breathes around 11 m³ of air each day, or about 115 L every 15 min [1]. Thus, the inhalation pathway has historically played an important role in the uptake of chemical and physical environmental contaminants, and the need to monitor potential human health hazards in air has become an important issue in environmental toxicity monitoring. Traditionally, the assessment of environmental air pollution has been done via two complementary approaches: 1) physicochemical analysis and 2) bioassay-based analysis [2].

Physicochemical analysis is often based on extensive analytical testing using a suite of analytical techniques that can sensitively and accurately identify the specific components within an environmentally-sampled air sample (mixture) to determine potential human health hazards. Not only is this process necessary for regulatory compliance monitoring, but it is also useful for providing information needed to establish environmental remediation measures. While it has demonstrated advantages, physicochemical analyses are often tedious, expensive, and inefficient. This inefficiency is highlighted when it comes to identifying the human health hazards associated with exposure to the mixture, as it produces little information on the bioavailability of the sample or the toxicity of the whole

* A version of this chapter has been accepted for publication. Moe et al. July 15, 2013. *Encyclopedia of Analytical Chemistry*.

sample due to the focus on the component parts. Therefore, the complementary approach of bioassay-based analysis is important for overcoming these limitations [2]. Using a bioassay, such as real-time cell analysis (RTCA), allows for the analysis of the toxicity of the sample as a whole, gaining a better understanding of any potential toxic effects of any components in the sample. Furthermore, it also allows for the evaluation of the bioavailable fraction of the sample, which is the most important from a human health perspective for understanding the hazards associated with exposure to particulate matter (PM).

Concerns over the human health and environmental impacts of PM have long been recognized. As such, PM has been under surveillance and/or regulation in the US and Canada for over 40 years [3, 4]. PM₁₀ and PM_{2.5} are the two size fractions of particulates currently regulated in North America (Table 3.1). The coarse fraction, PM₁₀, is defined as particles with an aerodynamic diameter between 2.5 and 10 μm , and corresponds to the fraction that penetrates beyond the larynx into the thoracic region [5, 6]. The fine fraction, PM_{2.5}, consists of particles with an aerodynamic diameter of 2.5 μm or less, and corresponds to the fraction that can penetrate the unciliated airways of the alveolar region [5, 6]. Hence, the regulatory distinction between the two classes is significant because PM_{2.5} poses the greater human health hazard due to its ability to penetrate the gas-exchange region of the lungs. This distinction is further supported by epidemiological studies [7-9]. A third fraction of particulates that is relevant from a human health perspective is PM_{0.1}, which is defined as particulates less than 0.1 μm (100 nm) in size, termed ultrafine particles (or nanoparticles). While they

are not regulated as a separate class (but are regulated within PM_{2.5}), ultrafine particles have been demonstrated to have high biological activity [10]. In rodent models, these particles are capable of not only penetrating the gas-exchange region of the lungs and entering the cardiovascular system, but they were also shown to enter directly into the brain by trans-synaptic transport after inhalation [11]. Thus, with increasing use and release of engineered nanomaterials into the environment, environmental toxicity monitoring of ultrafine particles (PM_{0.1}) is an important task in the near future for the protection of human health.

Table 3.1: Ambient Air Quality Standards for PM in North America

		Annual ^a	24 h ^b	Reference	
<u>Existing Standards</u>					
United States					
	<i>NAAQS</i>	PM₁₀	-	150 µg m ⁻³ *	[12]
		PM_{2.5}	12 µg m ⁻³	35 µg m ⁻³	
Canada					
	<i>CWS</i>	PM_{2.5}	-	30 µg m ⁻³	[13]
<u>Proposed Standards</u>					
Canada					
	<i>CAAQS for 2015</i>	PM_{2.5}	10 µg m ⁻³	28 µg m ⁻³	[14]
	<i>CAAQS for 2020</i>	PM_{2.5}	8.8 µg m ⁻³	27 µg m ⁻³	[14]
NAAQS = National Ambient Air Quality Standard; CWS = Canada-wide Standard; CAAQS=Canadian Ambient Air Quality Standard					
a = Annual average concentration, averaged over three years; b = Annual 98th percentile of the daily 24 h average concentrations, averaged over three years (for PM _{2.5}); * = Not to be exceeded more than once per year, averaged over three years					

Several studies have investigated the use of cell-based biosensors (CBBs) that rely on impedance detection for use in bioassay-based analysis of environmental particulate samples, demonstrating the usefulness of these

techniques for analysis of environmental particulates. In Huang et al., the 16-x RTCA system was used to screen and rank the cytotoxicity of four different particulate standard reference materials (SRMs), including two quartz SRMs (Q66 and Q70), a SRM for urban dust (SRM 1649a), and a SRM for diesel exhaust particles (DEP) (SRM 2975) (2008) [15]. Likewise, Chen et al. used the 96-x RTCA system to rank the cytotoxicity of cigarette smoke condensate (CSC) collected from five different cigarettes in a single cell line (2012) [16]. CSC is the particulate fraction of cigarette smoke, and is a highly complex mixture consisting of nicotine, tar, PAHs, and numerous other chemicals. While these studies demonstrated the efficacy of RTCA platforms as tools for toxicity ranking of environmentally-relevant particulates, they did not demonstrate the ability of the platform for use in cytotoxicity screening of particulate samples collected directly from the environment (environmentally-sampled particulates). The examination of environmentally-sampled PM has been demonstrated in two studies from Wang et al., who examined the cytotoxicity of PM collected from the Ft. McHenry Tunnel (Baltimore, MD) on a human pulmonary artery endothelial cell line using an electrical cell-substrate impedance sensing (ECIS) platform [17, 18]. Although these two studies demonstrated the use of impedance-based CBBs for cytotoxicity analysis of environmentally-sampled PM, the authors here only used the ECIS system to look specifically at the effects of the single PM sample to transendothelial electrical resistance (TER), not as a cytotoxicity ranking tool. Hence, this chapter will demonstrate the use of our 96-x RTCA method developed

in Chapter 2 for use as a cytotoxicity ranking tool for PM sampled directly from the environment.

To develop our 96x-RTCA method to quantitatively and qualitatively assess the cytotoxicity of environmentally-sampled particulates, we screened two different samples of PM: 1) size-fractionated coal fly ash (CFA) and 2) air particulates extracted from PM_{2.5} air quality monitoring filters. Because the lungs are a target organ for PM toxicity, we chose the two human lung carcinoma cell lines, A549 and SK-MES-1, as sensing probes. These two cell lines demonstrated adequate sensitivity to particle exposure with low experimental variability, as determined using our 96x-RTCA method developed in Chapter 2. This study will expand the method developed in Chapter 2 to further demonstrate its potential application to air quality monitoring. I will use this method to demonstrate the determination of concentration-, time-, particle-, and cell-dependent toxicological relationships for comprehensive cytotoxicity screening and prioritization of PM for *in vivo* and mechanistic toxicological studies.

3.2 Materials and Methods

3.2.1 Cell Culture Conditions

The A549 (CCL-185; American Type Culture Collection (ATCC), Manassas, VA) and SK-MES-1 (HTB-58; ATCC) cell lines were cultured in RPMI 1640 media (Gibco (Invitrogen), Burlington, ON, Canada). Media was supplemented with 10% fetal bovine serum (Sigma-Aldrich, Oakville, ON, Canada) and 1% penicillin-streptomycin (Invitrogen, Burlington, ON, Canada). The incubation conditions were maintained at 37 °C, 5.5% CO₂, and 90%

humidity. During the study, the cells were sub-cultured twice weekly into standard 10 cm x 20 mm cell culture dishes (Corning Incorporated, Corning, NY) containing fresh media, using 0.05% trypsin-EDTA (Invitrogen) for cell detachment.

3.2.2 Particulate Matter (PM) Preparation

3.2.2.1 Coal Fly Ash (CFA)

Coal fly ash (CFA) that was collected from a coal burning power plant in China and size-fractionated into three different size fractions was kindly provided by Dr. Chungang Yuan of the School of Environmental Sciences and Engineering, North China Electric Power University. Particles greater than 10 μm in size were designated as PM₁₀, those between 10 μm and 2.5 μm in size as PM_{10-2.5}, and particles less than 2.5 μm were designated as PM_{2.5}. The CFA was massed and sterilized with 70% ethanol (Commercial Alcohols, Brampton, ON, Canada) using methods previously published in the literature to prevent the loss of significant amounts of the ethanol soluble fraction [19]. For every 1.5 mg of PM, 10 μL of 70% ethanol was added to each sample. Samples were then dried in a vacuum desiccator (Desi-VacTM, Fisher Scientific, Nepean, ON, Canada), allowing the ethanol soluble fraction to settle back into the sample tube.

3.2.2.2 Concentrated Air Particulates (CAPs)

PM_{2.5} teflo membrane air filters [47 mm, 2 μm] (Pall Life Sciences, Port Washington, NY) used to collect PM over a 24 h period in Essex, Ontario were kindly provided by Dr. Ewa Dabek-Zlotorzynska of the Air Quality Research Division at Environment Canada (EC). The filters were massed pre- and post-

collection by EC, and we assumed a 100% mass recovery after extraction (1056 μg). Using methods described in the literature [20, 21], the filters were cut into small pieces and placed directly into cell culture media. The filter pieces were then sonicated for 20 min in a water sonicator (Fisher Scientific, Nepean, ON, Canada) to release the PM from the filter. Post-sonication, the filter pieces were removed with forceps and the extracted particulates in media were referred to as concentrated air particulates (CAPs). The CAPs were then ready for immediate use in RTCA analysis. Blank filters, identical to the ones used for collection, were prepared in the same manner and at the same time as the sample filter and were used as the negative controls.

3.2.3 RTCA Analysis

For the RTCA experiments, cells were sub-cultured after 24 h growth and seeded into the wells of the 96-well E-plate at concentrations that had previously been calibrated to allow the cells to reach a CI of 1, indicating a confluency of 50-60%, after 18-24 h growth. A549 cells were seeded at 5000 cells well⁻¹ and SK-MES-1 at 12,500 cells well⁻¹. The day of treatment, the sterile CFA PM samples were suspended in culture media (stock). These CFA stock solutions were then placed into a water sonicator (Fisher Scientific) for 20 min to disperse the particles in the media. CFA stock solutions were then serially-diluted in cell culture media to produce a concentration range from 1 $\mu\text{g mL}^{-1}$ to 20 mg mL^{-1} .

Freshly extracted CAPs in culture media were serially-diluted to produce a treatment range of 3.13-400 $\mu\text{g mL}^{-1}$. To compare the cytotoxicity of the CAPs to well-characterized particulates, two standard reference materials (SRMs) were

selected to run concurrently with the CAPs: 1) SRM Q66 (BCR[®] certified Reference Material), quartz particles with average particle diameter of 0.35-3.5 μm (Sigma-Aldrich, Oakville, ON, Canada) and 2) SRM1649a, an urban dust standard reference material (National Institute of Standards and Technology, Gaithersburg, MD). SRM1649a was suspended in methanol prior to dilution in cell culture media resulting in a final concentration of 0.1% (v/v) methanol in media (stock). Q66 was suspended directly into cell culture media (stock). These stock solutions of SRM1649a and Q66 were then sonicated in the water sonicator for 20 min before being serially-diluted in culture media to produce a treatment range of 6.25-200 $\mu\text{g mL}^{-1}$.

Each treatment concentration of PM was added at a volume of 200 μL to triplicate wells after vortexing for 1 min. Solvent controls (for SRM1649a) and non-treated controls (cell culture media) were run concurrently with the PM-treated cells and were also added at a volume of 200 μL to triplicate wells. Another 200 μL of each treatment concentration of PM was also placed into a single well with no cells present to ensure that there was no interference of the particulates with CI measurements. After treatment, CI was measured at hourly intervals until the CI of non-treated control wells plateaued.

3.2.4 Neutral Red Uptake (NRU) Assay

To confirm our IC_{50} values determined using our RTCA method, we examined cell viability using the neutral red uptake (NRU) assay. For this assay, both cell lines were seeded, grown, and treated with one of the three CFA PM fractions under the same conditions as those described above for the RTCA

experiments. Cells were analyzed at 24 h post-exposure using a previously described protocol [22]; however, modifications to this protocol were made to correspond to the same conditions used in the RTCA assays. Namely, cells were sub-cultured from standard 10 cm x 20 mm cell culture dishes instead of flasks before seeding into 96-well cell culture plates (Corning), and cells were seeded at a volume of 150 μ L instead of 200 μ L, with the same final concentrations of cells per well as seeded into the RTCA. In addition, a dual wavelength measurement was taken instead of a single wavelength measurement, with a reference wavelength of 690 nm subtracted from the 540 nm reference wavelength, using a microplate reader (Bio-Rad, Mississauga, ON, Canada).

3.2.5 Data Analysis

Analysis of data to determine viability curves, IC_{50} values, and t-tests was performed using Prism 5.0 (Graph Pad Software Inc., San Diego, CA). IC_{50} values were defined as the concentration of PM that resulted in a 50% reduction in normalized CI as compared to the normalized CI of non-treated control cells at a given timepoint.

3.3 Results and Discussion

3.3.1 RTCA Analysis of Size-fractionated Coal Fly Ash (CFA)

CFA is a by-product of coal combustion resulting from the incomplete conversion of coal to gas during the combustion process. CFA is one of several solid byproducts that remain after combustion, which are collectively referred to as coal combustion residues (CCRs) [23]. CFA is the predominant component of CCRs formed (62%), while other significant components include flue gas

desulfurization materials (19%) and bottom ash and boiler slag (18%) (Figure 3.1) [23]. While the specific composition of CFA depends on the type of coal that is burned, the principle components of CFA are silica, alumina, ferrous oxide, and calcium oxide [24], but CFA also contains several trace elements, of which As, B, Cr, Mo, and Se are of greatest concern from an environmental perspective [25].

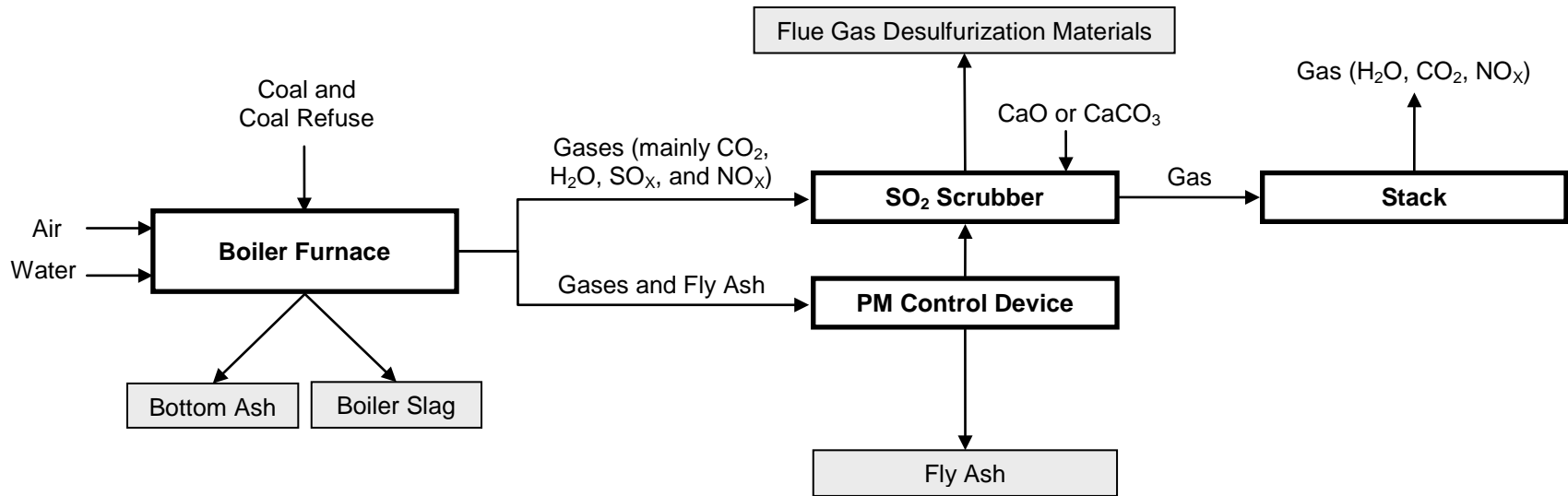


Figure 3.1: Production of coal combustion residues (CCRs) in a coal-powered plant. The CCRs are depicted in gray boxes. Adapted from the USGS Fact Sheet 076-01 (2001) [26].

Figure 3.2 shows the cytotoxicity profiles of A549 cells exposed to PM10 (Fig. 3.2A), PM10-2.5 (Fig. 3.2B), and PM2.5 (Fig. 3.2C). There is a clear dose-response in each profile, supported by the increase in normalized CI that occurs as the concentration of PM decreases. This is observed in the cells treated with each fraction of PM CFA.

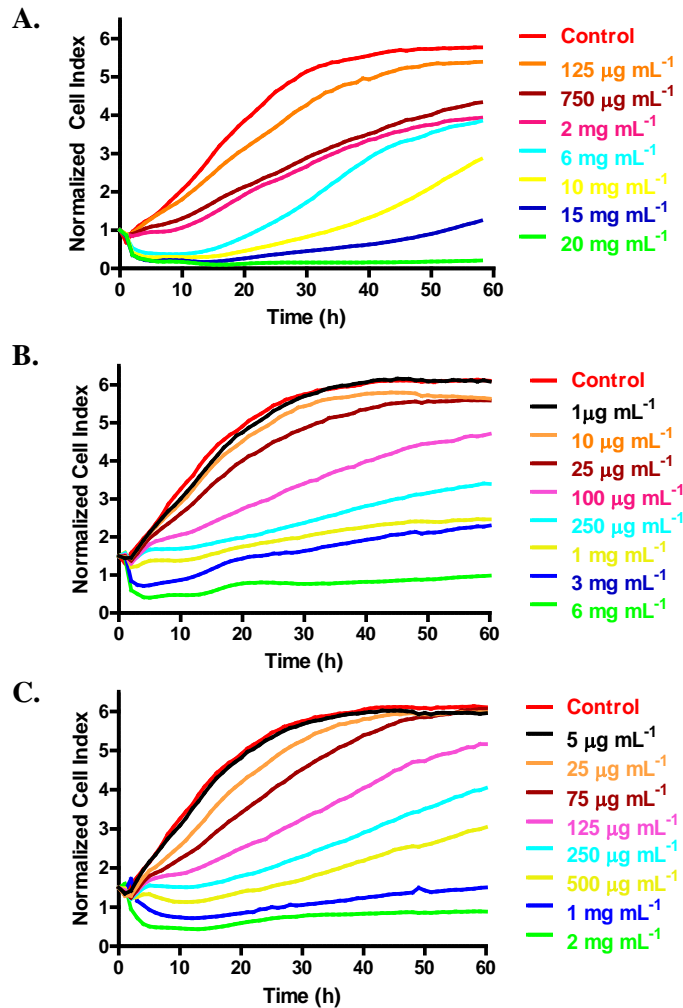


Figure 3.2: RTCA cytotoxicity profiles of the normalized cell index (CI) over time for A549 cells exposed to A) PM10, B) PM10-2.5 (x1.5), and C) PM2.5 (x1.5) coal fly ash (CFA). The CI scales were normalized using the multiplication factor (in parentheses) for easier visual analysis.

Figure 3.3 shows the RTCA cytotoxicity profiles for SK-MES-1 cells exposed to the three size fractions of CFA PM. Similar to the A549 profiles in

Figure 3.2, there is also a clear dose-response in the profiles for all three fractions of CFA PM.

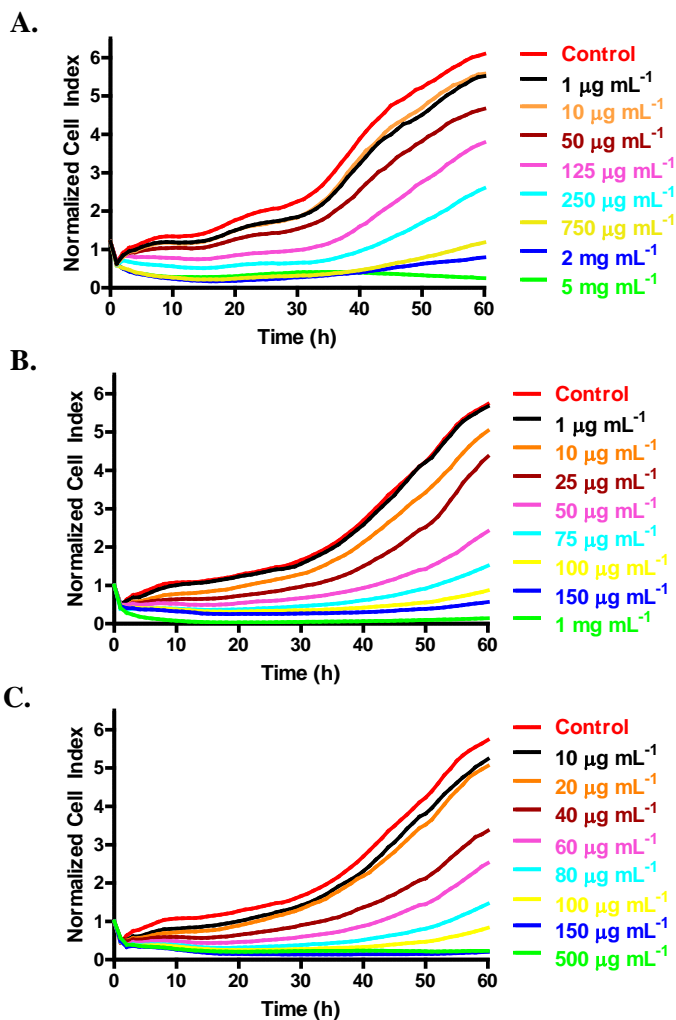


Figure 3.3: RTCA cytotoxicity profiles of the normalized cell index (CI) over time for SK-MES-1 cells exposed to A) PM₁₀ (x1.2), B) PM_{10-2.5}, and C) PM_{2.5} coal fly ash (CFA). The CI scales were normalized using the multiplication factor (in parentheses) for easier visual analysis.

To quantitatively assess the dose-response, IC₅₀ histograms were determined for both cell lines exposed to the three fractions of CFA PM. To generate these histograms, the CI values were first corrected for the minor interference of the larger concentrations of particulates (>1 mg mL⁻¹) on the electrodes. Figure 3.4 shows the interference of the particulates on the RTCA

electrodes. This interference is constant, and produces low CI readings (<0.5) throughout the exposure period in wells without cells present. The ACEA software built-in to the RTCA system calculates the normalized CI via the following equation:

$$NCI_{t_x} = \frac{CI_{t_x}}{CI_{t_N}} \quad (1)$$

where NCI_{t_x} is the normalized cell index at a given time (denoted as time t_x), CI_{t_x} is the cell index at time t_x , and CI_{t_N} is the cell index at the normalization time t_N (the time of cell treatment), all defined within a single well. To compensate for the interference of the PM on the electrodes, corrected normalized CI values were recalculated by subtracting the CI generated by the PM in the blank wells from the CI generated in the treated wells of the same PM concentration at the same time point via the following equation:

$$Corrected\ NCI_{t_x} = \frac{CI_{t_x} - Blank\ CI_{t_x}}{CI_{t_N}} \quad (2)$$

where Blank CI_{t_x} is the cell index generated by the PM in blank wells without cells present at time t_x . The corrected normalized CI values were then used to determine the IC_{50} values for each fraction of CFA PM on each cell line over the entire exposure period. To the best of our knowledge, this is the first report to demonstrate background correction can be used to reduce interference of any type of material with the RTCA system, based on a thorough search of the literature. Here I have demonstrated the means to overcome the interference to generate more accurate data by including blanks and subtracting out the background CI

readings. This can be used to reduce the background in the RTCA method for PM analysis.

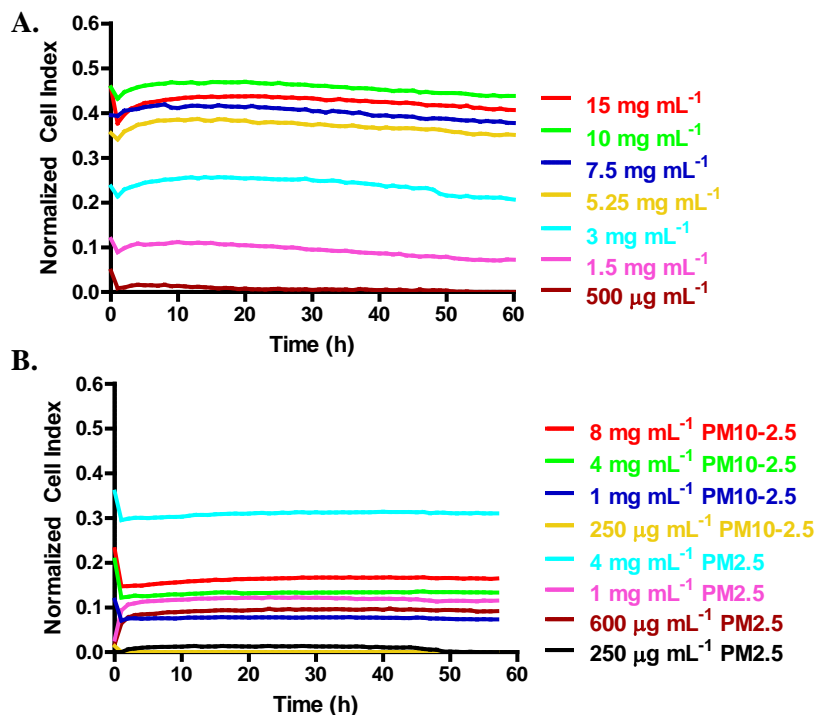


Figure 3.4: RTCA profiles of the cell index over time showing the interference of high concentrations of A) PM10 and B) PM10-2.5 and PM2.5 coal fly ash (CFA) on the RTCA electrodes in the absence of cells.

Figure 3.5 shows the IC₅₀ histograms generated using the corrected normalized CI values, calculated using Equations (1) and (2) above, for all three CFA fractions on A549 (Fig. 3.5A) and SK-MES-1 (Fig. 3.5B) cells. In each cell line, it is clear that the two smaller CFA fractions, PM10-2.5 and PM2.5, are more cytotoxic, as the IC₅₀ values are significantly lower than the IC₅₀ values for the largest fraction, PM10, on a mass per volume basis.

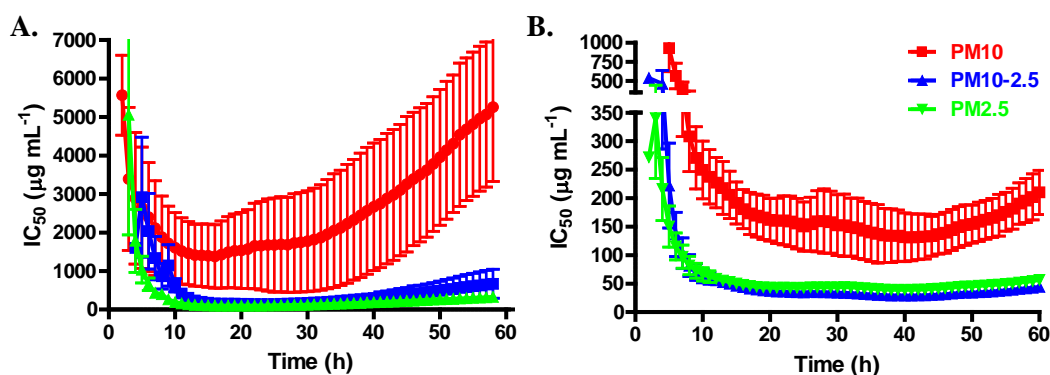


Figure 3.5: Temporal IC_{50} histograms of the hourly IC_{50} values ($\mu\text{g mL}^{-1} \pm \text{SEM}$) over the exposure period for A) A549 and B) SK-MES-1 cells exposed to the three size fractions of CFA: PM10, PM10-2.5, and PM2.5.

While the IC_{50} values for the PM10-2.5 and PM2.5 fractions are clearly lower than the values determined for the PM10 fraction, Figure 3.6 shows that the IC_{50} values for the two smaller size fractions of PM CFA in both cell lines do not appear to be significantly different. This was confirmed with a two-tailed t-test of the 24 h and 48 h IC_{50} values in each cell line. At 24 h and 48 h exposure, the IC_{50} values for these two fractions in each respective cell line were not statistically different. However, while the IC_{50} values for the two smaller fractions are not statistically different, it is interesting to compare the concentrations necessary to cause an almost complete loss in CI, as seen in the cytotoxicity profiles in Figures 3.2 and 3.3. In A549 cells, a concentration of 6 mg mL^{-1} of PM10-2.5 was needed to cause a reduction in normalized CI to less than 1, while a concentration of only 1 mg mL^{-1} of PM2.5 was needed to cause the same loss of normalized CI (Fig. 3.2). A similar trend in SK-MES-1 cells is also visible, with a complete loss of normalized CI (zero) caused by 1 mg mL^{-1} of PM10-2.5 compared to only 150 $\mu\text{g mL}^{-1}$ of PM2.5 necessary to produce the same response (Fig. 3.3). It is hypothesized that this observation is due to the number of

particles present in each treatment concentration. The three fractions of CFA are compared on a mass per volume basis, not a particle per volume basis. Hence, wells treated with 1 mg mL^{-1} PM_{2.5} would contain many more particles than a well treated with the same concentration of PM_{10-2.5}, which would in turn have more particles than wells treated with 1 mg mL^{-1} PM₁₀. Thus, it is likely that the number of particles present in each well is responsible for the observed differences in dose kinetics at the higher treatment concentrations. The smaller the size fraction of CFA, the lower the concentration needed to overwhelm the cells and their ability to maintain homeostasis.

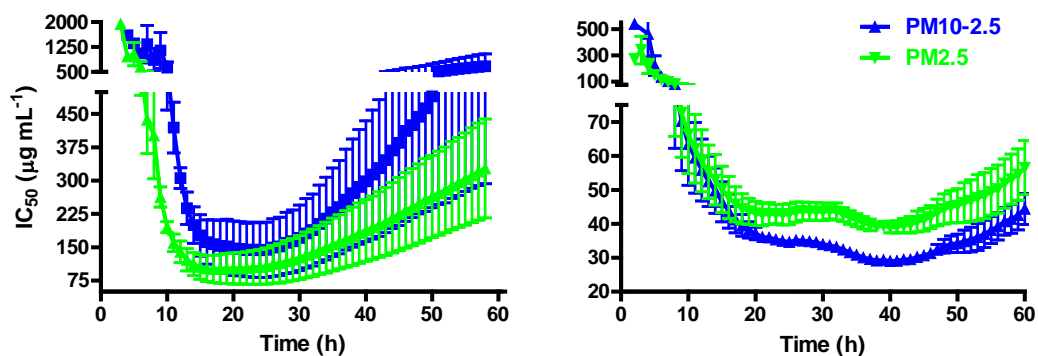


Figure 3.6: Temporal IC_{50} histograms of the hourly IC_{50} values ($\mu\text{g mL}^{-1} \pm \text{SEM}$) over the entire exposure period for A) A549 and B) SK-MES-1 cells exposed to the two smaller size fractions of CFA: PM_{10-2.5} and PM_{2.5}.

3.3.2 NRU Analysis of Size-fractionated CFA

The NRU assay was once again attempted to corroborate the IC_{50} values determined using our RTCA method, but interference of the PM with the assay made it unsuitable for IC_{50} determinations. We found that the large concentrations of CFA PM made the accurate determination of these values impossible. As the NRU assay requires the cells to be washed prior to lysing and analysis in order to

remove any extracellular neutral red dye from the wells, we found that washing could not remove all the excess PM from the wells without causing the loss of the adherent cells, particularly in wells treated with concentrations of CFA greater than 1 mg mL^{-1} . The presence of the excess PM in the wells then interfered with spectrophotometric analysis by generating false absorbance readings.

This demonstrates another benefit of our RTCA method for the cytotoxicity analysis of particulates, as no washing steps or absorbance measurements are required for analysis. While we have shown that these particulates can cause some interference with our RTCA method, we also found that this interference could easily be corrected for with proper blanks controls. This could potentially also be done with the NRU assay to subtract out the background interference, but the loss of cells due to excess washing cannot be corrected for.

3.3.3 RTCA Analysis of Filter-collected Particulate Matter

Due to the limited sample size of the PM_{2.5} air quality monitoring filters and the subsequent extracted CAPs, we chose to screen only a single cell line, SK-MES-1, as it has been shown previously to be highly sensitive to particulate exposure [15]. In addition to the CAPs, we also screened the two particulate standard reference materials, Q66 and SRM1649a, in the same experiments. Q66 is certified to contain quartz particles with an average size distribution between 0.35-3.5 μm . SRM 1649a is certified for 120 chemicals, including 44+ PAHs, 29 PCB congeners, chlorinated pesticides, and inorganic constituents. Both are well-characterized and their toxicological properties have been studied extensively.

Thus, they will serve as excellent comparisons for the cytotoxicity ranking of the CAPs. Figure 3.7 shows the RTCA cytotoxicity profiles for SK-MES-1 cells treated with CAPs (Fig. 3.7A), Q66 (Fig. 3.7B), and SRM1649a (Fig. 3.7C). There is a clear concentration-dependent response of these cells to all three types of PM.

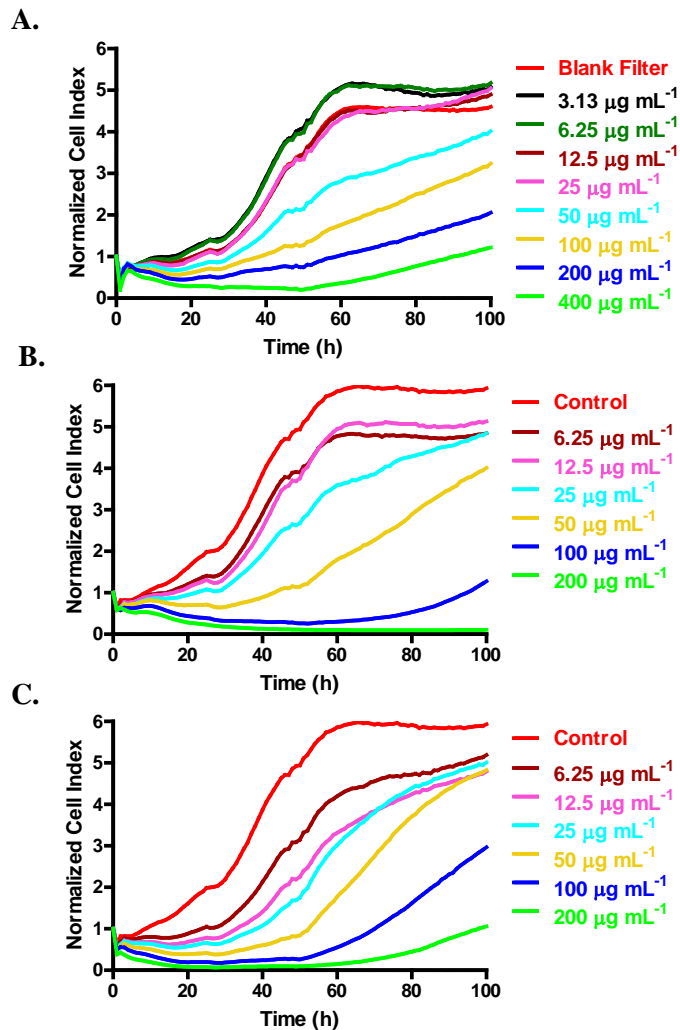


Figure 3.7: RTCA cytotoxicity profiles of the normalized cell index over time for SK-MES-1 cells exposed to A) concentrated air particulates (CAPs) extracted from a PM_{2.5} air quality monitoring filter (a 100% mass recovery was assumed), B) quartz standard reference material, Q66, and C) urban dust standard reference material, SRM 1649a.

We also determined the hourly IC₅₀ values over the exposure period of the CAPs, as seen in Figure 3.8. These values are compared to the hourly IC₅₀ values over time determined for Q66 and SRM1649a, with values for 24 h, 48 h, and 72 h exposure for all three PM included for easier comparison. The IC₅₀ values for the CAPs were clearly higher than the values for the two SRMs over the entire

exposure period, indicating that the CAPs extracted from the PM2.5 filter were less cytotoxic to the SK-MES-1 cells.

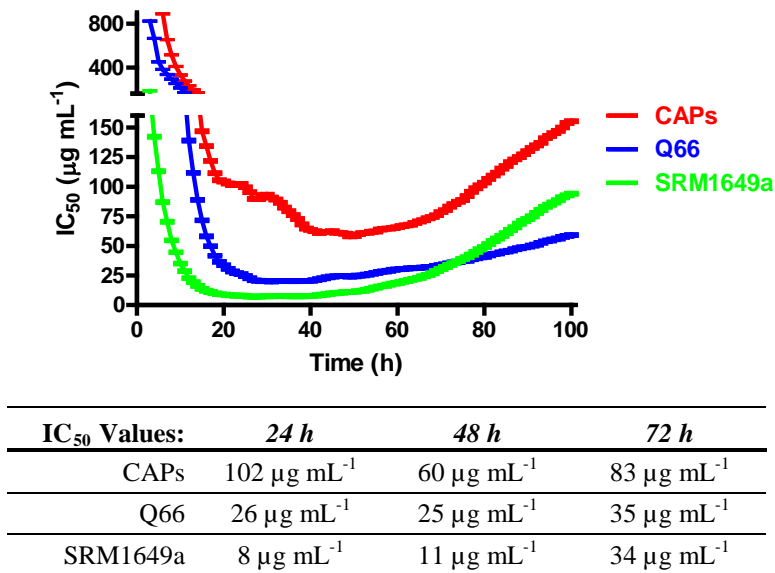


Figure 3.8: Temporal IC₅₀ histograms of the hourly IC₅₀ values (in µg mL⁻¹) over the exposure period for SK-MES-1 cells exposed to CAPs, quartz standard reference material, Q66, and an urban dust standard reference material, SRM1649a. Values are the mean ± SEM. The tabulated 24, 48, and 72 h IC₅₀ values for all three PM are included.

3.4 Conclusions

This demonstrates the ability of our 96-x RTCA method to examine the cytotoxicity of complex mixtures of particulate matter collected directly from the environment. While the PM selected for this study were not exclusively ultrafine, our method was able to distinguish size-dependent cytotoxicity, which is an important factor when assessing nanoparticles. Furthermore, it also overcame interference due to large concentrations of particulates on the RTCA electrodes, a problem that could not be overcome in the NRU assay. It also shows the utility of

this instrumentation to be used for environmental toxicity monitoring, as the RTCA was able to rank the toxicity of the CAPs sample compared to two well-studied and characterized SRMs. Using this technique, the hazards associated with exposure to the air in the area in which these PM were collected can be identified and prioritized for further testing. Hence, our RTCA method is a valuable tool for use in environmental toxicity monitoring for the protection of human health.

3.5 References

- [1] E. Laws, in: E.A. Laws (Ed.), *Environmental Toxicology*, Springer, New York, 2013, p. 565-594.
- [2] S. Magrisso, Y. Erel, S. Belkin, *Microb. Biotechnol.* 1 (2008) 320-330.
- [3] U.S. Environmental Protection Agency, *Integrated Review Plan for the National Ambient Air Quality Standards for Particulate Matter*, Washington, D.C., 2008, EPA 452/R-08-004.
- [4] E. Dabek-Zlotorzynska, T.F. Dann, P. Kalyani Martinelango, V. Celo, J.R. Brook, D. Mathieu, L. Ding, C.C. Austin, *Atmos. Environ.* 45 (2011) 673-686.
- [5] M. Krzyzanowski, in: J. Bower, O. Hänninen, B. Kotlik, H.-G. Mücke, H. Özkaynak, S. Tarkowski, and M. Krzyzanowski (Eds.), *Monitoring Ambient Air Quality for Health Impact Assessment*, WHO Regional Publications, Copenhagen, Denmark, 1999, p. 99-107.
- [6] C.A. Pope, D.W. Dockery, *J. Air Waste Manag. Assoc.* 56 (2006) 709-742.
- [7] R.T. Burnett, J. Brook, T. Dann, C. Delocla, O. Philips, S. Cakmak, R. Vincent, M.S. Goldberg, D. Krewski, *Inhal. Toxicol.* 12 Suppl 4 (2000) 15-39.
- [8] H.E. Wichmann, C. Spix, T. Tuch, G. Wolke, A. Peters, J. Heinrich, W.G. Kreyling, J. Heyder, *Res. Rep. Health Eff. Inst.* 98 (2000) 5-94.
- [9] C.A. Pope, M. Ezzati, D.W. Dockery, *N. Engl. J. Med.* 360 (2009) 376-386.
- [10] G. Oberdorster, E. Oberdorster, J. Oberdorster, *Environ. Health Perspect.* 113 (2005) 823-839.
- [11] P.J. Borm, D. Robbins, S. Haubold, T. Kuhlbusch, H. Fissan, K. Donaldson, R. Schins, V. Stone, W. Kreyling, J. Lademann, J. Krutmann, D. Warheit, E. Oberdorster, *Part. Fibre Toxicol.* 3 (2006) 11.
- [12] U.S. Environmental Protection Agency, *National Ambient Air Quality Standards for Particulate Matter - Final Rule - 40 CFR Parts 50, 51, 52, 53, and 58*, Washington, D.C., 2013, EPA-HQ-OAR-2007-0492; FRL-9761.
- [13] Canadian Council of Ministers of the Environment, *Canada-Wide Standards for Particulate Matter and Ozone* (2000).
- [14] Canadian Council of Ministers of the Environment, *Guidance Document on Achievement Determination Canadian Ambient Air Quality Standards for Fine*

- Particulate Matter and Ozone, 2012, PN1483. [15] L. Huang, L. Xie, J.M. Boyd, X.F. Li, *Analyst* 133 (2008) 643-648.
- [16] H. Chen, L. Cui, X.Y. Jiang, Y.Q. Pang, G.L. Tang, H.W. Hou, J.H. Jiang, Q.Y. Hu, *Food Chem. Toxicol.* 50 (2012) 612-618.
- [17] T. Wang, E.T. Chiang, L. Moreno-Vinasco, G.D. Lang, S. Pendyala, J.M. Samet, A.S. Geyh, P.N. Breysse, S.N. Chillrud, V. Natarajan, J.G. Garcia, *Am. J. Respir. Cell Mol. Biol.* 42 (2010) 442-449.
- [18] T. Wang, L. Wang, L. Moreno-Vinasco, G.D. Lang, J.H. Siegler, B. Mathew, P.V. Usatyuk, J.M. Samet, A.S. Geyh, P.N. Breysse, V. Natarajan, J.G. Garcia, *Part. Fibre Toxicol.* 9 (2012) 35-8977-9-35.
- [19] J.M. Veranth, T.A. Moss, J.C. Chow, R. Labban, W.K. Nichols, J.C. Walton, J.G. Watson, G.S. Yost, *Environ. Health Perspect.* 114 (2006) 341-349.
- [20] A. Imrich, Y.Y. Ning, H. Koziel, B. Coull, L. Kobzik, *Toxicol. Appl. Pharmacol.* 159 (1999) 117-124.
- [21] C.M. Long, H.H. Suh, L. Kobzik, P.J. Catalano, Y.Y. Ning, P. Koutrakis, *Environ. Health Perspect.* 109 (2001) 1019-1026.
- [22] G. Repetto, A. del Peso, J.L. Zurita, *Nat. Protoc.* 3 (2008) 1125-1131.
- [23] National Research Council, *Managing Coal Combustion Residues in Mines*, The National Academies Press, 2006.
- [24] R.S. Blissett, N.A. Rowson, *Fuel* 97 (2012) 1-23.
- [25] M. Izquierdo, X. Querol, *Int. J. Coal Geol.* 94 (2012) 54-66.
- [26] R.S. Kalyoncu, D.W. Olson, *Coal Combustion Products*, USGS Fact Sheet 076-01, 2001.

Chapter 4: Profiling Cytotoxicity of Thirteen Arsenic Species for Toxicity Ranking

4.1 Introduction

In humans, inorganic arsenic is enzymatically oxidized and reduced to promote elimination, resulting in the formation of several methylated intermediates and metabolites. The metabolism of inorganic arsenic is generally accepted to follow the pathway of $\text{As(V)} \rightarrow \text{As(III)} \rightarrow \text{MMA(V)} \rightarrow \text{MMA(III)} \rightarrow \text{DMA(V)} \rightarrow \text{DMA(III)}$ [1-3], although alternative pathways have been proposed [4]. Previously, the process of inorganic arsenic methylation was thought to be a detoxifying pathway. However, as toxicity testing of trivalent arsenic metabolites was conducted, it was found that these species were much more toxic than any of the pentavalent species and were either equally or more cytotoxic than As(III) [5-7]. Furthermore, these trivalent species were then discovered in human urine as a direct metabolite resulting from ingestion of inorganic arsenic, further demonstrating that this pathway is not a detoxifying one [1, 8].

Four As metabolites, MMA(III) , DMA(III) , MMA(V) , and DMA(V) have been repeatedly identified in human urine, and their toxicities have been studied using different assays. These are methylated arsenic metabolites containing oxygen. Several thio-arsenic metabolites have also been proposed or identified using improved analytical techniques. One of the S-arsenic metabolites that has been proposed is dimethylarsenic glutathione [DMAG(III)] [4]. It has been hypothesized that DMAG(III) plays a key role in the transport of methylated arsenic species from the liver to the bloodstream [9]. Another class of thiol-

containing arsenicals has been discovered in human urine [10] after first being identified as a metabolite in seaweed-fed sheep [11]. These pentavalent S-arsenic species include dimethylmonothioarsinate [DMMTA(V)], dimethyldithioarsinate [DMDTA(V)], and monomethylmonothioarsonate [MMMTA(V)], which have all been detected as metabolites in human or animal urine [10-12].

Monomethyltrithioarsonate [MMTTA(V)] is another thiol-containing pentavalent metabolite, but it has only been found as a metabolite of anaerobic microbiota *in vitro* [13].

While inorganic arsenic and its metabolites are often considered the most important from a human health perspective, other organoarsenic species (that are either naturally occurring or synthesized in a laboratory for industrial/consumer use) have become topics of recent research interest. One naturally occurring organoarsenic species that has recently been discovered is Arsenicin A. Isolated from the organic extract of a marine sponge, Arsenicin A is the first polyarsenical found in nature [14, 15]. While it has previously been shown to be a potent fungicide and bactericide in human pathogenic strains [14], the cytotoxicity of this novel arsenic species in human cell lines has not been demonstrated.

Two pentavalent arsenic species that have become heavily used in the poultry production industry are roxarsone (3-nitro-4-hydroxyphenylarsonic acid) and p-arsanilic acid (4-aminobenzenearsonic acid). As feed additives for broiler chickens, roxarsone and p-arsanilic acid not only improve feed efficiency, allowing for faster weight gain, but also help control intestinal coccidial parasites, preventing coccidiosis [16, 17]. However, while roxarsone has been approved for

use by the US Food and Drug Administration (FDA) since 1944 [17], little is known about the toxicity of these species of arsenic, not only in poultry, but in humans as well.

Another arsenic species that is used heavily in laboratory research as a known inhibitor in various biochemical reactions to elucidate toxicity mechanisms is phenylarsine oxide [PAO(III)]. This trivalent organoarsenic species is not naturally-occurring, but it is found in the environment at sites contaminated with chemical warfare agents, as it is a degradation product of the chemical warfare agent, diphenylarsine dichloride (also known as Pfiffikus) [18]. Studies have shown PAO(III) to be a potent cytotoxicant [19].

The toxicity of arsenic is dependent upon its chemical species, however, the mechanism of action and toxicity and the roles of specific metabolites or intermediates are poorly understood. The available toxicity data has been obtained using various assays on different cell lines. The species-dependent toxicity and variations in different assays make it difficult to compare the toxicity of different arsenic species. To address this issue, we propose to develop a real-time cell analysis (RTCA) method for uniform testing of the cytotoxicity of thirteen different arsenic species. RTCA is an impedance-based detection technique that can simultaneously perform 96 *in vitro* tests of cytotoxicity. This technique has been used by the US National Toxicology Program, the US EPA, and other regulatory agencies for high-throughput screening of chemical cytotoxicity [20, 21]. The RTCA technique is label- and dye-free, resulting in less interference. It provides continuous monitoring, revealing more dynamic and complete cytotoxic

response information. The features of high-throughput and accurate cytotoxicity data make RTCA a desirable tool for prioritizing chemicals for surveillance and regulatory consideration. In addition, as some arsenicals do have therapeutic uses, as with the treatment of acute promyelocytic leukemia (APL) with arsenic trioxide [19] and refractory solid tumors with DMAG(III) (alternate names: S-dimethylarsino-glutathione, ZIO-101, and darinaparsin) , understanding the cytotoxicity of various arsenic species may direct its exploitation for further therapeutic investigation. This will be of particular importance in later chapters of this thesis, as we will investigate the changes in cytotoxicity of these species due to the presence of nanoparticles (Chapter 6).

4.2 Materials and Methods

4.2.1 Cell Culture Conditions

Because our objective is to quantitatively rank the cytotoxicity of thirteen arsenic species, we chose to use continuous cell lines in order to reduce response variability between generations of cells used for testing. We selected a human lung carcinoma cell line and a human bladder cancer cell line for testing, as the lungs and bladder are target organs for arsenic toxicity. The human lung carcinoma cell line, A549, (CCL-185; American Type Culture Collection (ATCC), Manassas, VA) was cultured in RPMI 1640 media (Gibco (Invitrogen), Burlington, ON, Canada). The human bladder carcinoma cell line, T24, (HTB-4; ATCC) was cultured in McCoy's 5A modified media (ATCC). The human hepatocellular carcinoma cell line, HepG2, (HB-8065; ATCC) was cultured in EMEM (ATCC). All media were supplemented with 10% fetal bovine serum

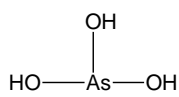
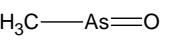
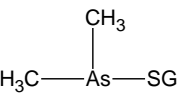
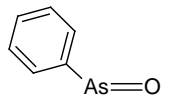
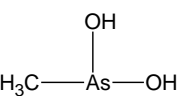
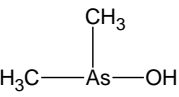
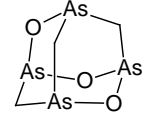
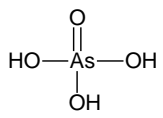
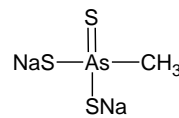
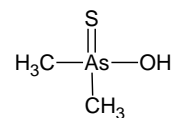
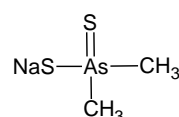
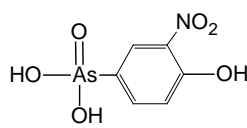
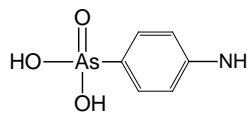
(Sigma-Aldrich, Oakville, ON, Canada) and 1% penicillin-streptomycin (Invitrogen, Burlington, ON, Canada). The incubation conditions were maintained at 37 °C, 5% CO₂, and 90% humidity. During the study, the cells were sub-cultured twice weekly into standard 10 cm x 20 mm cell culture dishes (Corning Incorporated, Corning, NY) containing fresh media, using 0.05% trypsin-EDTA (Invitrogen) for cell detachment.

4.2.2 Arsenic Solution Preparation

Solutions of As(III) and As(V) in deionized (DI) water were prepared from commercially available sodium arsenite and sodium arsenate (Sigma Chemical Co., St. Louis, MO). Solutions of MMA(III) in DI water were prepared from synthesized standards of methyl-diiodoarsine [MMA(III)] [22, 23] and methylarsine oxide [MAO(III)] [24], and the solution of DMA(III) in DI water was prepared from a synthesized standard of dimethyl-diiodoarsine [25]. Solutions of DMAG(III), DMMTA(V), MMTTA(V), and DMDTA(V) in DI water were also prepared from synthesized standards prepared in our laboratory. DMAG(III) solutions also contained 2% methanol (Fisher Scientific, Nepean, ON, Canada). Synthesized Arsenicin A stock was graciously provided by Dr. William Cullen at the University of British Columbia and contained 4% methanol. Solutions of PAO(III), roxarsone, and p-arsanilic acid in DI water were also prepared from commercially available standards (Sigma Chemical Co.). PAO(III) solutions contained 2% methanol, and p-arsanilic acid solutions contained up to 10% methanol (Fisher Scientific). Table 4.1 presents a list of all the above arsenic species, along with their chemical structure. Solutions were sterilized via filtration

(0.22 μm) and the final concentration of arsenic in each solution was calibrated using HPLC coupled with ICP-MS (Agilent Technologies, Japan). As(III), As(V), Arsenicin A, and PAO(III) solutions were stored at 4 °C until use. Roxarsone and p-arsanilic acid solutions re-precipitate in DI water at 4 °C over time and had to be used within a week of preparation. All remaining arsenic solutions are unstable at 4 °C and had to be prepared fresh the day of treatment.

Table 4.1: Structures of Thirteen Arsenic Species Profiled

Arsenic Species	Abbrev.	Structure
Arsenite	As(III)	
Methylarsine oxide	MAO(III)	
Dimethylarsenic glutathione	DMAG(III)	
Phenylarsine oxide	PAO(III)	
Monomethylarsonous acid	MMA(III)	
Dimethylarsinous acid	DMA(III)	
Arsenicin A	AA	
Arsenate	As(V)	
Monomethyltrithioarsenate	MMTTA(V)	
Dimethylmonothioarsinate	DMMTA(V)	
Dimethyldithioarsinate	DMDTA(V)	
3-nitro-4-hydroxyphenylarsonic acid	Roxarsone	
4-aminobenzearsonic acid	p-Arsanilic Acid	

4.2.3 RTCA Analysis

Cells were seeded into 96-well or 16-well E-plates of the 96x- or 16x- RTCA systems (ACEA Biosciences, San Diego, CA) at pre-calibrated concentrations that allowed for a Cell Index (CI) of 1, indicating 50-60% confluency, to be reached between 18-24 h after seeding. A549 cells were seeded at 4000-4500 cells well⁻¹, T24 cells at 3500-4000 cells well⁻¹, and HepG2 cells at 17,500-20,000 cells well⁻¹. When a CI of 1 was reached, the arsenic solutions described above were serially diluted in the respective media of the A549 and T24 cell lines to achieve the proper dose range for quantitative analysis. The HepG2 cell line was treated with As(III) and Arsenicin A only. 200 µL of each treatment concentration was added to triplicate wells. Negative controls (untreated media) and solvent controls (methanol) were also added when necessary at a volume of 200 µL to triplicate wells. After treatment, CI was measured at hourly intervals for at least 72 h post-exposure. At least three separate experimental runs with all corresponding negative and solvent controls were performed for each arsenic species on each cell line (n ≥ 3).

4.2.4 Data Analysis

Analysis of data to determine IC₅₀ values over time was performed using Prism 5.0 (Graph Pad Software Inc., San Diego, CA). IC₅₀ values were defined as the concentration of arsenic species that resulted in a 50% reduction in normalized CI as compared to the normalized CI of non-treated control cells at a given timepoint.

4.3 Results and Discussion

4.3.1 Inorganic Arsenicals

We first demonstrate the RTCA method for profiling the inorganic arsenicals, As(V) and As(III). Figure 4.1 shows the RTCA profiles of A549 cells (Fig. 4.1A) and T24 cells (Fig. 4.1B) responding to the exposure of As(V). Figure 4.1 clearly shows the dose-dependent and cell-dependent cytotoxicity of As(V). As the dose response for As(V) in T24 cells was in the μM range (20-500 μM) and in the mM range (1-5 mM) for A549 cells, it is clear that T24 cells are more sensitive to As(V) than A549.

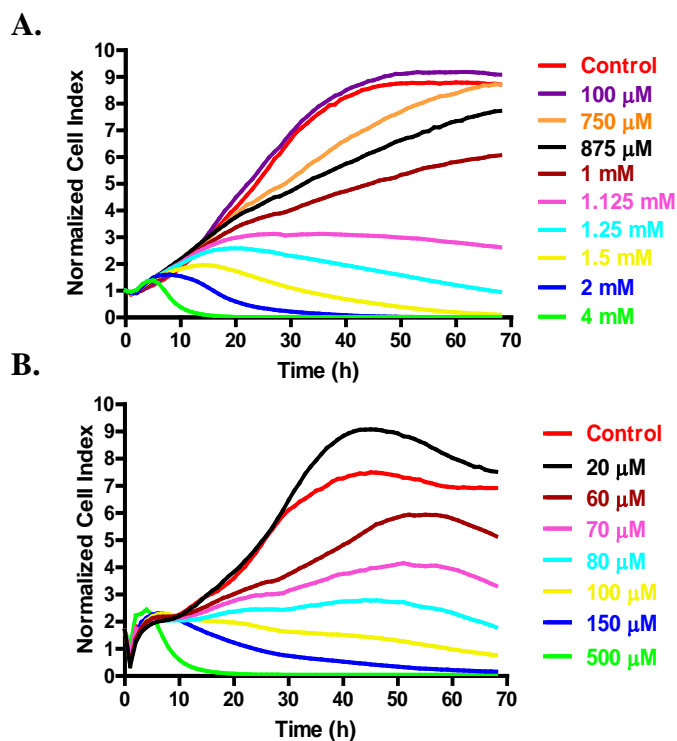


Figure 4.1: RTCA cytotoxicity profiles of the normalized cell index (CI) over time for A) A549 and B) T24 (x1.67) cells exposed to As(V). The CI scales were normalized using the multiplication factor (in parentheses) for easier visual analysis.

When treated with As(III), the A549 and T24 cells responded with the same trend as As(V), as shown in Figure 4.2. Dose-dependent cytotoxicity was observed for A549 cells between 40-250 μ M (Fig. 4.2A) and for T24 cells between 1-75 μ M (Fig. 4.2B). To further demonstrate cell-dependent cytotoxic response, Figure 4.2 also shows the RTCA cytotoxicity profile of HepG2 cells responding to As(III) (Fig. 4.2C). Comparing the shapes of the profiles in each of the three cell lines, HepG2 cells are clearly different from those of the A549 and T24 cells. This indicates that HepG2 cells respond to As(III) through different processes. Xing et al. reported a similarly-shaped RTCA profile for NIH 3T3 cells treated with As(III). They found As(III)-induced cell fusion resulted in an increase in CI at the beginning of exposure and was followed by cell dissociation resulting in the complete loss of CI, consistent with the induction of apoptosis [26]. Thus, Figure 4.2 also demonstrates the need for testing different cell lines for comprehensive profiling of arsenic toxicity, as cellular responses can vary significantly across cell lines.

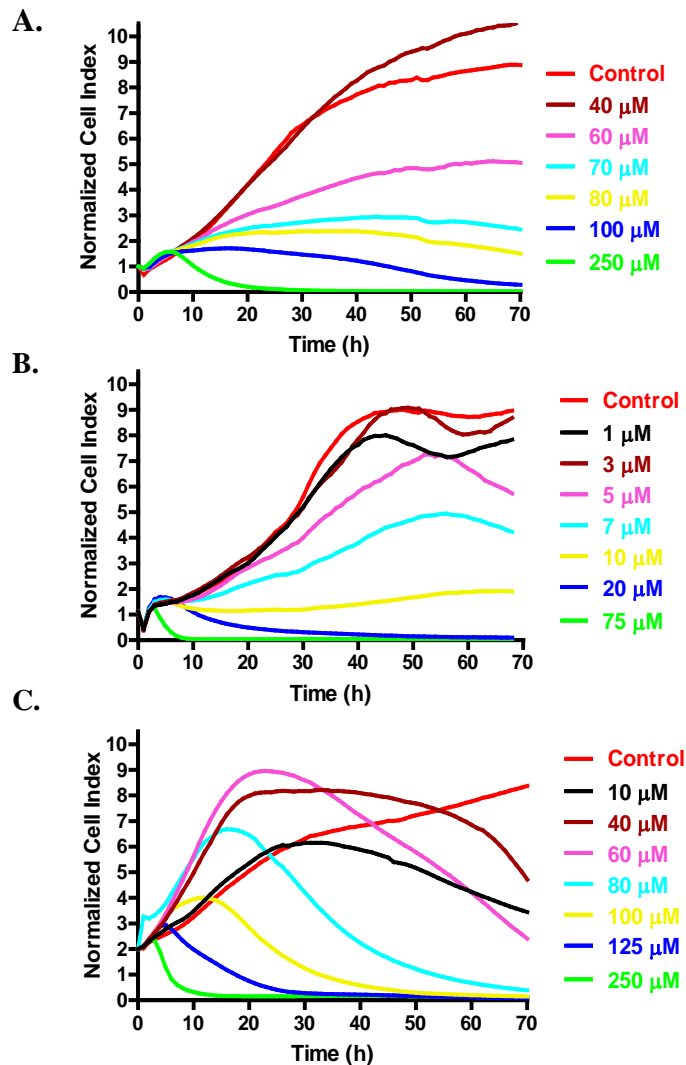


Figure 4.2: RTCA cytotoxicity profiles of the normalized cell index (CI) over time for A) A549, B) T24 (x1.11), and C) HepG2 (x2) cells exposed to As(III). The CI scales were normalized using the multiplication factor (in parentheses) for easier visual analysis.

To quantitatively compare the cytotoxicity of As(III) and As(V), we generated IC_{50} histograms (in $\mu\text{M} \pm \text{SEM}$) (Figure 4.3) from the data shown in Figures 4.1 and 4.2. This is a unique feature of RTCA cytotoxicity profiling, as it provides real-time response and high-throughput generation of cytotoxicity data for comparison. Figure 4.3 clearly shows that As(III) is much more cytotoxic than As(V) in both cell lines. This is consistent with the results reported in the previous

studies that As(III) was more cytotoxic than As(V) when examined in the same cell line [7, 19, 27, 28]. Tables 4.2 and 4.3 present the IC₅₀ values for As(III) and As(V) in both cell lines after 24 h and 48 h exposure. Our 24 h IC₅₀ value of 74.2 ± 4.1 μM for As(III) in the A549 cell line was in good agreement with reported literature values of around 100 μM for the same cell line, as determined using MTT and cell counting assays [29, 30].

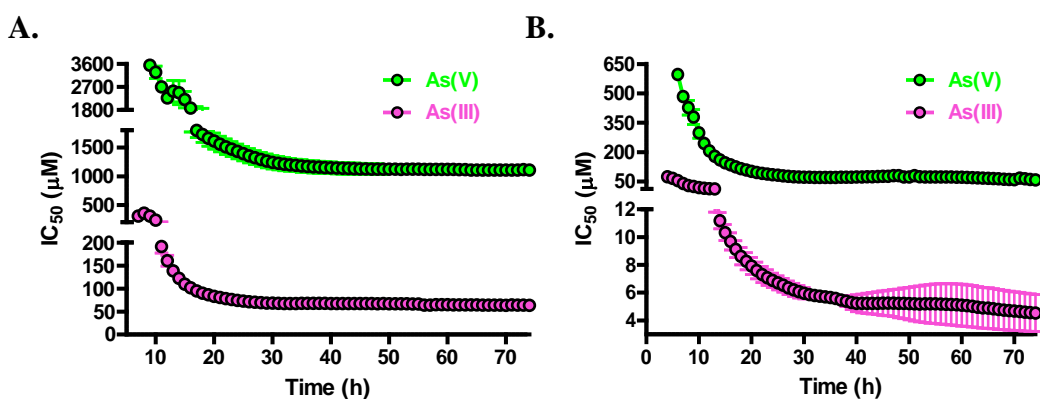


Figure 4.3: Temporal IC₅₀ histograms of the hourly IC₅₀ values (μM ± SEM) for A) A549 and B) T24 cells exposed to the inorganic arsenicals, As(V) and As(III).

The examination of the inorganic arsenicals highlights the benefits of real-time analysis provided by the RTCA assay. The RTCA cytotoxicity profiles provide qualitative kinetic information that indicates differences in cell-response patterns across cell lines and quantitative IC₅₀ values over the exposure period. In addition, the high-throughput capabilities of this assay allow for simultaneous examination of several cell lines.

Table 4.2: IC₅₀ Values (μM ± SEM) for all Arsenic Species on A549

	<i>24 h</i>	<i>48 h</i>
PAO(III)	0.70 ± 0.09	0.87 ± 0.11
Arsenicin A	7.3 ± 0.43	8.5 ± 0.25
MAO(III)	12.0 ± 1.7	14.5 ± 2.2
MMA(III)	13.6 ± 2.5	16.6 ± 2.9
DMA(III)	14.1 ± 2.2	17.1 ± 3.3
DMAG(III)	23.0 ± 1.3	29.2 ± 3.4
DMMTA(V)	20.5 ± 4.5	21.0 ± 6.6
As(III)	74.2 ± 4.1	67.1 ± 3.1
MMTTA(V)	600 ± 79	280 ± 22
As(V)	1400 ± 130	1100 ± 93
DMDTA(V)	4300 ± 3000	230 ± 74
Roxarsone	9300 ± 1600	9300 ± 1200
p-Arsanilic Acid	Not Toxic	Not Toxic

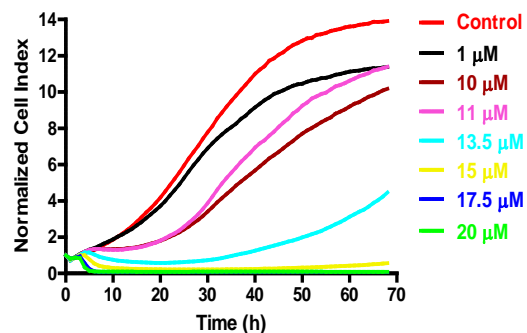
Table 4.3: IC₅₀ Values (μM ± SEM) for all Arsenic Species on T24

	<i>24 h</i>	<i>48 h</i>
PAO(III)	0.076 ± 0.0038	0.11 ± 0.0063
MAO(III)	1.2 ± 0.36	1.1 ± 0.19
MMA(III)	1.9 ± 0.10	2.2 ± 0.17
Arsenicin A	3.6 ± 0.24	3.6 ± 0.36
DMAG(III)	5.2 ± 1.1	4.8 ± 1.1
DMA(III)	5.2 ± 1.3	4.9 ± 1.4
DMMTA(V)	6.4 ± 1.4	7.6 ± 1.7
As(III)	6.9 ± 0.52	5.2 ± 1.0
MMTTA(V)	24.6 ± 2.5	28.8 ± 4.9
As(V)	85.0 ± 6.5	80.1 ± 7.7
DMDTA(V)	342 ± 95	63 ± 13
p-Arsanilic Acid	6300 ± 3200	7200 ± 1900
Roxarsone	6800 ± 740	6400 ± 620

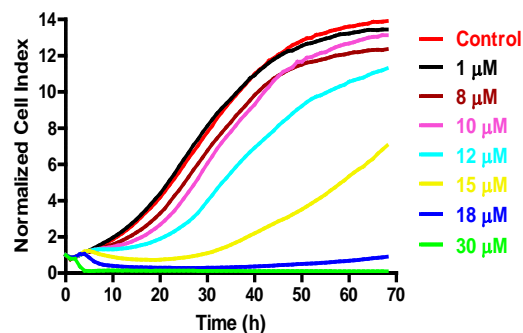
4.3.2 Arsenic Metabolites

Having demonstrated the RTCA assay for profiling the cytotoxicity of the inorganic arsenicals, As(V) and As(III), we then examined the methylated As(III) metabolites, MAO(III), MMA(III), and DMA(III). Figure 4.4 shows the real-time response profiles of A549 (A-C) and T24 (D-F) cells generated using data from RTCA. MAO(III) and MMA(III) both dissociate to form the same monomethylarsonous acid species in solution. Hence, their effects on cells are expected to be similar. This is clearly observed in the RTCA profiles of MAO(III) (Fig. 4.4A and D) and MMA(III) (Fig. 4.4B and E), where both the curve shape and the slopes of initial responses are similar in both cell lines. Both A549 and T24 cells exposed to DMA(III) show similar response profiles (Fig. 4.4C and F). However, the response profiles of both cell lines to DMA(III) are noticeably different from those of MAO(III) and MMA(III). In Figure 4.4C, when A549 cells are exposed to DMA(III) at the doses of 7.5 μM and 10 μM , the response curves have a step-wise shape. The step-wise shape is also apparent in Figure 4.4F when T24 cells are exposed to DMA(III) at doses between 5-7 μM . The step-wise shape is not observed in the response profiles of A549 and T24 cells exposed to MAO(III) or MMA(III). The step-wise response may be explained by a chemical response caused by the conversion of DMA(III) in solution over time. Further research is warranted to elucidate the mechanisms of the step-wise cellular response observed, as it could be due to chemical (e.g. species conversion over time) or biological effects (e.g. cell cycle arrest).

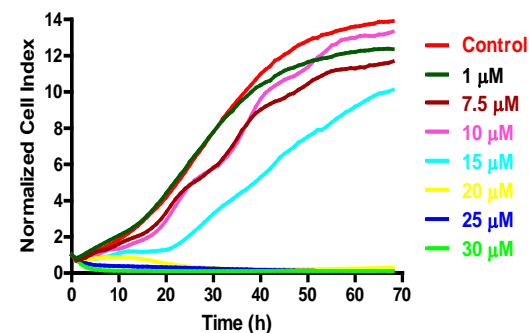
A. MAO(III) on A549



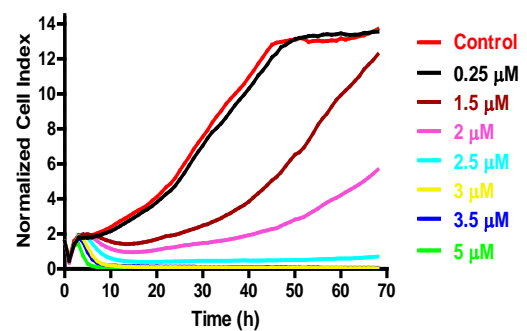
B. MMA(III) on A549



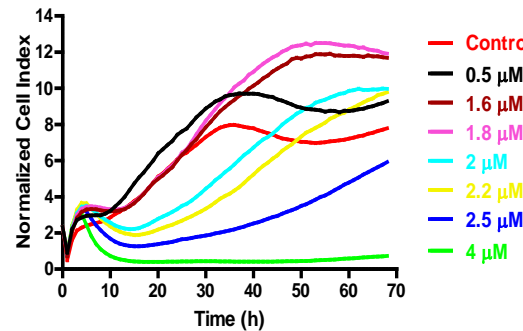
C. DMA(III) on A549



D. MAO(III) on T24



E. MMA(III) on T24



F. DMA(III) on T24

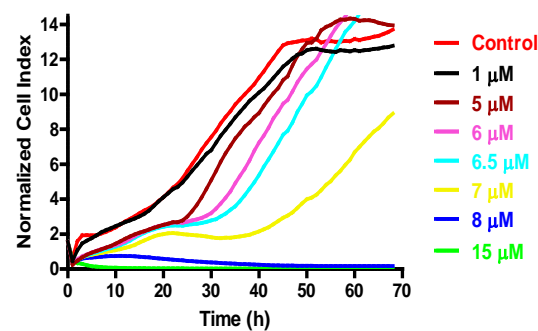


Figure 4.4: RTCA cytotoxicity profiles of the normalized cell index over time for A549 cells exposed to A) MAO(III), B) MMA(III), and C) DMA(III), and T24 cells exposed to D) MAO(III) (x1.56), E) MMA(III) (x2.33), and F) DMA(III) (x1.56). The CI scales were normalized using the multiplication factor (in parentheses) for easier visual analysis.

To quantitatively compare the toxicity of these three trivalent arsenic metabolites with that of the inorganic arsenicals, we generated the temporal IC_{50} histograms from the response profiles. Figure 4.5 shows the hourly IC_{50} values over the exposure period for the three metabolites, MAO(III), MMA(III), and DMA(III), and the inorganic arsenicals, As(III) and As(V). In A549 cells (Fig. 4.5A), the IC_{50} values of MAO(III), MMA(III), and DMA(III) over time have similar toxicity. The 24 h and 48 h IC_{50} values for these species (Table 4.2) support this. However, T24 cells responding to these arsenic metabolites (Fig. 4.5B) show a difference in temporal IC_{50} histograms. The IC_{50} values for MAO(III) and MMA(III) are similar, but they are significantly lower than those of DMA(III). The temporal IC_{50} values of DMA(III) begin to overlap with those of the inorganic arsenical, As(III), after 24 h exposure. Table 4.3 presents the 24 h and 48 h IC_{50} values of these species on T24 cells. Our data rank the toxicity of these species as $MAO(III) \approx MMA(III) \approx DMA(III) > As(III) \gg As(V)$ in A549 cells and $MAO(III) > MMA(III) > DMA(III) \geq As(III) \gg As(V)$ in T24 cells. Our results support the trend reported in the literature that trivalent methylated arsenic metabolites are more cytotoxic than the inorganic species in human cells [5-7].

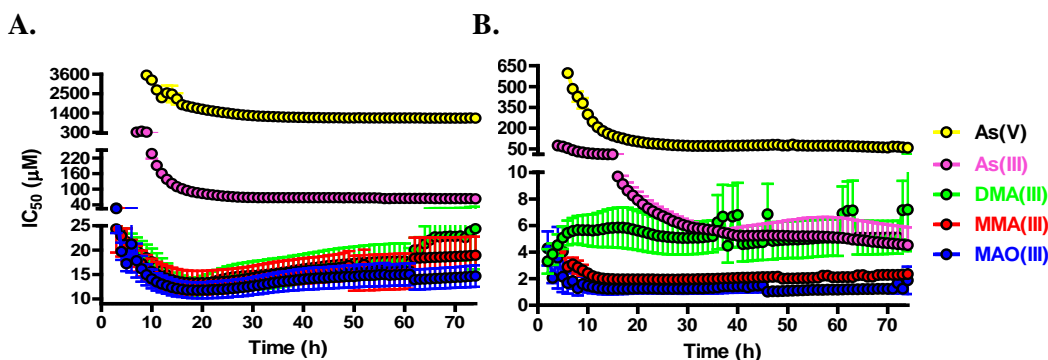


Figure 4.5: Temporal IC_{50} histograms of the hourly IC_{50} values ($\mu\text{M} \pm \text{SEM}$) for A) A549 and B) T24 cells exposed to the inorganic arsenicals, As(V) and As(III), in comparison to the trivalent arsenic metabolites, MAO(III), MMA(III), and DMA(III).

4.3.3 Thiolated Arsenic Metabolites

Figure 4.6 shows RTCA cytotoxicity profiles for A549 (Fig. 4.6A) and T24 cells (Fig. 4.6B) exposed to the thiolated trivalent arsenic species, DMAG(III). Interestingly, the profile shape for this species in both cell lines is very similar to the profile shapes of DMA(III) in both cell lines (Fig. 4.4C and F). Here, that step-wise profile shape is again clearly visible in the doses between 10-25 μM in A549 cells and 2.5-5 μM in T24 cells. These profiles suggest that either DMAG(III) may convert to DMA(III) in media, or that dimethylated trivalent arsenicals may have a similar mode of action in these two cell lines which is specific to the dimethylated nature of the arsenic species.

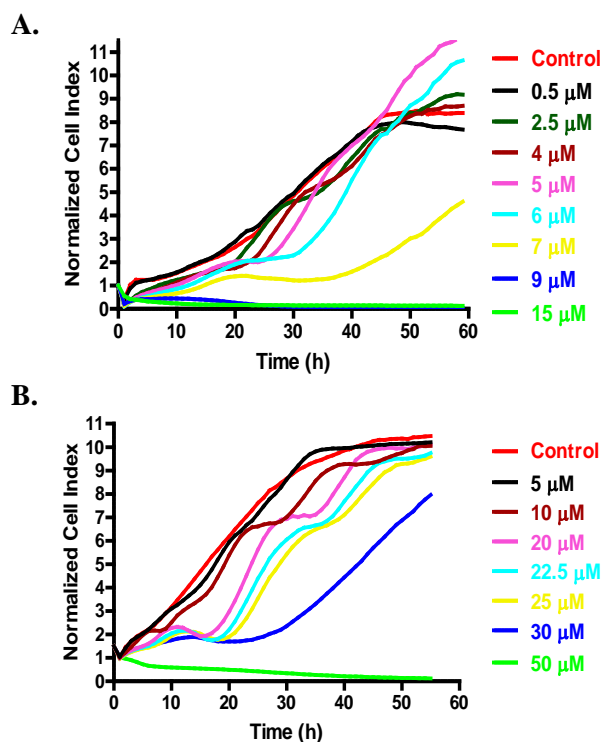


Figure 4.6: RTCA cytotoxicity profiles of the normalized cell index over time for A) A549 (x1.5) and B) T24 cells exposed to the trivalent thiolated arsenic species, DMAG (III). The CI scales were normalized using the multiplication factor (in parentheses) for easier visual analysis.

Figure 4.7 compares temporal IC_{50} values of the two dimethylated trivalent arsenicals, DMAG(III) and DMA(III), with those of As(III). In A549 cells (Fig. 4.7A), the cytotoxicity of these species clearly rank as $DMA(III) > DMAG(III) > As(III)$. However, in T24 cells, the temporal IC_{50} values for DMAG(III) $>$ As(III). However, in T24 cells, the temporal IC_{50} values for DMA(III) and DMAG(III) almost fully overlap, supporting that DMAG(III) and DMA(III) have similar cytotoxicity to T24 cells. In A549 cells, the dimethylated trivalent metabolites are much more toxic than As(III), but in T24 cells, the three trivalent species are equally cytotoxic. This trend is consistent with the previous report that the cytotoxicity of DMAG(III) was similar to that of As(III) in most of the tested cell lines [7].

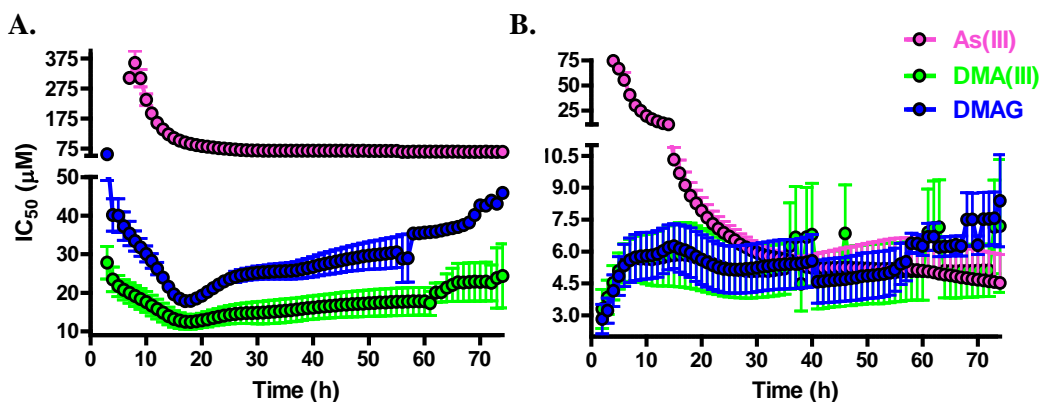
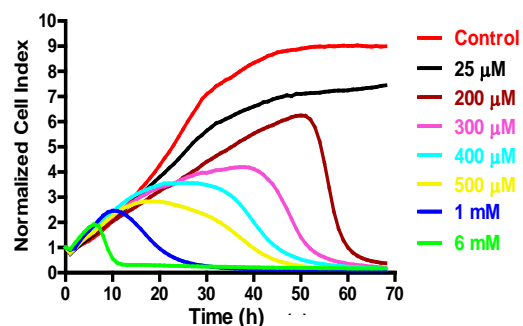


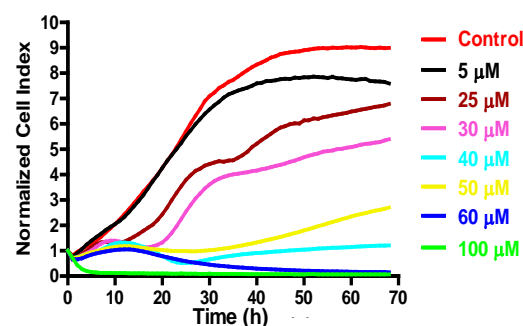
Figure 4.7: Temporal IC₅₀ histograms showing the hourly IC₅₀ values (µM ± SEM) over the exposure period for A) A549 and B) T24 cells exposed to the trivalent inorganic arsenical, As(III), in comparison to the dimethylated trivalent arsenic species, DMA(III) and DMAG(III).

Figure 4.8 presents the RTCA cytotoxicity profiles for the pentavalent thiolated arsenic metabolites, MMTTA(V), DMMTA(V), and DMDTA(V) in A549 (A-C) and T24 (D-F) cells. Here, several interesting compound-dependent cellular responses are clearly visible. When examining the MMTTA(V) RTCA profiles (Fig. 4.8A and D), a similar profile shape characterized by an increasing CI that rapidly drops to zero can be seen in most of the concentrations tested in both cell lines. The time of CI drop is inversely correlated with dose, so as the dose increases, the time for the CI drop becomes earlier.

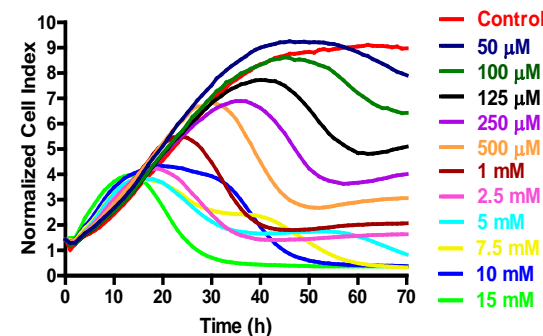
A. MMTTA(V) on A549



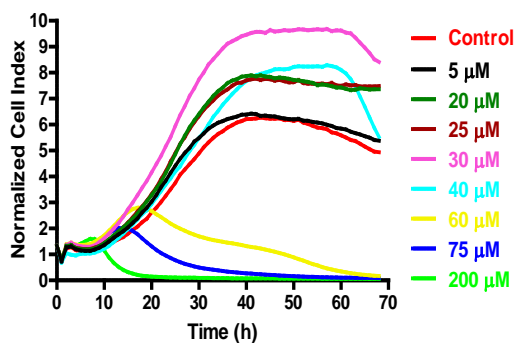
B. DMMTA(V) on A549



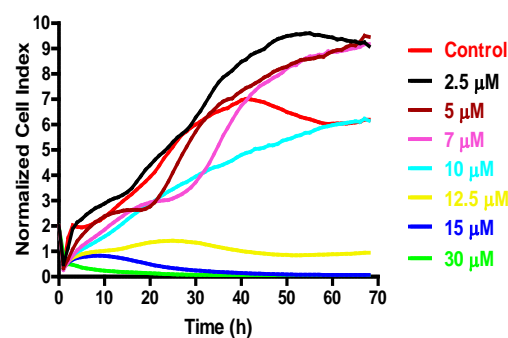
C. DMDTA(V) on A549



D. MMTTA(V) on T24



E. DMMTA(V) on T24



F. DMDTA(V) on T24

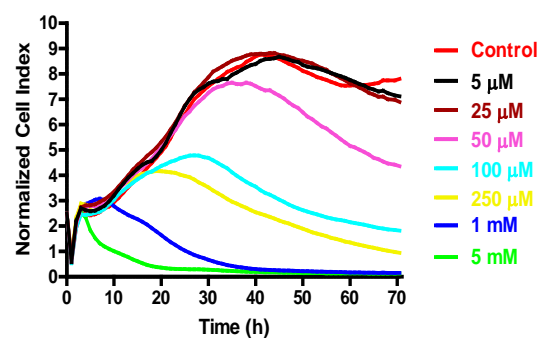


Figure 4.8: RTCA cytotoxicity profiles of the normalized cell index over time for A549 cells exposed to A) MMTTA(V), B) DMMTA(V), and C) DMDTA(V) (x1.43) and T24 cells exposed to D) MMTTA(V) (x1.33), E) DMMTA(V) (x2), and F) DMDTA(V) (x2.5). The CI scales were normalized using the multiplication factor (in parentheses) for easier visual analysis.

For both cell lines exposed to the dimethylated pentavalent arsenical, DMMTA(V) (Fig. 4.8B and E), we again see the step-wise profile shape that we saw earlier in the trivalent dimethylated arsenic metabolites (Fig. 4.4C, 4.4F, 4.6). In A549 cells (Fig. 4.8B), this step-wise profile shape is clearly seen with the doses between 25-30 μ M, while in T24 cells, it is seen with doses between 5-7 μ M (Fig. 4.8E). Thus, our hypothesis from above regarding a unique mode of action of dimethylated arsenicals must be modified to not only include trivalent dimethylated arsenic species, but also pentavalent dimethylated arsenic species as well. However, when examining the profile shapes for DMDTA(V) in A549 cells (Fig. 4.8C), this trend does not seem as clear. While the other dimethylated arsenic metabolites appeared to have an ascending step-wise pattern in A549 cells, DMDTA(V) appears to have a descending step-wise pattern in this cell line, as is most clearly visible in the treatment dose of 7.5 mM DMDTA(V). Again, while these unique profile shapes may be the result of a specific biological effect, they may also be a result of a change in the chemical speciation of arsenic present over time, or even a combination of both.

To quantitatively assess the relationship between these pentavalent arsenicals, we generated IC_{50} histograms, as can be found in Figure 4.9. DMMTA(V) is clearly the most cytotoxic of the pentavalent species examined, and this result has been shown in the literature [31]. Another interesting result from Figure 4.9 is the noticeable decrease in IC_{50} values that occurs over time for both MMTA(V) and DMDTA(V). This corresponds with what was seen in the RTCA cytotoxicity profiles for these species (Fig. 4.8), but the significance of the

decrease appears to point more toward a chemical conversion of the arsenic present in solution or within the cell. These species may convert to the less toxic pentavalent arsenicals, MMA(V) and DMA(V), which in turn can be reduced within the cell to the more toxic trivalent arsenicals, MMA(III) and DMA(III). This further supports the necessity to test arsenic conversion over time using HPLC-ICP-MS analysis.

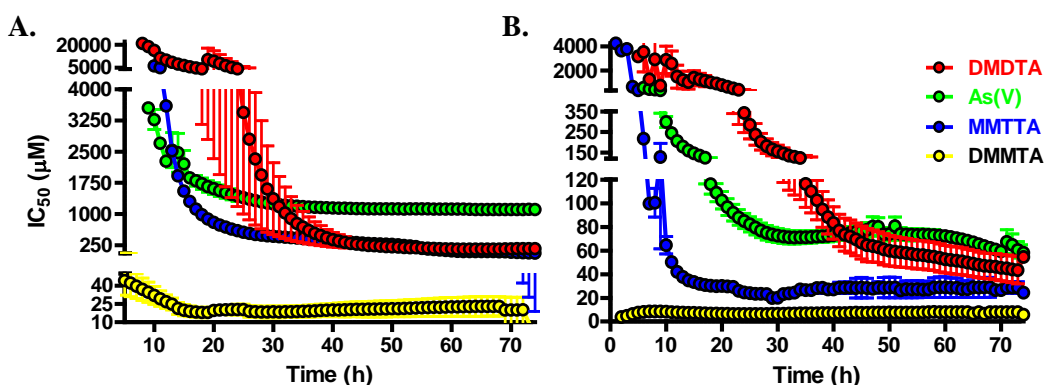


Figure 4.9: Temporal IC_{50} histograms of the hourly IC_{50} values ($\mu\text{M} \pm \text{SEM}$) for A) A549 and B) T24 cells exposed to the pentavalent inorganic arsenical, As(V), in comparison to the pentavalent arsenic metabolites, MMTTA(V), DMMTA(V), and DMDTA(V).

4.3.4 Non-metabolite Organoarsenicals

Figure 4.10 shows the RTCA cytotoxicity profiles for A549 (Fig. 4.10A), T24 (Fig. 4.10B), and HepG2 (Fig. 4.10C) cells exposed to the non-metabolite polyarsenical, Arsenicin A. This data presents the first known *in vitro* human toxicity data collected on this unique arsenical. It is interesting to note that the profile shapes seen here in Figure 4.10 appear to mimic the profile shapes for each cell line exposed to As(III), as seen in Figure 4.2. This is particularly clear for HepG2 cells, where the profile shape for many of the concentrations in Figure

4.10C exhibit the same transient increase in CI during the initial hours of exposure, which is then followed by a decrease in CI, producing a characteristic “bump” in the profiles. Further investigation is needed to characterize this response.

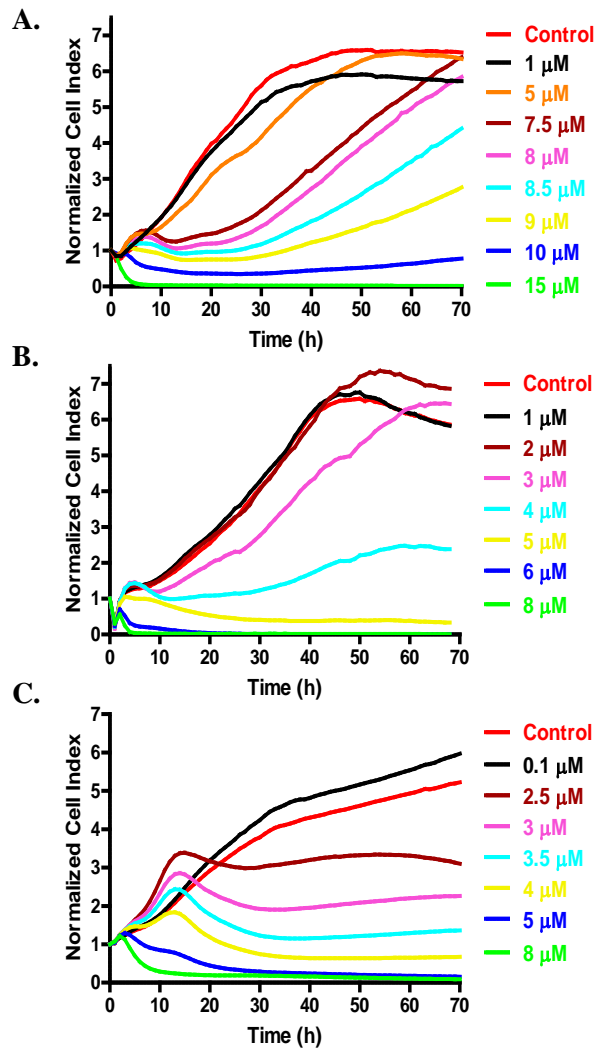


Figure 4.10: RTCA cytotoxicity profiles of the normalized cell index over time for A) A549, B) T24, and C) HepG2 cells exposed to Arsenicin A.

To quantify the concentration-response observed in Figure 4.10, IC_{50} histograms were generated, as seen in Figure 4.11. Arsenicin A had significantly lower IC_{50} values in the A549 and HepG2 cell lines compared to As(III) over the

entire exposure period, indicating that Arsenicin A (Fig. 4.11A) is considerably more cytotoxic than As(III) (Fig. 4.11B) in these cell lines. However, in the T24 cell line, the IC_{50} values for Arsenicin A were only slightly lower than those for As(III). Of the cell lines, T24 was the most sensitive to As(III), while HepG2 was slightly more sensitive to Arsenicin A than T24. A549 was the least sensitive to both species. The enhanced cytotoxicity of Arsenicin A in comparison to As(III) indicates it may have potential use in cancer therapy, as it was highly cytotoxic to a broad range of human carcinoma cell lines. Thus, further investigation into the mechanisms of biological activity of this novel arsenic species is warranted.

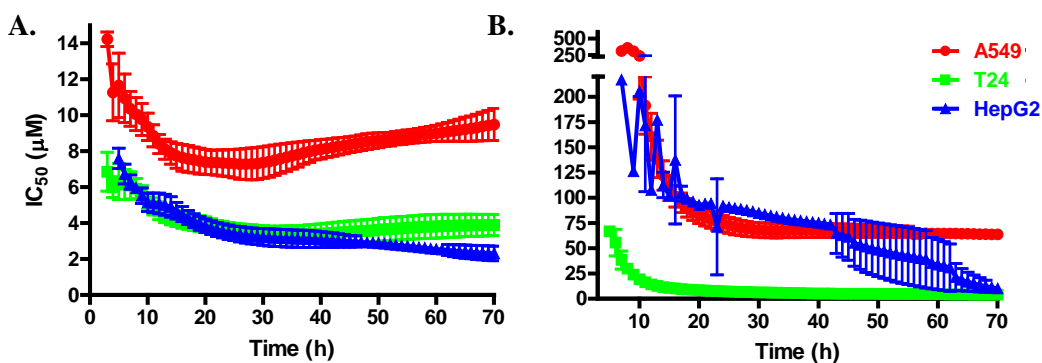
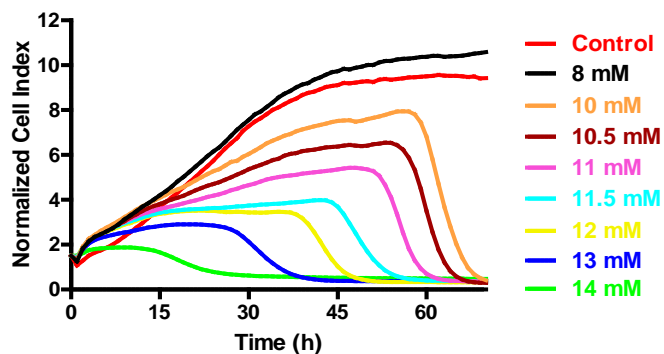


Figure 4.11: Temporal IC_{50} histograms showing the hourly IC_{50} values ($\mu M \pm SEM$) over the exposure period for A549, T24, and HepG2 cells exposed to A) Arsenicin A and B) the trivalent inorganic arsenical, As(III).

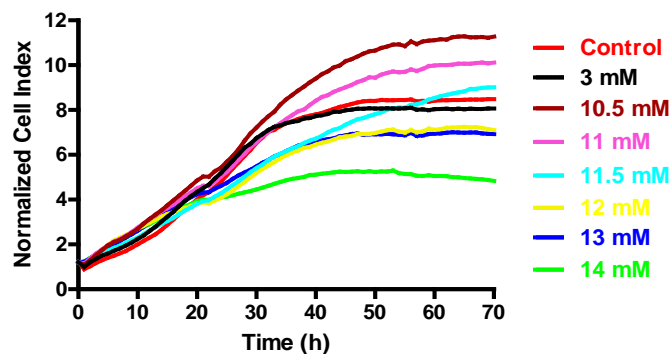
Figure 4.12 show the RTCA cytotoxicity profiles for A549 and T24 cells exposed to the pentavalent organoarsenicals, roxarsone and p-arsanilic acid. The profiles for A549 (Fig. 4.12A) and T24 (Fig. 4.12C) cells exposed to roxarsone show a unique pattern that is characterized by increasing CI over time (albeit at different rates for each concentration), followed by an abrupt crash in CI to 0, where the higher the concentration, the earlier the time at which the crash occurs. However, the crash observed in A549 cells (Fig. 4.12A) appears to be much more

abrupt than in T24 cells (Fig. 4.12B). This seems to indicate a change in speciation of the two pentavalent organoarsenicals over time, again indicating the necessity of testing arsenic conversion over time using HPLC-ICP-MS analysis. T24 cells also appear to have a similar response to p-arsanilic acid (Fig. 4.12D), with the same wide curve of increasing and then decreasing CI. A549 cells, however, exhibited little response to the tested concentration range of p-arsanilic acid (Fig. 4.12B).

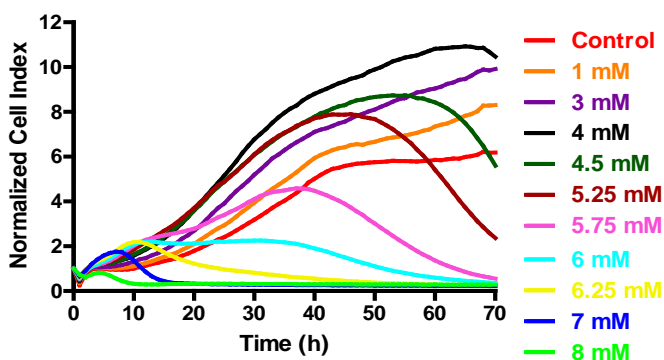
A. Roxarsone on A549



B. p-Arsanilic Acid on A549



C. Roxarsone on T24



D. p-Arsanilic Acid on T24

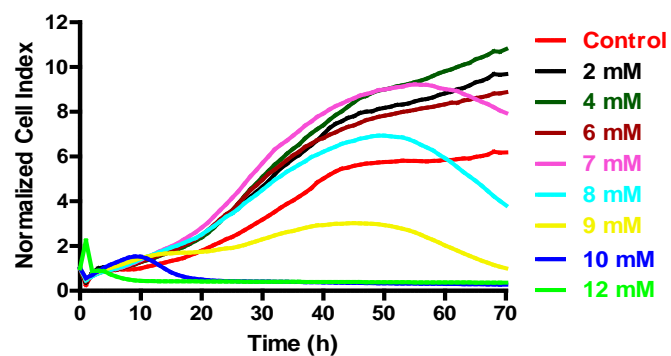


Figure 4.12: RTCA cytotoxicity profiles of the normalized cell index over time for A549 cells exposed to A) roxarsone (x1.5) and B) p-arsanilic acid (x1.2) and T24 cells exposed to C) roxarsone and D) p-arsanilic acid. The CI scales were normalized using the multiplication factor (in parentheses) for easier visual analysis.

The final arsenic species we investigated was the trivalent organoarsenical, PAO(III). Figure 4.13 shows the RTCA cytotoxicity profiles for A549 (Fig. 4.13A) and T24 (Fig. 4.13B) cells exposed to PAO(III).

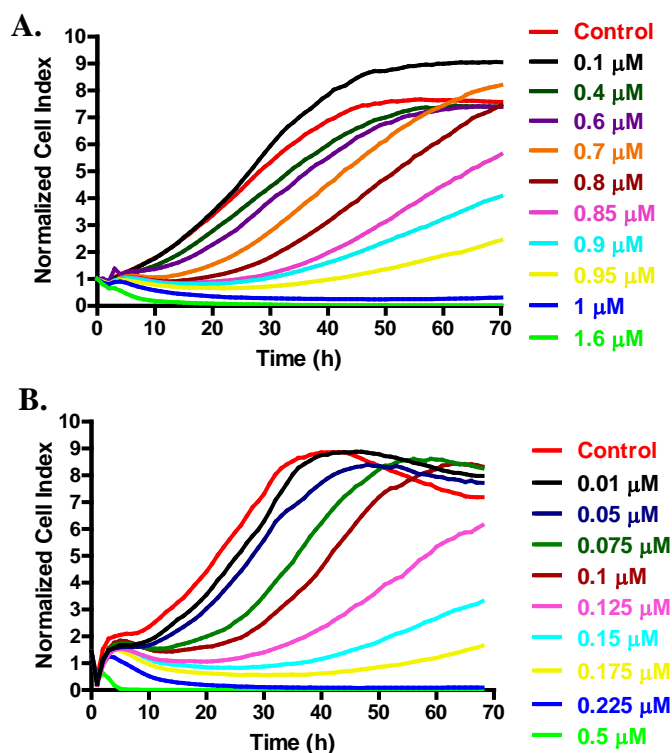


Figure 4.13: RTCA cytotoxicity profiles of the normalized cell index over time for A) A549 and B) T24 (x1.43) cells exposed to the trivalent organoarsenical, PAO(III). The CI scales were normalized using the multiplication factor (in parentheses) for easier visual analysis.

As is clear from the concentration range screened in each cell line, PAO(III) is a highly potent cytotoxicant, with a clear dose-response in the nM range. To quantitate this response, IC₅₀ values over time were determined using the data in Figure 4.13. To illustrate the significant gap in IC₅₀ values that were determined amongst the thirteen screened species of arsenic, Figure 4.14 shows the IC₅₀ values over time for the most potent cytotoxicant tested, PAO(III),

compared with inorganic As(III), and the low toxicity pentavalent organoarsenical, roxarsone, in both the A549 (Fig. 4.14A) and T24 (Fig. 4.14B) cell lines. Figure 4.14A in particular demonstrates this range, as the IC_{50} values for roxarsone are in the mM range, while the values for As(III) are in the μM , and the values for PAO(III) are in the nM range. Hence, Figure 4.14 clearly demonstrates that arsenic toxicity is strongly dependent upon the chemical species. This is further supported by the 24 h and 48 h IC_{50} values we determined for all thirteen species in A549 (Table 4.2) and T24 (Table 4.3) cells. The species are listed in each table based on increasing 24 h IC_{50} values.

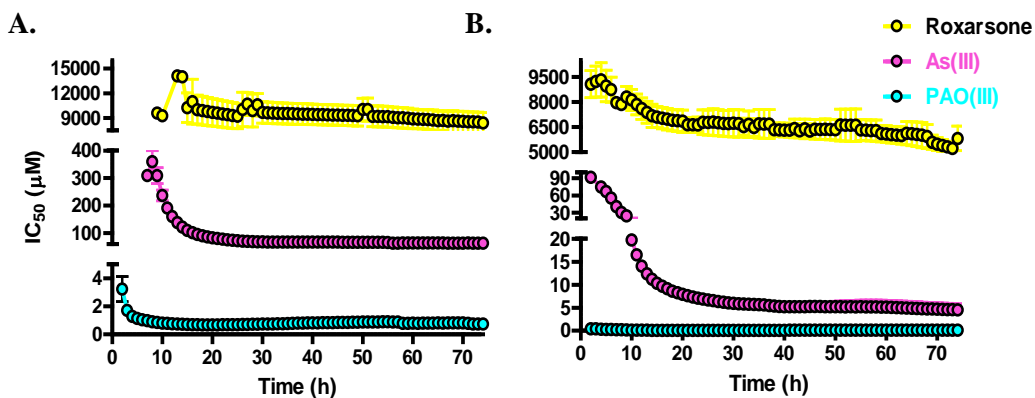


Figure 4.14: Temporal IC_{50} histograms of the hourly IC_{50} values ($\mu M \pm SEM$) for A) A549 and B) T24 cells exposed to PAO(III), inorganic As(III), and roxarsone.

4.4 Conclusions

RTCA cytotoxicity profiling has been demonstrated to be highly effective in arsenic cytotoxicity studies, as it is high-throughput (multiple cell lines screened with limited user manipulation), it revealed important kinetic information about cellular response, and allowed for the toxicity ranking of thirteen arsenic species to provide a comprehensive study on the cytotoxicity of key inorganic and organic arsenic species.

Using our IC_{50} histograms generated through RTCA cytotoxicity profiling, we can accurately rank the cytotoxicity of all thirteen arsenicals tested in each of the cell lines examined. In the A549 cell line, $PAO(III) > Arsenicin\ A > MAO(III) \approx MMA(III) \approx DMA(III) > DMAG \approx DMMTA > As(III) > MMTA > DMDTA \geq As(V) > Roxarsone > p\text{-Arsanilic\ Acid}$. In the T24 cell line, $PAO(III) > MAO(III) > MMA(III) > Arsenicin\ A > DMAG \approx DMA(III) \geq DMMTA \geq As(III) > MMTA > As(V) \geq DMDTA > p\text{-Arsanilic\ Acid} \approx Roxarsone$.

4.5 References

- [1] X.C. Le, X. Lu, M. Ma, W.R. Cullen, H.V. Aposhian, B. Zheng, *Anal. Chem.* 72 (2000) 5172-5177.
- [2] M. Styblo, Z. Drobna, I. Jaspers, S. Lin, D.J. Thomas, *Environ. Health Perspect.* 110 Suppl 5 (2002) 767-771.
- [3] U. Schuhmacher-Wolz, H.H. Dieter, D. Klein, K. Schneider, *Crit. Rev. Toxicol.* 39 (2009) 271-298.
- [4] T. Hayakawa, Y. Kobayashi, X. Cui, S. Hirano, *Arch. Toxicol.* 79 (2005) 183-191.
- [5] M. Styblo, S.V. Serves, W.R. Cullen, D.J. Thomas, *Chem. Res. Toxicol.* 10 (1997) 27-33.
- [6] S. Lin, W.R. Cullen, D.J. Thomas, *Chem. Res. Toxicol.* 12 (1999) 924-930.
- [7] M. Styblo, L.M. Del Razo, L. Vega, D.R. Germolec, E.L. LeCluyse, G.A. Hamilton, W. Reed, C. Wang, W.R. Cullen, D.J. Thomas, *Arch. Toxicol.* 74 (2000) 289-299.
- [8] X.C. Le, M. Ma, W.R. Cullen, H.V. Aposhian, X. Lu, B. Zheng, *Environ. Health Perspect.* 108 (2000) 1015-1018.
- [9] A.J. Percy, J. Gailer, *Bioinorg. Chem. Appl.* (2008) 539082.
- [10] R. Raml, A. Rumpler, W. Goessler, M. Vahter, L. Li, T. Ochi, K.A. Francesconi, *Toxicol. Appl. Pharmacol.* 222 (2007) 374-380.
- [11] H.R. Hansen, A. Raab, M. Jaspars, B.F. Milne, J. Feldmann, *Chem. Res. Toxicol.* 17 (2004) 1086-1091.
- [12] H. Naranmandura, N. Suzuki, K. Iwata, S. Hirano, K.T. Suzuki, *Chem. Res. Toxicol.* 20 (2007) 616-624.
- [13] T.S. Pinyayev, M.J. Kohan, K. Herbin-Davis, J.T. Creed, D.J. Thomas, *Chem. Res. Toxicol.* 24 (2011) 475-477.
- [14] I. Mancini, G. Guella, M. Frostin, E. Hnawia, D. Laurent, C. Debitus, F. Pietra, *Chemistry* 12 (2006) 8989-8994.
- [15] D. Lu, A.D. Rae, G. Salem, M.L. Weir, A.C. Willis, S.B. Wild, *Organometallics* 29 (2010) 32-33.

- [16] W.R. Chen, C.H. Huang, *J. Hazard. Mater.* 227-228 (2012) 378-385.
- [17] K.E. Nachman, P.A. Baron, G. Raber, K.A. Francesconi, A. Navas-Acien, D.C. Love, *Environ. Health Perspect.* 121 (2013) 818-824.
- [18] M. Leermakers, W. Baeyens, M. De Gieter, B. Smedts, C. Meert, H.C. De Bisschop, R. Morabito, P. Quevauviller, *Trends in Anal. Chem.* 25 (2006) 1-10.
- [19] V. Charoensuk, W.P. Gati, M. Weinfeld, X.C. Le, *Toxicol. Appl. Pharmacol.* 239 (2009) 64-70.
- [20] M. Xia, R. Huang, K.L. Witt, N. Southall, J. Fostel, M.H. Cho, A. Jadhav, C.S. Smith, J. Inglese, C.J. Portier, R.R. Tice, C.P. Austin, *Environ. Health Perspect.* 116 (2008) 284-291.
- [21] R.S. Judson, K.A. Houck, R.J. Kavlock, T.B. Knudsen, M.T. Martin, H.M. Mortensen, D.M. Reif, D.M. Rotroff, I. Shah, A.M. Richard, D.J. Dix, *Environ. Health Perspect.* 118 (2010) 485-492.
- [22] I.T. Millar, H. Heaney, D.M. Heinecky, C. Fernelius, *Inorg. Synthesis* 6 (1960) 113-115.
- [23] R.A. Zingaro, *Synthetic Meth. of Organometal. Inorg. Chem.* 3 (1996) 198-200.
- [24] W.R. Cullen, B.C. McBride, H. Manji, A.W. Pickett, J. Reglinski, *Appl. Organometal. Chem.* 3 (1989) 71-78.
- [25] I.T. Millar, *Inorg. Synthesis* 6 (1960) 116-118.
- [26] J.Z. Xing, L. Zhu, J.A. Jackson, S. Gabos, X.J. Sun, X.B. Wang, X. Xu, *Chem. Res. Toxicol.* 18 (2005) 154-161.
- [27] L. Vega, M. Styblo, R. Patterson, W. Cullen, C. Wang, D. Germolec, *Toxicol. Appl. Pharmacol.* 172 (2001) 225-232.
- [28] S. Hirano, X. Cui, S. Li, S. Kanno, Y. Kobayashi, T. Hayakawa, A. Shraim, *Arch. Toxicol.* 77 (2003) 305-312.
- [29] H.C. Chiang, T.C. Tsou, *Toxicol. In Vitro* 23 (2009) 897-905.
- [30] S. Talbot, R. Nelson, W.T. Self, *Br. J. Pharmacol.* 154 (2008) 940-948.
- [31] H. Naranmandura, M.W. Carew, S. Xu, J. Lee, E.M. Leslie, M. Weinfeld, X.C. Le, *Chem. Res. Toxicol.* 24 (2011) 1586-1596.

Chapter 5: Cellular Accumulation of Arsenic Species in Human Cell Lines and Conversion of Arsenic Species in Culture Media

5.1 Introduction

The toxic effects of arsenic both *in vivo* and *in vitro* are well-documented [1-4]. However, the exact mechanisms by which arsenic induces those observed effects are still under debate. Figure 5.1 presents some of the known interactions of arsenic with cellular components or processes resulting in toxicity [3]. As can be seen from this figure, the cellular interactions of arsenic are extensive. This can make the determination of the causes of observed cytotoxic responses very difficult. Nevertheless, one cellular process that is a key precondition for the induction of any cytotoxic effect by arsenic is cellular uptake. Hence, the examination of cellular uptake and accumulation is an important starting point for understanding arsenic-induced cytotoxic effects.

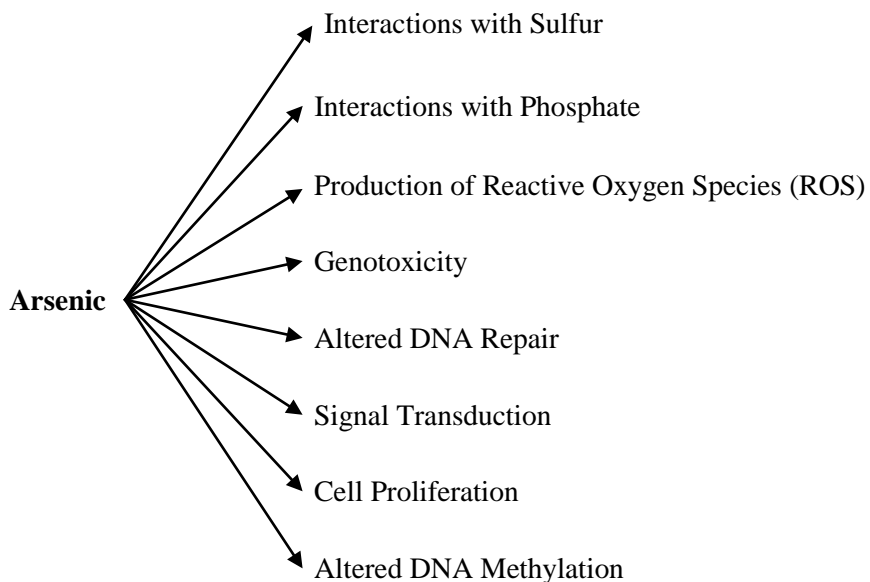


Figure 5.1: Proposed modes of action for arsenic. Adapted from Hughes et al. (2011) [3].

The cellular uptake of arsenic is a complex process that is dependent on cell type as well as the species of arsenic [5]. The difference in uptake of trivalent versus pentavalent species has long been known, and much of this difference is due to the ionization of these species at physiological pH (7.2) [4, 6]. The pKa value for inorganic arsenite [As(III)] is 9.2 and is therefore neutral at physiological pH. Conversely, as the pKa values for inorganic arsenate [As(V)] are 2.3, 6.7, and 11.6, As(V) is negatively charged at physiological pH. Neutral molecules easily penetrate cell membranes, and As(III) is readily taken up through aquaporins (AQP) 7/9, which transport neutral solutes [4, 7, 8]. As(V) is most likely taken up through phosphate transporters, which has also led to the suggestion that slower uptake of As(V) compared to As(III) is due to competition between As(V) and other oxyanions (such as phosphate) for transport, reducing As(V) uptake [4, 6]. Nevertheless, several studies have shown that trivalent arsenicals are much more efficiently taken up than (non-thiolated) pentavalent species into cells, and this difference in uptake is believed to be one of the major factors contributing to the observed differences in cytotoxicity between these species [5, 6, 9-11].

In Chapter 4, real-time cell analysis (RTCA) of the cytotoxicity of thirteen arsenic species revealed several interesting arsenic-induced cellular responses. One of these findings was the relative toxicity of Arsenicin A, the first known naturally-occurring polyarsenical. In three human cell lines, laboratory synthesized Arsenicin A produced significantly lower IC₅₀ values than inorganic As(III). Based on studies that have shown that cell uptake and retention play an

important role in the cytotoxicity of arsenic species, I hypothesize that the difference in cytotoxicity between Arsenicin A and As(III) may be due to differences in intracellular accumulation. Accumulation may also play an important role in the observed cell-dependent cytotoxicity of trivalent arsenicals in Chapter 4. In A549 cells, 24 h IC₅₀ values rank the cytotoxicity of As(III), MMA(III), and DMA(III) as MMA(III) \approx DMA(III) > As(III). In T24 cells, these species rank as MMA(III) > DMA(III) \approx As(III). I hypothesize that these differences are also influenced by intracellular accumulation.

Another interesting finding from Chapter 4 was the identification of a unique step-wise profile shape in the RTCA cytotoxicity profiles for several dimethylated arsenicals. One of the hypotheses for the cause of this unique profile shape observed in cells treated with DMA(III), DMAG(III), or DMMTA(V) was the chemical conversion of these species in cell culture media over time. The conversion of dimethylated trivalent species to the dimethylated pentavalent species in culture media would result in reduced cellular uptake and, hence, cytotoxicity. Thus, I hypothesize that the changes in cell index (CI) observed in Chapter 4 for the dimethylated arsenicals is due to the conversion of these arsenic species over time in culture media.

5.2 Materials and Methods

5.2.1 Cell Culture Conditions

The human lung carcinoma cell line, A549, (CCL-185; American Type Culture Collection (ATCC), Manassas, VA) was cultured in RPMI 1640 media (Gibco (Invitrogen), Burlington, ON, Canada). The human bladder carcinoma cell

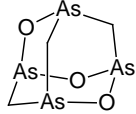
line, T24, (HTB-4; ATCC) was cultured in McCoy's 5A modified media (ATCC). Media was supplemented with 10% fetal bovine serum (Sigma-Aldrich, Oakville, ON, Canada) and 1% penicillin-streptomycin (Invitrogen, Burlington, ON, Canada). The incubation conditions were maintained at 37 °C, 5% CO₂, and 90% humidity. During the study, the cells were sub-cultured twice weekly into standard 10 cm x 20 mm cell culture dishes (Corning Incorporated, Corning, NY) containing fresh media, using 0.05% trypsin-EDTA (Invitrogen) for cell detachment.

5.2.2 Arsenic Solution Preparation

Solutions of As(III) and As(V) in deionized (DI) water were prepared from commercially available sodium arsenite and sodium arsenate (Sigma Chemical Co., St. Louis, MO). Solutions of MMA(III) and DMA(III) in DI water were prepared from synthesized standards of methyl-diiodoarsine and dimethyl-diiodoarsine, respectively [12-14]. Solutions of DMAG(III), DMMTA(V), and DMDTA(V) in DI water were also prepared from synthesized standards prepared in our laboratory. The solution of DMAG(III) in DI water also contained 2% methanol. Synthesized Arsenicin A stock was graciously provided by Dr. William Cullen at the University of British Columbia and contained 4% methanol. Table 5.1 presents a list of the above arsenic species, along with their chemical structure. Solutions were sterilized via filtration (0.22 µm) and the final concentration of arsenic in each solution was calibrated using HPLC coupled with ICP-MS (Agilent Technologies, Japan). As(III) and Arsenicin A solutions were

stored at 4 °C until use. All remaining arsenic solutions are unstable at 4 °C and had to be prepared fresh the day of treatment.

Table 5.1: Structures of Arsenic Species Studied in this Chapter

Arsenic Species	Abbrev.	Structure
Arsenite	As(III)	$\begin{array}{c} \text{OH} \\ \\ \text{HO}-\text{As}-\text{OH} \end{array}$
Dimethylarsenic glutathione	DMAG(III)	$\begin{array}{c} \text{CH}_3 \\ \\ \text{H}_3\text{C}-\text{As}-\text{SG} \end{array}$
Monomethylarsonous acid	MMA(III)	$\begin{array}{c} \text{OH} \\ \\ \text{H}_3\text{C}-\text{As}-\text{OH} \end{array}$
Dimethylarsinous acid	DMA(III)	$\begin{array}{c} \text{CH}_3 \\ \\ \text{H}_3\text{C}-\text{As}-\text{OH} \end{array}$
Arsenicin A	AA	
Arsenate	As(V)	$\begin{array}{c} \text{O} \\ \\ \text{HO}-\text{As}-\text{OH} \\ \\ \text{OH} \end{array}$
Dimethylmonothioarsinate	DMMTA(V)	$\begin{array}{c} \text{S} \\ \\ \text{H}_3\text{C}-\text{As}-\text{OH} \\ \\ \text{CH}_3 \end{array}$
Dimethyldithioarsinate	DMDTA(V)	$\begin{array}{c} \text{S} \\ \\ \text{NaS}-\text{As}-\text{CH}_3 \\ \\ \text{CH}_3 \end{array}$

5.2.3 Cellular Accumulation of Arsenic

Cells were seeded into standard 6-well culture dishes (Greiner BioOne, Oakville, ON, Canada) at concentrations that had previously been determined to allow the cells to reach 50-60% confluency after 18-24 h growth. A549 cells were

seeded at a density of 4.5×10^4 cells mL^{-1} and T24 cells at 4.0×10^4 cells mL^{-1} . When the cells had reached the proper confluency, the As(III), Arsenicin A, MMA(III), and DMA(III) solutions described above were serially diluted in media to produce the desired treatment concentrations based on the 24 h IC_{50} determinations described in Chapter 4 (Tables 4.2 and 4.3). The 24 h IC_{50} value determined using RTCA analysis for As(III) was $76.6 \mu\text{M}$, while the 24 h IC_{50} value determined using RTCA analysis for this specific solution of Arsenicin A standard was $3.5 \mu\text{M}$ [N.B. this solution is not the same Arsenicin A standard solution as in Chapter 4]. The following concentration treatments were prepared for Arsenicin A and As(III) in A549 cells: IC_{50} , $\frac{1}{2} \text{IC}_{50}$, and $\frac{1}{4} \text{IC}_{50}$. The following concentrations were prepared for MMA(III) and DMA(III) in A549 cells and for As(III), MMA(III), and DMA(III) in T24 cells: IC_{50} and $\frac{1}{2} \text{IC}_{50}$. The old media in each well was aspirated and replaced with the treated media, with triplicate wells prepared for each concentration. Non-treated control wells (without arsenic treatment) were also prepared in triplicate. Cells were incubated for 24 h.

After 24 h exposure, cells were washed twice with phosphate buffered saline (PBS; Gibco), detached using 0.05% trypsin-EDTA, and suspended in fresh media. Cells were pelleted by centrifugation at 1700 rpm for 3 min and washed with ice-cold PBS. The cells were then counted using a hemocytometer. After pelleting again at 1000 rpm for 10 min, the PBS was carefully aspirated to avoid disturbing the pellet. The cell pellets were then resuspended in 2% HNO_3 (Fisher Scientific, Nepean, ON, Canada) and sonicated in a water sonicator (Fisher

Scientific) for 30 min for lysis. After pelleting the now lysed cells at 2500 rpm for 30 min, the supernatant (containing the intracellular components) was carefully collected to avoid disturbing the pellet and placed into a fresh 0.5 mL microcentrifuge tube (Fisher Scientific). Because these samples were prepared for total arsenic analysis, samples were parafilmed and stored at 4 °C until analysis by ICP-MS.

5.2.4 Conversion of Arsenic over Time in Culture Media

Cells were seeded into standard 96-well culture dishes (Corning) at concentrations that had previously been determined to allow the cells to reach 50-60% confluency after 18-24 h growth. A549 cells were seeded at a density of 4.5×10^4 cells mL⁻¹. When the cells had reached the proper confluency (60-70%), the As(III), DMAG(III), MMA(III), DMA(III), As(V), DMMTA(V), and DMDTA(V) solutions described above were serially diluted in media to produce the desired treatment concentrations based on the 24 h IC₅₀ values for A549 cells that have been described in Chapter 4 (Table 4.2). The 24 h IC₅₀ values determined using RTCA analysis were: 74.2 μM for As(III), 23 μM for DMAG, 13.6 μM for MMA(III), 14.1 μM for DMA(III), 1.4 mM for As(V), 20.5 μM for DMMTA(V), and 4.3 mM for DMDTA(V). Due to the available quantity of DMDTA(V) standard, a treatment concentration of only $\frac{1}{4}$ IC₅₀ (1.05 mM) was prepared. An aliquot of 326 μL of each treatment concentration was added to 24 wells so that 150 μL could be separately collected from 3 wells at each of the 8 post-exposure timepoints. Similarly, an aliquot of 326 μL of each treatment concentration was added to 8 control wells that contained no cells so that an

aliquot of 150 μL could be collected from one well at each of 8 post-exposure timepoints. The selected timepoints for analysis were at the time of treatment (0 h) and at 3, 6, 9, 12, 24, 26, 48, and 56 h post-exposure.

High-performance liquid chromatography (HPLC) (Agilent 1100 series; Agilent Technologies, Germany) separation of arsenic species was performed on a Prodigy™ ODS-3 column (3 μm particle size, 100 \AA , 100 x 4.6 mm; Phenomenex, USA). The mobile phase was prepared as follows: 5 mM tetrabutylammonium hydroxide (TBA), 200 mM malonic acid (MA), and 5% methanol, with the pH adjusted to 5.85. The flow rate was maintained at 1.2 mL min^{-1} for the entire 6 min. The column temperature was maintained at 50 $^{\circ}\text{C}$. The injection volume was 30 μL . An Agilent 7500cs ICP-MS was used as the detector, and arsenic was measured at 75 m/z.

5.3 Results and Discussion

5.3.1 Cellular Accumulation of Arsenic

5.3.1.1 Arsenicin A and As(III) in A549 Cells

One of the key findings in Chapter 4 was the identification of the high cytotoxicity of the novel synthesized polyarsenical, Arsenicin A. The toxicity of this compound in human cell lines was previously unknown. Table 5.2 shows the 24 and 48 h IC_{50} values for Arsenicin A and As(III) determined for the three cell lines screened, A549, T24, and HepG2. The IC_{50} values for Arsenicin A are significantly lower than the IC_{50} values for As(III), particularly in the A549 and HepG2 cell lines. Here, the IC_{50} values are an order of magnitude lower. We suspect this difference in cytotoxicity may be due to a difference in arsenic

accumulation. In addition, because the amount of data regarding the toxicological properties of Arsenicin A is poor, this information will be of particular importance in future toxicity studies.

Table 5.2: IC₅₀ Values for Human Cell Lines Exposed to As(III) and Arsenicin A

		As(III)	Arsenicin A
A549	24 h	74.2 ± 4.1	7.3 ± 0.43
	48 h	67.1 ± 3.1	8.5 ± 0.25
T24	24 h	6.9 ± 0.52	3.6 ± 0.24
	48 h	5.2 ± 1.0	3.6 ± 0.36
HepG2	24 h	91.9 ± 2.4	3.5 ± 0.23
	48 h	51.5 ± 12.7	2.9 ± 0.14

N.B. Values expressed as $\mu\text{M} \pm \text{SEM}$

Due to the large difference in dose range in which Arsenicin A (1-15 μM) and As(III) (40-250 μM) exert their cytotoxicity in A549 cells (Fig. 4.10), it was determined that a comparison of arsenic accumulation should be based on IC₅₀ values, and not on equal concentration, as an equal concentration of Arsenicin A or As(III) would either result in unacceptable levels of cell death (Arsenicin A) or intracellular concentrations of arsenic below the level of detection with ICP-MS [As(III)]. Hence, the concentrations determined for dosing were based on the 24 h IC₅₀ values (cell survival $\geq 50\%$). Table 5.3 shows the concentration of total intracellular arsenic determined by ICP-MS analysis in the cell lysate of A549 cells exposed to Arsenicin A for 24 h. To normalize the data by the number of cells contributing to the total intracellular arsenic, the data has been expressed as arsenic (As) atoms cell⁻¹. It is clear that as the concentration of Arsenicin A in the treatment media increases, so does the concentration of As atoms cell⁻¹.

Table 5.3: Concentrations of Total Arsenic in A549 Cells after 24 h Arsenicin A (AA) Exposure

	[AA]	Equivalent [As]	Number of cells	As atoms cell ⁻¹
Control	0.3 μM	1.2 μM	26.3 ± 3.6 x 10 ⁴	0.6 ± 0.1 x 10 ⁶
¼ IC₅₀	0.9 μM	3.5 μM	24.4 ± 3.4 x 10 ⁴	77 ± 5 x 10 ⁶
½ IC₅₀	1.8 μM	7.1 μM	19.2 ± 2.1 x 10 ⁴	313 ± 23 x 10 ⁶
IC₅₀	3.5 μM	14.1 μM	13.6 ± 4.0 x 10 ⁴	986 ± 150 x 10 ⁶

Table 5.4 shows the concentration of total intracellular arsenic determined by ICP-MS analysis in the cell lysate of A549 cells exposed to As(III) for 24 h. Again, to normalize the data by the number of cells contributing to the total intracellular arsenic, the data has been expressed as As atoms cell⁻¹. Compared to the data in Table 5.3, it is clear that at the respective IC₅₀ values (and fractions there of) for each species, there were more As atoms cell⁻¹ present in A549 cells exposed to Arsenicin A than As(III).

Table 5.4: Concentrations of Total Arsenic in A549 Cells after 24 h As(III) Exposure

	[As(III)]	Number of cells	As atoms cell ⁻¹
Control	1 μM	26.4 ± 3.5 x 10 ⁴	0.4 ± 0.1 x 10 ⁶
¼ IC₅₀	19.2 μM	22.0 ± 4.4 x 10 ⁴	3 ± 1 x 10 ⁶
½ IC₅₀	38.3 μM	19.3 ± 1.3 x 10 ⁴	59 ± 21 x 10 ⁶
IC₅₀	76.6 μM	12.7 ± 2.8 x 10 ⁴	255 ± 9 x 10 ⁶

To better compare the differences in intracellular accumulation of these species, Table 5.5 shows the concentration of total intracellular arsenic determined by ICP-MS analysis of A549 cells exposed to either Arsenicin A or

As(III) for 24 h. Here, the data is also expressed as the number of arsenic molecules cell⁻¹. Although A549 cells were treated with concentrations of As(III) nearly 20 times larger than the concentrations of Arsenicin A, the same number of molecules of each species were detected on a per cell basis. However, as a single molecule of Arsenicin A contains four arsenic atoms compared to the one arsenic atom present in each molecule of As(III) (Table 5.1), it is clear that A549 cells treated with Arsenicin A accumulate four times as many arsenic atoms per cell than A549 cells treated with As(III) even when treated with a fraction of the concentration (e.g. 3.5 μM vs. 76.6 μM). Thus, these results suggest that intracellular accumulation of arsenic plays a key role in the observed difference in cytotoxicity of Arsenicin A compared to As(III) in human cell lines. The observed increase in cytotoxicity of Arsenicin A is likely due to the higher intracellular concentration of arsenic atoms present, although it is unknown why Arsenicin A is more readily taken up and/or retained.

Table 5.5: Concentrations of Total Arsenic in A549 cells after 24 h Exposure

		Arsenic (μM)	Molecules cell⁻¹ (×10⁶)	As atoms cell⁻¹ (×10⁶)
¼ IC₅₀	AA	0.9	19 ± 1	77 ± 5
	As ^{III}	19.2	3 ± 1	3 ± 1
½ IC₅₀	AA	1.8	78 ± 6	313 ± 23
	As ^{III}	38.3	59 ± 21	59 ± 21
IC₅₀	AA	3.5	247 ± 38	986 ± 150
	As ^{III}	76.6	255 ± 9	255 ± 9

5.3.1.2 As(III), MMA(III), and DMA(III) in A549 and T24 Cells

Cytotoxicity ranking of the trivalent arsenicals by 24 h IC₅₀ values determined using RTCA analysis in Chapter 4 indicated cell-dependent cytotoxicity for A549 and T24 cells. While the cytotoxicity of MMA(III) [13.6 μM] ≈ DMA(III) [14.1 μM] > As(III) [76.6 μM] in A549 cells, the cytotoxicity of MMA(III) [1.9 μM] > DMA(III) [6.4 μM] ≈ As(III) [6.9 μM] in T24 cells. Methylated trivalent arsenicals are generally considered to be more cytotoxic than inorganic arsenic, which is what was observed in the A549 cell line. However, it was interesting that in T24 cells, As(III) was equally as cytotoxic as DMA(III). Hence, the determination of differences in intracellular accumulation may help explain the difference in observed cytotoxicity between A549 and T24 cells.

Table 5.6 shows the concentration of total intracellular arsenic determined by ICP-MS analysis of A549 and T24 cells exposed to MMA(III), DMA(III), or As(III) for 24 h. Here, the data is expressed as the number of arsenic (As) atoms cell⁻¹. The data suggests that A549 and T24 cells are capable of accumulating equal concentrations of MMA(III), as the concentrations of intracellular arsenic were similar in each cell line at around 40x10⁶ As atoms cell⁻¹. However, the concentration of MMA(III) present in the cell culture media of the A549 cells was nearly seven times higher than the media of the T24 cells. This suggests that T24 cells are capable of more efficient uptake and/or retention of MMA(III). This is consistent with the lower IC₅₀ values for MMA(III) in T24 cells (1.9 μM) compared to A549 cells (13.6 μM) determined with RTCA analysis. Enhanced uptake and/or retention of MMA(III) would result in increased cytotoxicity.

Table 5.6: Concentrations of Total Arsenic in A549 and T24 Cells after 24 h Arsenical Exposure

	A549			T24	
		[As]	As atoms cell ⁻¹ (x 10 ⁶)	[As]	As atoms cell ⁻¹ (x 10 ⁶)
Control	---	---	2.2 ± 0.7	---	1.5 ± 0.6
MMA(III)	IC ₅₀	13.6 μM	36 ± 3	1.9 μM	40 ± 5
	½ IC ₅₀	6.8 μM	6.8 ± 0.6	0.95 μM	5.3 ± 0.4
DMA(III)	IC ₅₀	14.1 μM	80 ± 7	6.4 μM	44 ± 15
	½ IC ₅₀	7.05 μM	23 ± 4	3.2 μM	22 ± 6
As(III)	IC ₅₀	76.6 μM	255 ± 9	6.9 μM	435 ± 43
	½ IC ₅₀	38.3 μM	59 ± 21	3.45 μM	114 ± 9.3

N.B. [As] represents the treatment concentrations for each cell line (IC₅₀ and ½ IC₅₀ Values)
 Values represented as ± SEM (n=3)

While the concentration of As atoms cell⁻¹ for cells treated with MMA(III) were similar in both cell lines, the concentration of As atoms cell⁻¹ for cells treated with DMA(III) were not. A549 cells contained nearly 80x10⁶ As atoms cell⁻¹ after 24 h treatment with DMA(III), while T24 cells contained roughly half that concentration at 44x10⁶ As atoms cell⁻¹ (Table 5.6). However, this is consistent with the concentration of DMA(III) present in the respective culture media, as T24 cells (6.4 μM) were treated with roughly half the concentration of DMA(III) used to treat A549 cells (14.1 μM). Hence, accumulation of DMA(III) in these two cell lines appears to correlate with the concentration of DMA(III) present in the media at the time of treatment, indicating similar accumulation of DMA(III) in A549 and T24 cells.

Table 5.6 also shows the concentrations of As atoms cell⁻¹ for A549 and T24 cells treated with As(III) for 24 h. The concentration of As atoms cell⁻¹ in treated T24 cells (435x10⁶ As atoms cell⁻¹) was almost twice the concentration cell⁻¹ found in treated A549 cells (255x10⁶ As atoms cell⁻¹). Hence, the accumulation of As(III) appears to be higher in T24 cells than in A549 cells. This difference becomes even more apparent when the concentration of As(III) present in the respective media used to treat the cells is considered. A549 cells were treated with 76.6 μM, which is 10 times the concentration of As(III) used to treat T24 cells (6.9 μM). Thus, T24 cells are capable of much more efficient uptake and/or retention of As(III) than A549 cells, as the concentration of As atoms cell⁻¹ was significantly higher. This is consistent with the observed difference in cytotoxicity of As(III) in A549 and T24 cells, where the 24 h IC₅₀ value for

As(III) in T24 cells is an order of magnitude less than the corresponding value in A549. The enhanced uptake and/or retention of As(III) in T24 cells also helps to explain the observed similarity in cytotoxicity of inorganic As(III) compared to the methylated trivalent arsenicals, particularly DMA(III).

While our intracellular accumulation findings are consistent with the observed cell-dependent cytotoxicity in A549 and T24 cells exposed to trivalent arsenicals, an important distinction must be made concerning the ability of these cells to methylate inorganic arsenic. Studies have shown that methylation of inorganic arsenic is an important step in arsenic metabolism to promote detoxification and/or elimination, as observed in the proposed pathways of inorganic arsenic methylation discussed in Chapter 1 (Figure 1.5) [15, 16]. A549 cells, derived from a human alveolar adenocarcinoma, have been shown to express arsenic(+3 oxidation state)-methyltransferase (As3MT), which catalyzes the oxidative methylation of As(III) [17]. T24 cells, derived from a human urinary bladder carcinoma, on the other hand, lack the ability to methylate inorganic As(III) [18]. Hence, the difference in observed cytotoxicity of As(III) in T24 and A549 cells may also be influenced by the inability of T24 cells to methylate As(III), resulting in the higher cytotoxicity observed for the trivalent arsenicals in this cell line.

5.3.2 Conversion of Arsenic over Time in Culture Media

Another important finding from Chapter 4 of this thesis was the unique step-wise profiles of the dimethylated arsenicals (Figs. 4.4, 4.6, 4.8). We hypothesized this may be due to the conversion of the trivalent species to

pentavalent species. An increasing presence of pentavalent species in the culture media would affect the uptake of arsenic into cells, reducing the observed cytotoxicity. In addition to the dimethylated trivalent arsenicals, DMA(III) and DMAG(III), we also examined the trivalent arsenicals As(III) and MMA(III) for comparison. Likewise, in addition to the dimethylated pentavalent arsenicals, DMMTA(V) and DMDTA(V), we also examined the pentavalent inorganic arsenical, As(V). Figure 5.2 shows the chromatograms from the HPLC-ICP-MS analyses of As(III) in cell culture media at all nine timepoints investigated. From this data, it is clear that As(III) is fairly stable in cell culture media, as there is little conversion of trivalent As(III) to pentavalent As(V). However, by 24 h, there is a small As(V) peak present in the chromatogram, indicating that there is some conversion of As(III) over time.

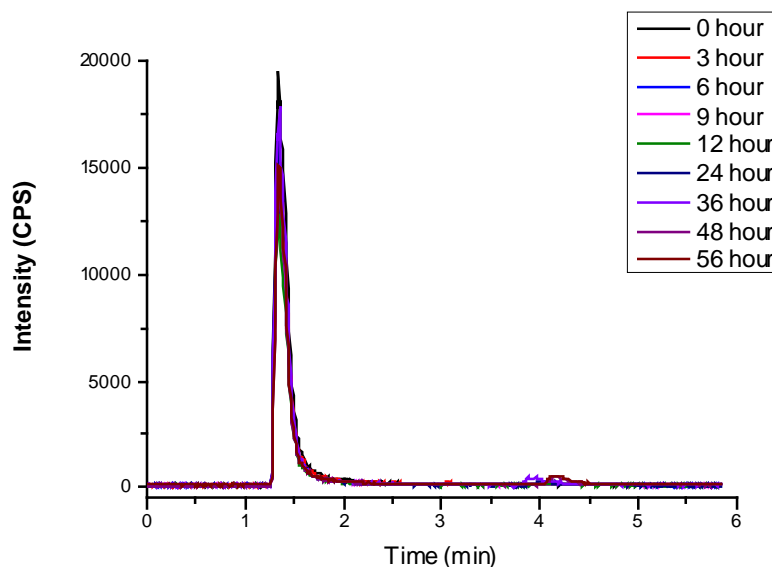


Figure 5.2: Chromatograms showing the speciation analysis for the As(III) samples collected at all nine timepoints. By 24 h, there is a small As(V) peak present, indicating some conversion of As(III) to As(V) in culture media.

Figure 5.3A shows the concentrations of As(III) and As(V) present in the As(III) treated culture media over time determined from HPLC-ICP-MS analyses. As(III) is fairly stable in cell culture media, as the concentration of As(III) present in the media changes little over time. This is consistent with the RTCA cytotoxicity profile for A549 cells exposed to As(III), as seen in Figure 5.3B. Here, the changes in CI over time vary little over the exposure period, particularly for the concentrations around the 24 h IC₅₀ value (70 μ M and 80 μ M), where the values almost appear static. Hence, with little conversion of As(III) to As(V), there should be little change in observed cytotoxicity, as the same concentration of As(III) is capable of exerting the same effects over the exposure period.

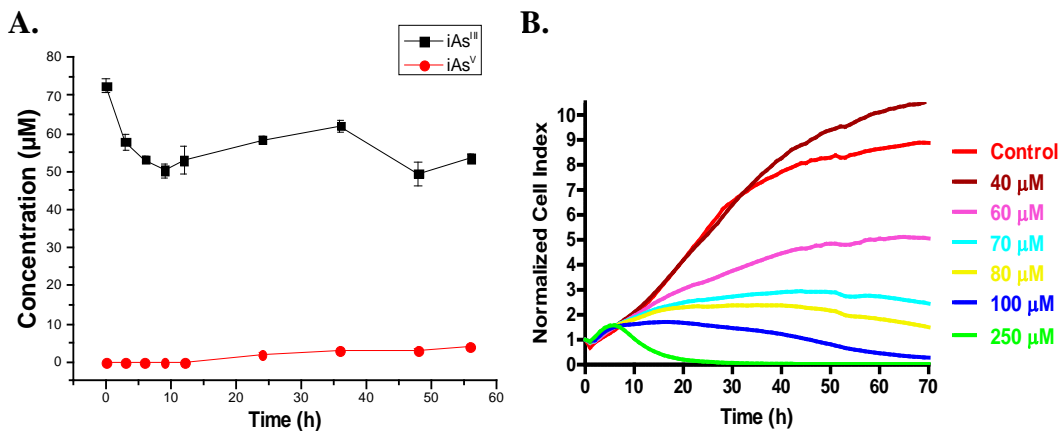


Figure 5.3: A) Concentrations of As(III) and As(V) detected in cell culture media over time by HPLC-ICP-MS analyses. B) RTCA profile of the normalized CI over time for A549 cells treated with As(III).

The chromatograms from HPLC-ICP-MS analyses of MMA(III) in cell culture media at all nine timepoints investigated can be seen in Figure 5.4. Here, conversion of MMA(III) to MMA(V) in the culture media occurs throughout the

exposure period, as there is a distinct peak for MMA(V) present at all timepoints except for time 0 h.

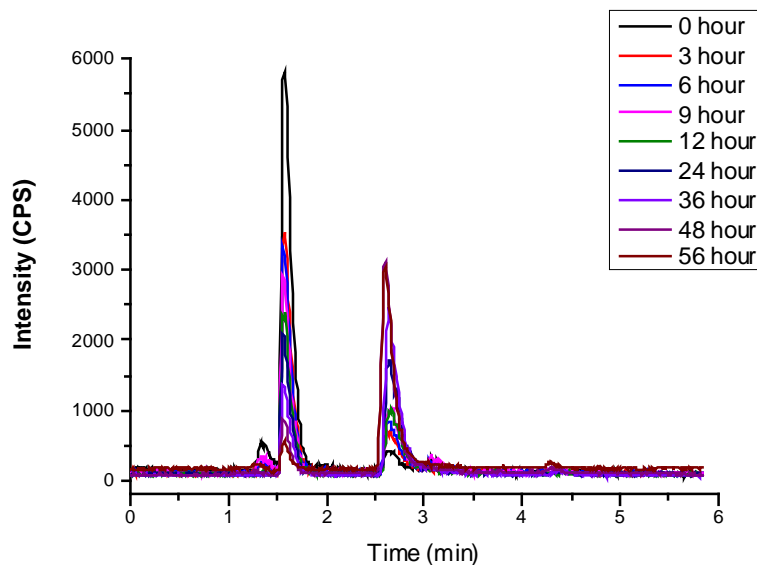


Figure 5.4: Chromatograms showing the speciation analysis for the MMA(III) samples collected at all nine timepoints. By 3 h, there is a small MMA(V) peak present, indicating conversion of MMA(III) to MMA(V) in culture media. The MMA(V) peak continues to increase in area over the exposure period, as the peak area for MMA(III) decreases.

The concentrations of MMA(III) and MMA(V) present in the MMA(III) treated culture media over time determined from HPLC-ICP-MS analyses are found in Figure 5.5A. It is also clear from this figure that conversion of MMA(III) to MMA(V) occurs throughout the exposure period. The conversion of MMA(III) to MMA(V) not only begins immediately, as there is a small amount of MMA(V) detected at 0 h, but the conversion of the trivalent to pentavalent species is complete, as there is no MMA(III) detected by 48-56 h. This is consistent with the RTCA cytotoxicity profile for A549 cells exposed to MMA(III), as seen in Figure 5.5B. Here, the concentrations around the 24 h IC_{50} value (12 μ M and 15 μ M) initially exhibit little change in CI for the first 10-20 h exposure, but then the CI

values begin to increase over time, indicating reduced cytotoxicity. As MMA(V) is known to be far less cytotoxic than MMA(III), the increase in CI values is consistent with the decreasing presence of MMA(III) and the concomitant increase in MMA(V) present in the culture media.

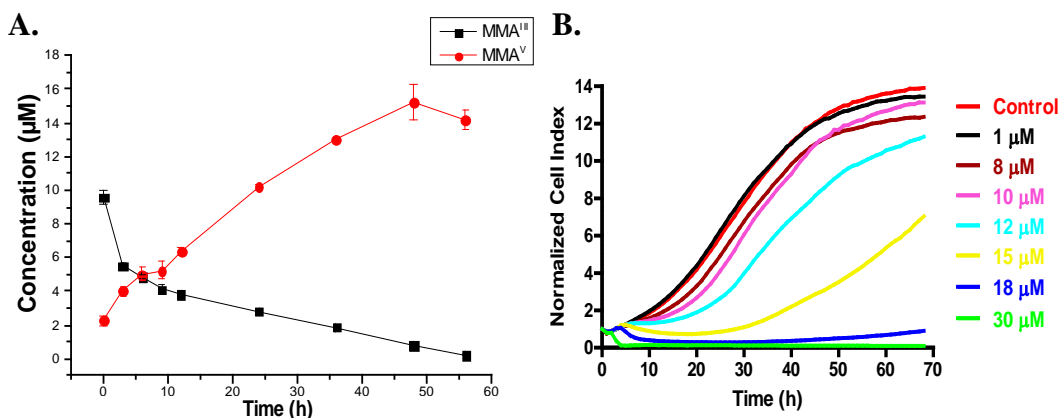


Figure 5.5: A) Concentrations of MMA(III) and MMA(V) detected in cell culture media over time by HPLC-ICP-MS analyses. B) RTCA profile of the normalized CI over time for A549 cells treated with MMA(III).

Figure 5.6 shows the chromatograms from the HPLC-ICP-MS analyses of DMA(III) in cell culture media at the first five timepoints investigated. It is clear that DMA(III) is highly unstable in cell culture media, as the peak for DMA(III) is gone by 9 h, with complete conversion of DMA(III) to DMA(V) by this point. The only clearly visible peak for DMA(III) is present at 0 h.

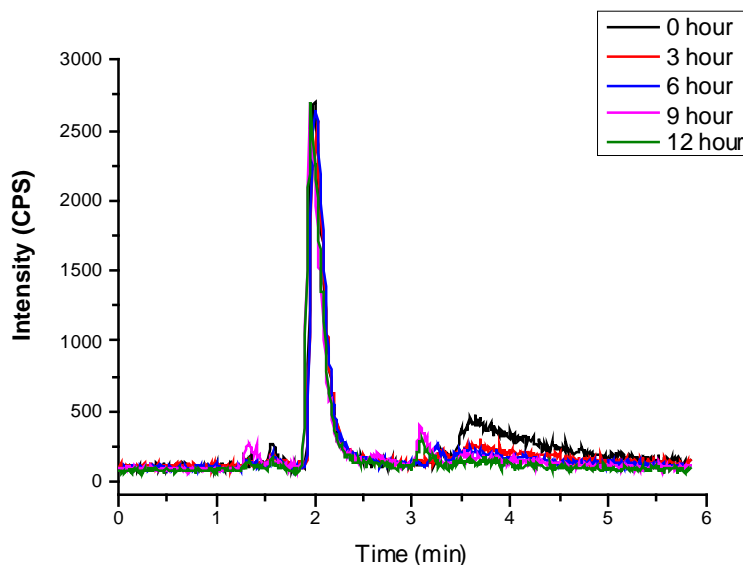


Figure 5.6: Chromatograms showing the speciation analysis for the DMA(III) samples collected at the first five timepoints. There is clear, rapid conversion of DMA(III) to DMA(V) in culture media, as the DMA(III) peak is not visible by 9 h.

Figure 5.7A shows the concentrations of DMA(III) and DMA(V) present in the DMA(III) treated culture media over time determined from HPLC-ICP-MS analyses. DMA(III) conversion to DMA(V) is rapid and complete, as there is no detectable concentration of DMA(III) present by 9 h. This is consistent with the RTCA cytotoxicity profile for A549 cells exposed to DMA(III), as seen in Figure 5.7B. Here, the concentrations around the 24 h IC_{50} value ($10 \mu\text{M}$ and $15 \mu\text{M}$) initially exhibit little change in CI for the first 10-20 h exposure, but then the CI values begins to increase more visibly over time, indicating reduced cytotoxicity. As DMA(V) is known to be far less cytotoxic than DMA(III), the increase in CI values is consistent with the decreasing presence of DMA(III) and the concomitant increase in DMA(V) present in the culture media.

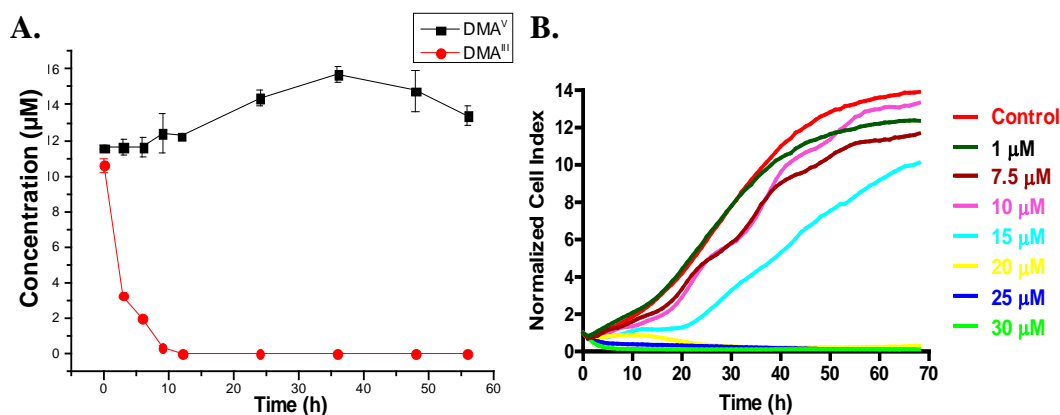


Figure 5.7: A) Concentrations of DMA(III) and DMA(V) detected in cell culture media over time by HPLC-ICP-MS analyses. B) RTCA profile of the normalized CI over time for A549 cells treated with DMA(III).

The chromatograms from the HPLC-ICP-MS analyses of DMAG(III) in cell culture media at all nine timepoints investigated are found in Figure 5.8. DMAG(III) conversion to DMA(V) in the culture media occurs throughout the exposure period, as there is a distinct peak for DMA(V) present at all timepoints, with the complete conversion of DMAG(III) to DMA(V) by 36 h. Interestingly, this trend is more consistent with the chromatograms in Figure 5.4 for the monomethylated trivalent species, MMA(III), than the chromatograms in Figure 5.6 for the dimethylated trivalent species, DMA(III). As DMA(III) and DMAG(III) are both dimethylated trivalent arsenic species, it was assumed that they would have a similar trend in conversion to DMA(V). Hence, the presence of the glutathione group must stabilize this species in culture media compared to DMA(III).

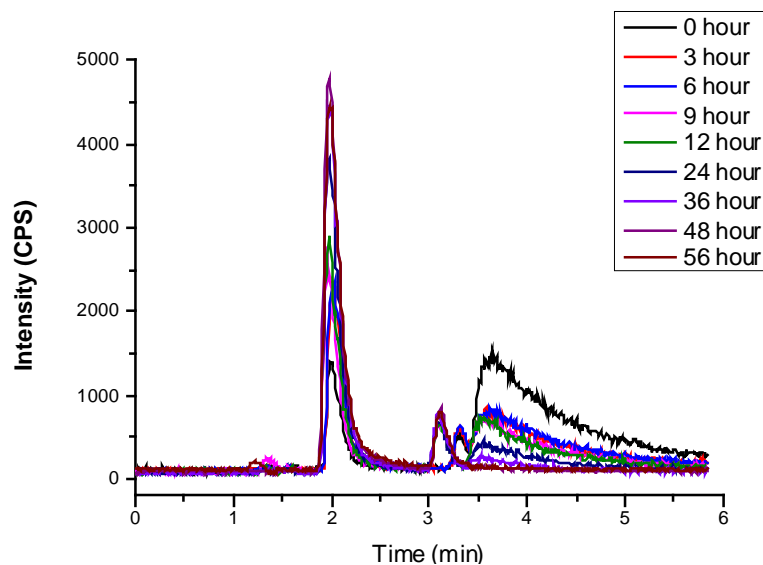


Figure 5.8: Chromatograms showing the speciation analysis for the DMAG(III) samples collected at all nine timepoints. At 0 h, there is a small DMA(V) peak present, indicating conversion of DMAG(III) to DMA(V) in culture media. The DMA(V) peak continues to increase in area over the exposure period, as the peak area for DMAG(III) decreases.

The concentrations of DMAG(III) and DMA(V) present in the DMAG(III) treated culture media over time determined from HPLC-ICP-MS analyses can be seen in Figure 5.9A. As was also observed in Figure 5.8, DMAG(III) conversion to DMA(V) occurs throughout the exposure period, with a small concentration of DMA(V) present at 0 h and complete conversion by 36 h. This rate of conversion is faster than that observed in the MMA(III) culture media, where complete conversion to MMA(V) occurred by 56 h. This is consistent with the RTCA cytotoxicity profile for A549 cells exposed to DMAG(III), as seen in Figure 5.9B. The concentrations around the 24 h IC_{50} value (20-30 μ M) initially exhibit little change in CI for the first 10-20 h exposure, but then the CI values begin to increase over time, indicating reduced cytotoxicity. Hence, the increase in CI

values is consistent with the decreasing presence of DMAG(III) and the increasing presence of DMA(V), as DMA(V) is less cytotoxic than DMAG(III).

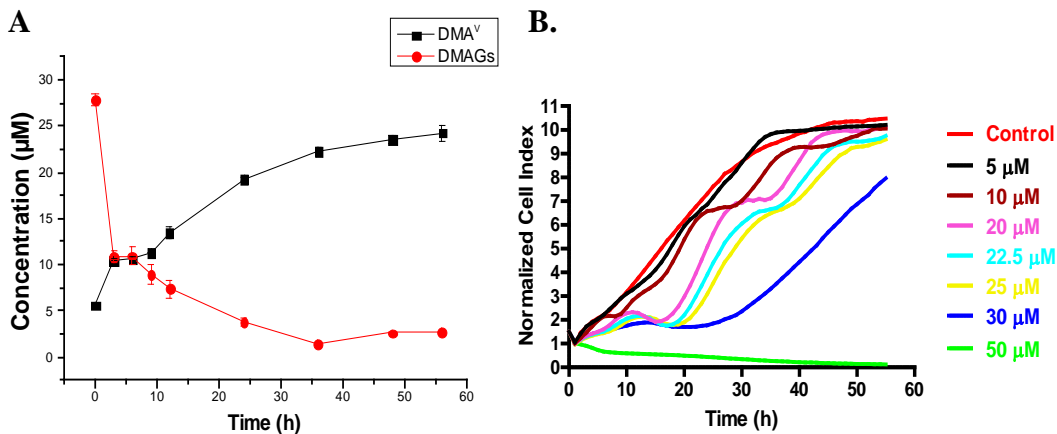


Figure 5.9: A) Concentrations of DMAG(III) and DMA(V) detected in cell culture media over time by HPLC-ICP-MS analyses. B) RTCA profile of the normalized CI over time for A549 cells treated with DMAG(III).

Figure 5.10 shows a chromatogram from HPLC-ICP-MS analyses of As(V) in cell culture media at 48 h, the last timepoint investigated. From here, it is clear that As(V) is highly stable in cell culture media. The As(V) peak was the only peak observed in any of the derived chromatograms, indicating there was no conversion of As(V) in media during any point of the investigated time period.

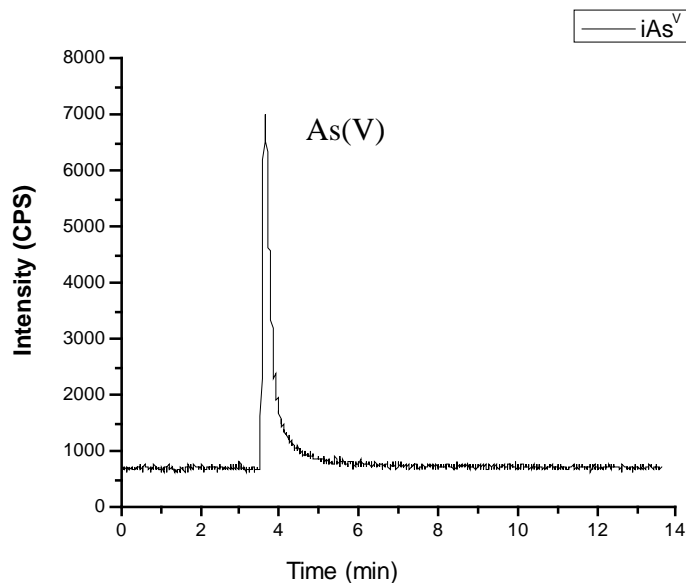


Figure 5.10: HPLC-ICP-MS chromatogram showing the speciation analysis for the As(V) samples collected at the final timepoint, 48 h, indicating that As(V) is highly stable in cell culture media.

The quantification of As(V) in the cell culture media over time can be seen in Figure 5.11A. Again, it is clear that As(V) is highly stable in culture media, as the concentration of As(V) in the culture media is unchanged over the exposure period. This is consistent with the RTCA cytotoxicity profile for A549 cells exposed to As(V), as seen in Figure 5.11B. As observed in the cytotoxicity profile for A549 cells treated with As(III) (Fig. 5.3B), the changes in CI over time vary little over the exposure period for the concentrations of As(V) around the 24 h IC₅₀ value (1.125 - 1.5 mM), where the values almost appear static. Hence, with no conversion of As(V), there should be little change in observed cytotoxicity over the exposure period..

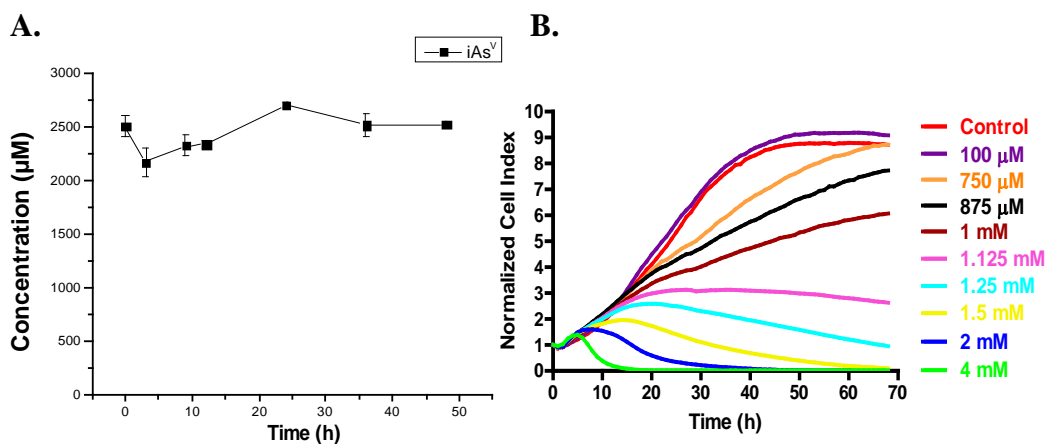


Figure 5.11: A) Concentration of As(V) detected in cell culture media over time by HPLC-ICP-MS analyses. B) RTCA profile of the normalized CI over time for A549 cells treated with As(V).

Figure 5.12 shows the chromatograms from HPLC-ICP-MS analyses of DMMTA(V) in cell culture media at eight timepoints investigated. The analysis of DMMTA(V) conversion in culture media was complicated by two factors. The first factor being that the synthesized standard of DMMTA(V) provided for these experiments and for those in Chapter 4, is not 100% pure. Hence, the presence of other species of arsenic within the standard makes the analysis of DMMTA(V)-mediated effects difficult. The second factor making these analyses difficult, particularly for HPLC-ICP-MS analysis is the lack of a DMMTA(V) standard for comparison. As there is no DMMTA(V) standard available to compare peak retention times, the identity of the peaks on the chromatograms from HPLC-ICP-MS analysis cannot be confirmed. Nevertheless, the identity of the peaks can be tentatively determined by analysis of retention time, and from Figure 5.12, it is clear that DMMTA(V) conversion over time in culture media is occurring throughout the exposure period. Peak 1 has the same retention time as DMA(V), peak 3 the same as DMA(III), and peak 4 has the same retention time as

DMDTA(V). Hence, peak 2 is most likely that of the DMMTA(V). Peaks 1, 2, and 4 were present at every timepoint over the exposure period. Peak 3 was highest at time 0 h, but was gone by 9 h, consistent with the presence of the unstable arsenical, DMA(III), in the culture media.

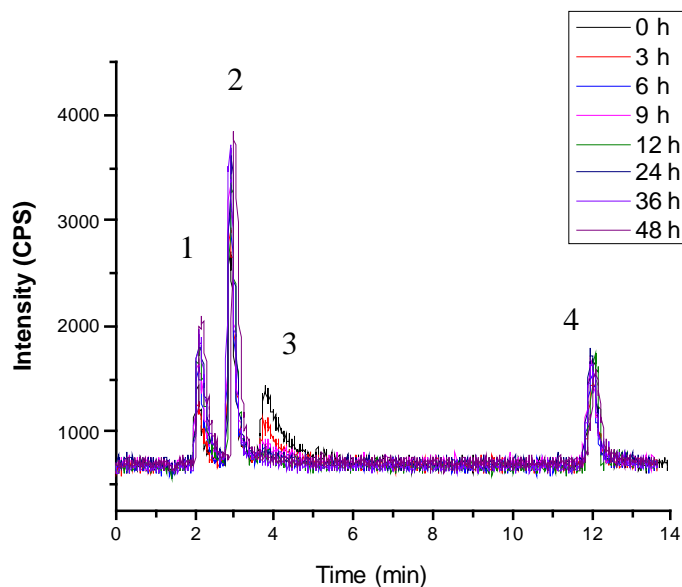


Figure 5.12: HPLC-ICP-MS chromatograms showing the speciation analysis for the DMMTA(V) samples collected at eight timepoints. The impurity of the DMMTA(V) standard as well as the lack of an HPLC-ICP-MS standard for retention time comparison made analysis of this data difficult.

Figure 5.13 shows the concentrations of the four species of arsenic present in the DMMTA(V) samples over the exposure period. Again, it is clear that the arsenical that elutes at peak 3 is unstable in culture media, as it is gone by 9 h. This is similar to what was observed for DMA(III), whose conversion to DMA(V) was complete by 9 h. The arsenicals found in peaks 2 and 4 do not appear to convert in media over time, as there is little change in concentration of these arsenicals over time. The arsenical that elutes in peak 1 [at the same retention time as DMA(V)] increases in concentration as the concentration of the arsenical

in peak 3 decreases. If the identity of the arsenical in peak 1 is indeed DMA(V), while the arsenical in peak 3 is DMA(III), then these results would correlate with our previous findings of DMA(III) conversion in media. This would also correlate with step-wise profile for DMMTA(V) in A549 cells, as seen in Figure 5.13B. Similar to the profiles for DMA(III) and DMAG(III), the presence of DMA(V) over time in culture media would indicate that the step-wise profile is DMA(V)-mediated.

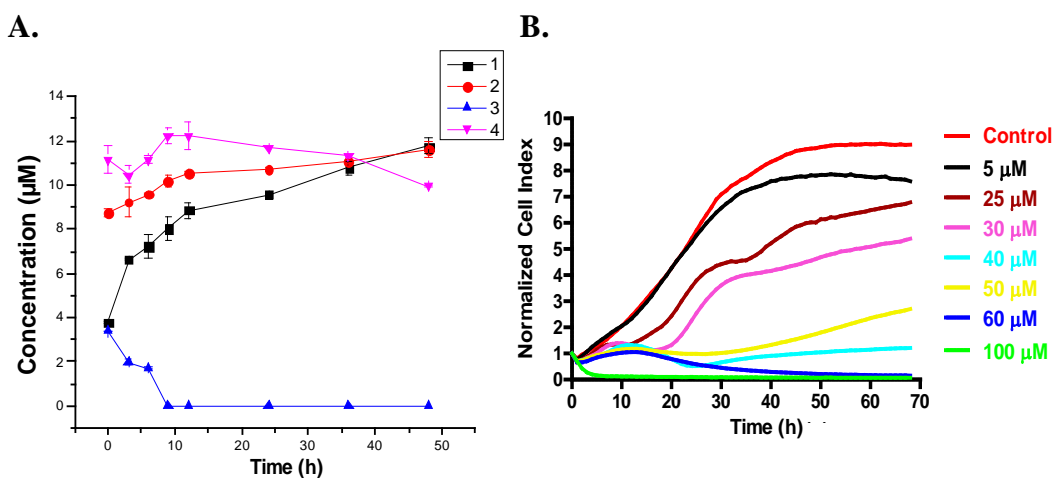


Figure 5.13: A) Concentrations of four arsenicals detected in cell culture media treated with DMMTA(V) over time by HPLC-ICP-MS analyses. B) RTCA profile of the normalized CI over time for A549 cells treated with DMMTA(V).

The only dimethylated arsenical tested in Chapter 4 that did not produce a step-wise profile in the RTCA cytotoxicity profiles was DMDTA(V). HPLC-ICP-MS analysis revealed that DMDTA(V) is highly stable in cell culture media over time, and did not convert into DMA(V), as seen in Figure 5.14. Hence, with no DMA(V) present in culture media over the exposure period, this further supports our hypothesis that the step-wise profiles observed in Chapter 4 for the

dimethylated arsenicals, DMA(III), DMAG(III), and DMMTA(V), is mediated by the presence of DMA(V).

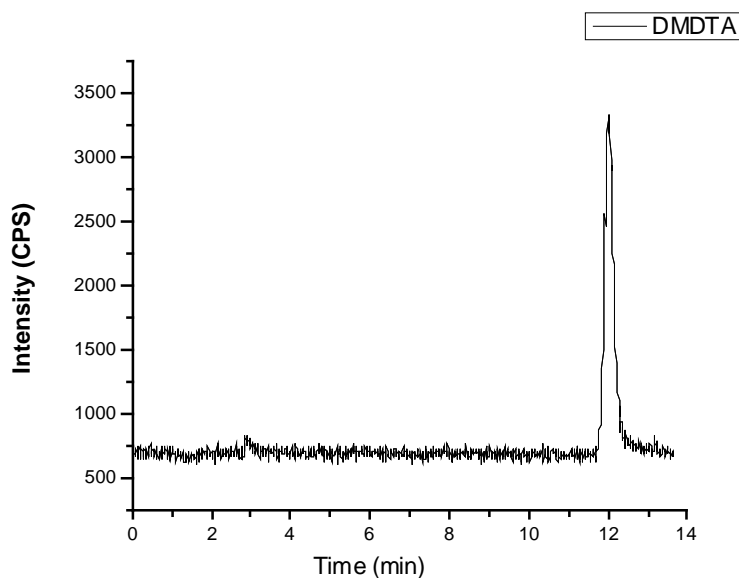


Figure 5.14: HPLC-ICP-MS chromatogram showing the speciation analysis for DMDTA(V) samples collected at the last of eight timepoints at 48 h. DMDTA(V) is highly stable in cell culture media.

5.4 Conclusions

Analysis of intracellular accumulation of Arsenicin A and As(III) has revealed that accumulation of Arsenicin A plays a key role in the observed increase in cytotoxicity for this novel polyarsenical compared to inorganic As(III). The enhanced accumulation of Arsenicin A compared to As(III) by A549 cells is consistent with the cytotoxicity data determined for these two species in Chapter 4, where Arsenicin A was found to be significantly more cytotoxic than As(III). Investigation of accumulation of the trivalent arsenicals, As(III), MMA(III), and DMA(III), by A549 and T24 cells indicates that intracellular accumulation also plays a key role in the cell-dependent cytotoxicity of these arsenicals observed in Chapter 4.

Using HPLC-ICP-MS analysis, we were also able to demonstrate the conversion of arsenic species over time in cell culture media. While As(III) demonstrated little conversion to As(V) over the 56 h exposure period, the trivalent methylated arsenicals, MMA(III), DMA(III), and DMAG(III) all exhibited significant conversion over time. The fastest rate of conversion was determined for DMA(III), where a complete conversion to DMA(V) occurred in less than 9 h. DMAG conversion to DMA(V) was also rapid, with complete conversion by 36 h. MMA(III) was the slowest of the three methylated arsenicals, with complete conversion by the end of the exposure period at 56 h. All three methylated species demonstrated much more rapid and complete conversion than inorganic As(III). As(V) and DMDTA(V) did not convert at all in cell culture media over the 48 h exposure period, while DMMTA(V) did exhibit some conversion, although the identities of the arsenicals present cannot be confirmed. These findings are consistent with the cytotoxicity results obtained in Chapter 4, where the conversion of the trivalent methylated arsenicals to the less toxic pentavalent methylated arsenicals over time corresponds with the increase in cell index (CI) observed in the RTCA cytotoxicity profiles, indicating reduced cytotoxicity. Furthermore, the step-wise profile shapes observed in Chapter 4 are likely due to the decrease in DMA(III) over time in solutions of DMA(III), DMAG(III), and DMMTA(V) in culture media.

5.5 References

- [1] D.J. Thomas, *Toxicol. Appl. Pharmacol.* 222 (2007) 365-373.
- [2] U. Schuhmacher-Wolz, H.H. Dieter, D. Klein, K. Schneider, *Crit. Rev. Toxicol.* 39 (2009) 271-298.
- [3] M.F. Hughes, B.D. Beck, Y. Chen, A.S. Lewis, D.J. Thomas, *Toxicol. Sci.* 123 (2011) 305-332.
- [4] T. Watanabe, S. Hirano, *Arch. Toxicol.* 87 (2013) 969-979.
- [5] E. Dopp, U. von Recklinghausen, R. Diaz-Bone, A.V. Hirner, A.W. Rettenmeier, *Environ. Res.* 110 (2010) 435-442.
- [6] S. Hirano, X. Cui, S. Li, S. Kanno, Y. Kobayashi, T. Hayakawa, A. Shraim, *Arch. Toxicol.* 77 (2003) 305-312.
- [7] Z. Liu, J.M. Carbrey, P. Agre, B.P. Rosen, *Biochem. Biophys. Res. Commun.* 316 (2004) 1178-1185.
- [8] T.C. Lee, I.C. Ho, W.J. Lu, J.D. Huang, *J. Biol. Chem.* 281 (2006) 18401-18407.
- [9] E. Dopp, L.M. Hartmann, A.M. Florea, U. von Recklinghausen, R. Pieper, B. Shokouhi, A.W. Rettenmeier, A.V. Hirner, G. Obe, *Toxicol. Appl. Pharmacol.* 201 (2004) 156-165.
- [10] E. Dopp, L.M. Hartmann, U. von Recklinghausen, A.M. Florea, S. Rabieh, U. Zimmermann, B. Shokouhi, S. Yadav, A.V. Hirner, A.W. Rettenmeier, *Toxicol. Sci.* 87 (2005) 46-56.
- [11] E. Dopp, U. von Recklinghausen, L.M. Hartmann, I. Stueckradt, I. Pollok, S. Rabieh, L. Hao, A. Nussler, C. Katier, A.V. Hirner, A.W. Rettenmeier, *Drug Metab. Dispos.* 36 (2008) 971-979.
- [12] I.T. Millar, H. Heaney, D.M. Heinecky, C. Fernelius, *Inorg. Synthesis* 6 (1960) 113-115.
- [13] R.A. Zingaro, *Synthetic Meth. Organometal. Inorg. Chem.* 3 (1996) 198-200.
- [14] I.T. Millar, *Inorg. Synthesis* 6 (1960) 116-118.
- [15] F. Challenger, *Chem. Rev.* 36 (1945; 1945) 315-361.

- [16] T. Hayakawa, Y. Kobayashi, X. Cui, S. Hirano, *Arch. Toxicol.* 79 (2005) 183-191.
- [17] D. Sumi, K. Fukushima, H. Miyataka, S. Himeno, *Biochem. Biophys. Res. Commun.* 415 (2011) 48-53.
- [18] Z. Drobna, S.B. Waters, V. Devesa, A.W. Harmon, D.J. Thomas, M. Styblo, *Toxicol. Appl. Pharmacol.* 207 (2005) 147-159.

Chapter 6: Altered Cytotoxicity of Arsenic Species by Carbon Nanotubes in Human Cancer Cell Lines

6.1 Introduction

One of the more promising applications of nanomaterials has been the development of nanoparticle-based drug delivery systems [1, 2]. Targeted drug delivery using nanoparticles is often used in order to improve the bioavailability of the drug, to improve the uptake of drugs with poor solubility, or to target the delivery of drugs to a specific site [1]. Of the nanomaterials used to this end, one of the most important classes of transporters are single-walled carbon nanotubes (SWCNT). SWCNT are cylindrical in shape and composed entirely of carbon (a graphite sheet rolled into a seamless cylinder) [3]. This unique structure is one of the characteristics that make SWCNT desirable for drug delivery, as they have an ultrahigh surface area available for functionalization (addition of functional groups) and, hence, for drug (cargo) loading [4]. Because pure SWCNT are composed only of carbon, they are completely insoluble in any type of solvent. Hence, functionalization is an important facet of SWCNT utilization, as it is needed to make SWCNT compatible with biological systems [5]. Furthermore, it is often utilized to improve interactions between the SWCNT and its delivery cargo, promoting both its delivery into target cells and intracellular release [6, 7].

Several studies have shown the capability of specially-designed functionalized SWCNT to enhance the observed cytotoxic effects of antineoplastic drugs in human cancer cells. Feazell et al. used amine-functionalized soluble SWCNT to significantly enhance the cytotoxicity of a

platinum (IV) complex to testicular cancer cells, in which the drug complex alone is nearly nontoxic [8]. Likewise, Zhang et al. used SWCNT functionalized with two polysaccharides to attach folic acid, a targeting agent, and doxorubicin, an anticancer drug, for targeted delivery of doxorubicin into human cervical carcinoma cells (HeLa), dramatically enhancing the observed cytotoxicity [7]. In another example, Liu et al. functionalized SWCNT with phospholipid-branched polyethylene glycol (PEG) to conjugate the cancer chemotherapy drug, paclitaxel, onto the surface. These functionalized SWCNT were then used both *in vitro* and *in vivo* to demonstrate the enhanced toxicity of paclitaxel when used as part of a SWCNT-drug delivery system [4].

Arsenic species as therapeutics have been in use for over 2,400 years. Fowler's solution, a potassium bicarbonate-based solution of arsenic trioxide (As_2O_3), was used extensively in the 18th, 19th, and 20th centuries to treat a variety of ailments including leukemia, pernicious anemia, asthma, and psoriasis [9, 10]. Salvarsan, the first organoarsenical used therapeutically, was developed in 1910 and used to treat syphilis and trypanosomiasis (African sleeping sickness) [9, 10]. The use of arsenic as a therapeutic rapidly declined in the 20th century, as the carcinogenic effects of arsenic became more widely understood [10]. However, in the 1970's, As_2O_3 was found to be an effective treatment for acute promyelocytic leukemia (APL), and further studies have shown it is highly effective in relapsed cases of APL [11], leading the US Food and Drug Administration (FDA) to approve it for treatment of relapsed or refractory APL in 2000 [9]. The approval of As_2O_3 as a cancer therapeutic has led to renewed interest in the development

of arsenic-based drugs for cancer treatment, and several studies have sought to examine the efficacy of other arsenic species as well, including dimethylarsinic acid [DMA(V)], 4-(*N*-(*S*-glutathionylacetyl)amino) phenylarsonous acid (GSAO), and dimethylarsenic glutathione (alternate names: *S*-dimethylarsino-glutathione, ZIO-101, and darinaparsin) [10, 12]. While As₂O₃ has shown promise in the treatment of other hematological malignancies [10, 13], As₂O₃ treatment for other types of cancers has had limited efficacy due to its non-selectivity and resulting higher general toxicity and side effects [14].

Thus, with the known limitations of current applications of arsenic-based treatments, I propose to investigate the ability of functionalized SWCNT to alter the cytotoxicity of arsenic species in the human lung cancer cell line, A549. Having examined the cytotoxicity of thirteen different arsenic species in Chapter 4, I propose to investigate the species with the highest observed cytotoxicity [PAO(III)], a PAO(III) derivative [PAPAO(III)], and a species with low observed cytotoxicity (roxarsone). I will examine the change in cytotoxicity of these species during co-treatment with oxidized SWCNT (o-SWCNT) using RTCA methods developed in Chapters 2 and 4 for the examination of nanoparticle- and arsenic-mediated cytotoxicity. The development of these RTCA methods for the measurement of nanoparticle-altered cytotoxicity will provide an important tool for use in drug discovery and development.

6.2 Materials and Methods

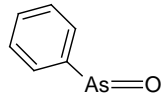
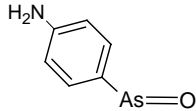
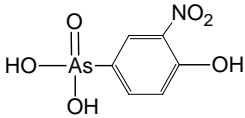
6.2.1 Cell Culture Conditions

The human lung carcinoma cell line, A549, (CCL-185; American Type Culture Collection (ATCC), Manassas, VA) was cultured in RPMI 1640 media (Gibco (Invitrogen), Burlington, ON, Canada). Media was supplemented with 10% fetal bovine serum (Sigma-Aldrich, Oakville, ON, Canada) and 1% penicillin-streptomycin (Invitrogen, Burlington, ON, Canada). The incubation conditions were maintained at 37 °C, 5% CO₂, and 90% humidity. During the study, the cells were sub-cultured twice weekly into standard 10 cm x 20 mm cell culture dishes (Corning Incorporated, Corning, NY) containing fresh media, using 0.05% trypsin-EDTA (Invitrogen) for cell detachment.

6.2.2 Arsenic Solution Preparation

Solutions of phenylarsine oxide [PAO(III)] and roxarsone in deionized (DI) water were prepared from commercially available standards (Sigma Chemical Co., St. Louis, MO). The solution of PAO(III) contained 2% methanol (Fisher Scientific, Nepean, ON, Canada), and the solution of roxarsone contained 4% DMSO (Sigma). p-Amino-phenylarsine oxide [PAPAO(III)] in DI water was prepared from a synthesized standard. Table 6.1 presents the chemical structure of each arsenic species. Solutions were sterilized via filtration (0.22 µm) and the final concentration of arsenic in each solution was calibrated using HPLC coupled with ICP-MS (Agilent Technologies, Japan). PAO(III) and PAPAO(III) solutions were stored at 4 °C until use. Roxarsone solutions re-precipitate in DI water at 4 °C over time and had to be used within a week of preparation.

Table 6.1: Structures of Arsenic Species Studied in this Chapter

Arsenic Species	Abbrev.	Structure
Phenylarsine oxide	PAO(III)	
p-Amino-phenylarsine oxide	PAPAO(III)	
Roxarsone	-	

6.2.3 o-SWCNT Preparation

o-SWCNT were kindly provided by Professor Hanfa Zou from the Dalian Institute of Chemical Physics, Chinese Academy of Sciences and were prepared as follows: 200 mg of carbon nanotubes (CNTs) (Sino-nano Company, Beijing, China) were suspended in 30 mL of 3:1 concentrated H_2SO_4 : HNO_3 by stirring and refluxing at 120 °C for 30 min. After cooling to room temperature, the CNT solution was diluted with water to a volume of 1 L, filtrated (45 μm), and rinsed with water until a pH of 7 was reached. To release the now oxidized-CNT (o-SWCNT) from the membrane filter, the membranes were placed into 50 mL of water, sonicated for 15 min, and the membrane was removed. This solution was then centrifuged for 10 min at 10,000 g to remove large agglomerates. The supernatant was re-filtered, collected, hydrolyzed, and stored at 4 °C until use. We received the o-SWCNT as dried samples, and the average diameter of the o-SWCNT was reported to be 30-50 nm. To prevent exposure, the dry o-SWCNT

were massed in a glovebox and placed into glass vials with a syringe cap. A syringe was then used to suspend the massed o-SWCNT in DI H₂O. This technique prevented the release of dry o-SWCNT into the air. The caps on each vial were removed, and the o-SWCNT solutions were autoclaved for 20 min at 120 °C.

6.2.4 RTCA Analysis

Cells were seeded into 96-well E-plates of the 96x-RTCA systems (ACEA Biosciences, San Diego, CA) at pre-calibrated concentrations that allowed for a Cell Index (CI) of 1, indicating 50-60% confluency, to be reached between 18-24 h after seeding. A549 cells were seeded at 4000-5000 cells well⁻¹. When a CI of 1 was reached, the arsenic solutions described above were serially diluted in media to produce double the desired treatment concentration. Sterile o-SWCNT in DI H₂O were sonicated in a water sonicator for 30 min and were then diluted in media to produce double the desired treatment concentration. Arsenic solutions in media and o-SWCNT in media were then mixed at 1:1 ratios to produce the desired treatment concentrations. Each treatment concentration of arsenic, o-SWCNT, and arsenic + o-SWCNT was added at a volume of 200 µL to triplicate wells after vortexing for 1 min. Solvent controls and non-treated controls (cell culture media) were run concurrently with the nanoparticle-treated cells and were also added at a volume of 200 µL to triplicate wells. The highest concentration of o-SWCNT-treatment was also placed in duplicate wells with no cells present to ensure that there was no interference of the nanoparticles with CI measurements. CI was measured at hourly intervals for at least 72 h post-exposure.

6.2.5 ICP-MS

An Agilent 7500ce octopole reaction system ICP-MS (Agilent Technologies, Japan) was used as the detector. The ICP was operating at a radio frequency power of 1550 W and the argon carrier gas flow rate was 0.9-1.0 L min⁻¹. ICP-MS was operated with a helium mode, and the use of helium (3.5 mL min⁻¹) in the octopole reaction cells aimed to reduce isobaric and polyatomic interference. Arsenic was monitored at m/z 75. HPLC separation was performed on a Phenomenex column (BioSep-SEC-S 2000, 300 x 4.6 mm, 5 μm particle size) with a mobile phase consisting of 10 mM ammonium bicarbonate and 5% methanol (2 mL min⁻¹). Chromatograms from HPLC separation and ICP-MS detection were recorded by ICP-MS ChemStation (Agilent Technologies, Santa Clara, CA).

6.3 Results and Discussion

6.3.1 PAO(III)

Unmodified PAO(III) is often precluded from investigation as an antineoplastic agent due to its high toxicity *in vivo* and its non-selectivity for cancer cells, having demonstrated high toxicity to both cancer and normal cells in the same concentration range [13]. However, this cell selectivity issue could be improved through use of a SWCNT delivery system to allow for targeted delivery of PAO(III) into the desired cells. Furthermore, studies have shown that nanomaterials can be modified to improve the delivery of their cargo to cancer cells through the addition of biomolecules to the structure that are recognized by cancer cells and promote their uptake [7]. For example, folic acid is a commonly

used targeting biomolecule, as it has a high binding affinity to folate receptors, which are highly overexpressed on the surface of tumors of epithelial origin compared to normal tissues [14]. Chen et al. even utilized this biomolecule (folate) on the surface of 100-nm-scale liposomes encapsulating As_2O_3 for delivery into cancer cells [14]. Hence, because of the potent cytotoxicity we observed for PAO(III) in Chapter 4 and the recognized need to increase its selectivity for cancer cells, it was believed that PAO(III) would be an excellent candidate for targeted delivery, as the use of highly toxic arsenic species would also reduce the overall body burden of arsenic during treatment. In addition, because PAO(III) is stable, it would reduce the probability of arsenic conversion *in vivo*, allowing for a better understanding of any potential pharmacokinetic effects.

Figure 6.1A shows an RTCA cytotoxicity profile of A549 cells treated with 1 μM PAO(III) in the presence and absence of varying concentrations of o-SWCNT, from 5-100 $\mu\text{g mL}^{-1}$. Here, a very interesting dose-response was observed. Figure 6.1A clearly shows that during this experiment, the concentration of 1 μM PAO(III) resulted in a complete loss of cell viability, supported by the fact that the normalized cell index (CI) is 0 throughout the entire exposure period. However, as the concentration of o-SWCNT increases in the presence of the 1 μM PAO(III) treatment, the normalized CI also increases, indicating an increase in cell viability. Hence, the o-SWCNT may be preventing or reducing the toxicity of PAO(III) in solution by unknown mechanisms. As shown in Figure 6.1B, the same concentrations of o-SWCNT alone without

PAO(III) are not cytotoxic, as the CI values over time do not differ from the CI values of the untreated control cells. The o-SWCNT also do not interfere with RTCA detection, as the presence of o-SWCNT in wells without cells generated no CI values over the exposure period (CI = 0).

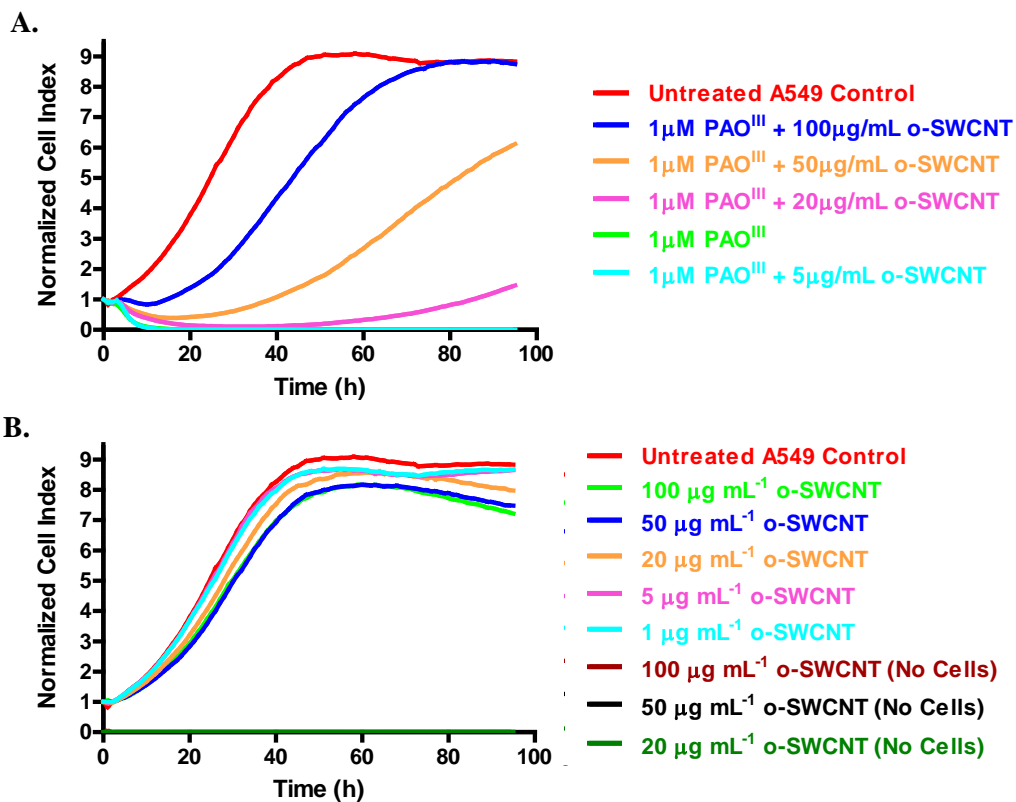


Figure 6.1: A) RTCA profile of the CI over time for A549 cells treated with 1 μM PAO(III) and 0-50 μg mL⁻¹ o-SWCNT. B) RTCA profile of the CI over time for A549 cells treated with 0-50 μg mL⁻¹ o-SWCNT (as in Fig. 6.1A) and the CI over time for wells without cells present to show the effects of o-SWCNT on the RTCA electrodes (CI = 0).

The results of Figure 6.1 indicate that the interactions of o-SWCNT with PAO(III) may contribute to the reduced cytotoxicity of PAO(III) observed in Figure 6.1A. We hypothesize that PAO(III), when mixed with o-SWCNT, may generate complexes of o-SWCNT-PAO(III), resulting in reduced free PAO(III).

To test this hypothesis, we examined the interactions of PAO(III) with o-SWCNT using size exclusion LC-ICP-MS. The size exclusion LC will separate the o-SWCNT-PAO(III) complex from the free PAO(III). In the first set of experiments, 0.8 μM PAO(III) was prepared with o-SWCNT at varying concentrations from 0 to 50 $\mu\text{g mL}^{-1}$. These solutions were analyzed using the size exclusion LC-ICP-MS after two different incubation times. A complex peak was eluted before the free PAO(III). Therefore, both the complex and the free PAO(III) in solution were determined. The results of the samples at time 0 and after storage for 1 week at room temperature are summarized in Table 6.2. Analysis of these samples reveals the formation of an o-SWCNT-PAO(III) complex. It is clear that as the concentration of o-SWCNT increases (left to right), the peak area of PAO(III) (representing the free PAO(III) in solution) decreases in both the freshly prepared and week old solutions. Furthermore, the area of the peak representing the o-SWCNT-PAO(III) complex also increases with increasing o-SWCNT concentration in both the freshly prepared and week old solutions. In fact, after 1 week at room temperature, 50 $\mu\text{g mL}^{-1}$ o-SWCNT reduces the concentration of free PAO(III) in solution to levels that are below the detection limit of the ICP-MS. This demonstrates that o-SWCNT are capable of fully capturing PAO(III) after a one week incubation. Hence, the increased viability of the A549 cells in the presence of increasing concentrations of o-SWCNT in solution observed in Figure 6.1 is due to the formation of the o-SWCNT-PAO(III) complex. The formation of this complex reduces the free PAO(III) in solution, thereby reducing the observed cytotoxic effects (Fig. 6.1). These results suggest

that using o-SWCNT can modify the toxicity of PAO(III) through the formation of a complex. Further research is needed to develop a method for delivery of this low toxicity o-SWCNT-PAO(III) complex to the treatment site and enhance uptake, and also to release free PAO(III) at the site once it is taken up.

Table 6.2: o-SWCNT-PAO(III) Complex Formation in 0.8 μ M PAO(III)

o-SWCNT (μg mL⁻¹):	0	0.5	5	50
<i>Freshly prepared:</i>				
Free PAO(III)	547009	525335	519606	471575
Complex	11398	19074	21785	83961
<i>After 1 week at RT:</i>				
Free PAO(III)	813406	744725	441771	N.D.
Complex	27317	73473	411986	956017
N.B. Complex and Free PAO(III) measured as Peak Area; RT = Room Temperature				

6.3.2 PPAO(III)

Having determined that PAO(III) forms a complex with o-SWCNT, we decided to examine a second species of arsenic to exploit the carboxylic acid functionalization present on the oxidized SWCNT surface. p-Amino-phenylarsine oxide [PPAO(III)] contains the same structure as PAO(III), but contains an amino group (-NH₂) on the para-location of the phenyl- group (Table 6.1). SWCNT have been shown previously to easily penetrate mammalian cells through clathrin-dependent endocytosis [8, 15, 16]. During this process, the SWCNT interact with receptors on the surface of the cell membrane, which prompts the recruitment of the clathrin adaptor protein 2 and clathrin to the plasma membrane. A clathrin-coated pit is formed and accessory proteins pinch off the clathrin-coated domain to form a vesicle around the SWCNT. As the

vesicles fuse and proteins (e.g. clathrin) are recycled, the vesicle becomes an early endosome with pH around 5.9-6.0, which then matures into a late endosome with pH around 5.0-6.0 (Figure 6.2). The late endosome will then progress to a lysosome to drop the pH to 5.0-5.5 to attempt to process the SWCNT present [17]. Because amide bonds are cleaved during a pH drop from 7 to 5, we hypothesized that if PAPA0(III) formed an amide bond with the carboxylic acid groups present on the surface of o-SWCNT, we could then use o-SWCNT to deliver low concentrations of PAPA0(III) into A549 cells and release the PAPA0(III) into the endosomes/lysosomes after uptake.

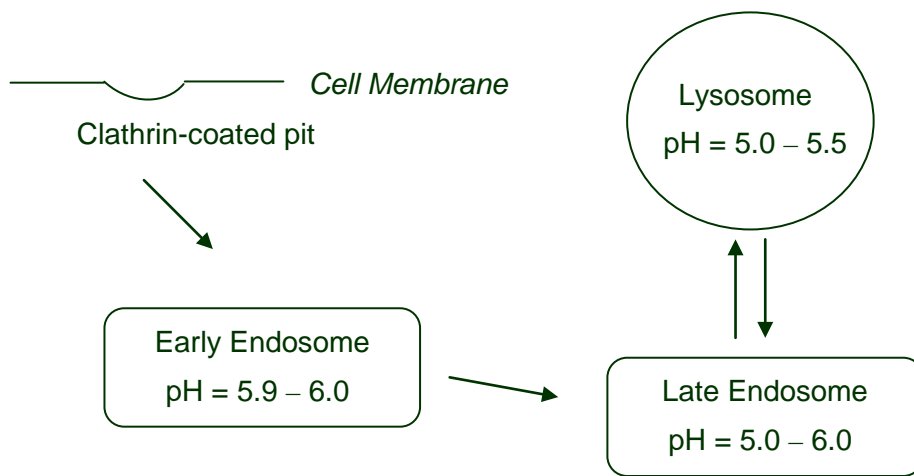


Figure 6.2: Change in pH during various stages of clathrin-dependent endocytosis.

Figure 6.3A shows the RTCA cytotoxicity profile of A549 cells exposed to 12 μM PAPA0(III) with o-SWCNT at varying concentrations from 0-50 $\mu\text{g mL}^{-1}$. Figure 6.3B shows the RTCA cytotoxicity profile of A549 cells exposed to o-SWCNT alone, at the same concentrations used in Figure 6.3A. The o-SWCNT solutions alone are not cytotoxic and they do not interfere with RTCA measurements. In Figure 6.3A, there appears to be a dose-response with the

higher concentrations of o-SWCNT in the presence of 12 μM PAPAO(III) (blue, orange, and pink profiles in Fig. 6.3A). The CI decreases when the concentration of o-SWCNT present in the PAPAO(III) solution increases from 5 to 50 $\mu\text{g mL}^{-1}$. This toxic response is observed at 36 h after treatment with 12 μM PAPAO(III) + 50 $\mu\text{g mL}^{-1}$ o-SWCNT (Fig. 6.3A). This delay may be due to the slow intracellular accumulation of the complex. Studies have shown that cellular uptake and expulsion/recycling of SWCNT occur simultaneously, and the rate of uptake is faster than the rate of expulsion [18, 19]. Hence, the delayed effect observed in Figure 6.3A could be caused by the time required for the intracellular concentration of o-SWCNT + PAPAO(III), and thus, free PAPAO(III) as well, to increase to a level where cytotoxicity is observed. As this is merely a hypothesis, more research is needed to confirm this delay in observed cytotoxicity for o-SWCNT and PAPAO(III).

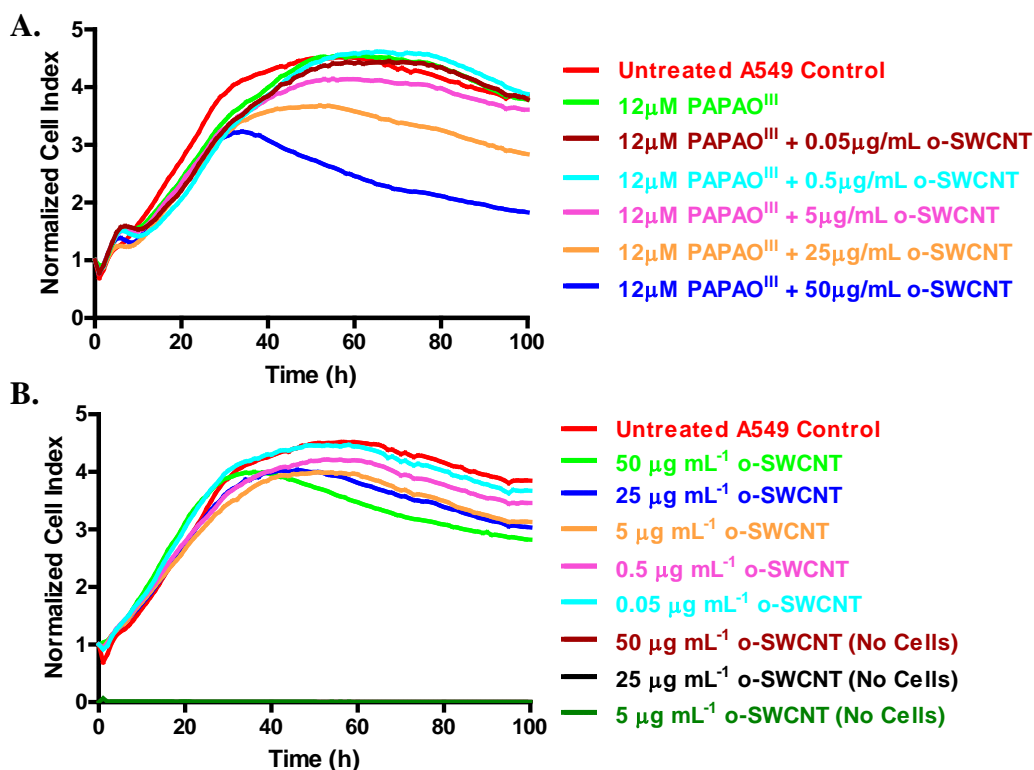


Figure 6.3: A) RTCA profile of the CI over time for A549 cells treated with 12 μ M PAPA0(III) and 0-50 μ g mL⁻¹ o-SWCNT. B) RTCA profile of the CI over time for A549 cells treated with 0-50 μ g mL⁻¹ o-SWCNT (as in Fig. 6.3A) and the CI over time for wells without cells present to show the effects of o-SWCNT on the RTCA electrodes (CI = 0).

6.3.3 Roxarsone

Uptake of pentavalent arsenic species [e.g., As(V), DMA(V)] has been shown to be much slower and the species less efficiently retained than the uptake of trivalent species [DMA(III), MMA(III), As(III)] [20-22]. While it is generally accepted that trivalent species are taken up more readily into cells than pentavalent species, it is a source of contention if the more efficient uptake of trivalent over pentavalent species is a cause of the observed increase in cytotoxicity of trivalent over pentavalent species. Hence, the examination of o-SWCNT-altered cytotoxicity of the low toxicity pentavalent species, roxarsone, will provide evidence to support the potential effect of enhanced uptake of

pentavalent species. To this end, we examined the cytotoxicity of the pentavalent species, roxarsone, in the presence of o-SWCNT, as roxarsone showed little cytotoxicity in A549 cells (Chapter 4).

Figure 6.4 shows the RTCA cytotoxicity profiles of A549 cells exposed to A) 7.5 mM or B) 5 mM roxarsone with o-SWCNT concentrations from 0 to 400 $\mu\text{g mL}^{-1}$. Both sets of results show a clear dose-response. In the presence of 5 or 7.5 mM roxarsone, as the concentration of o-SWCNT increases, the treated A549 cells show toxic effects, demonstrated by the decreasing CI values. The observed decrease in CI, however, is different from what was observed in Figure 6.3A when A549 cells were treated with o-SWCNT and PAPA(OIII). In Figure 6.3A, the cytotoxicity (or reduction in CI) was observed after 36 h exposure, while the decrease of CI observed in Figure 6.4 occurs much earlier in the exposure period (approximately 12 h after exposure). It should be noted that a comparison between the profiles of the two species in the presence of o-SWCNT is difficult to make as the range of tested concentrations for both the species and the o-SWCNT tested vary significantly. The concentration of 5 mM roxarsone is over 400 times larger than the concentration of 12 μM PAPA(OIII) that was screened. Although both of these concentrations had little quantifiable cytotoxicity, the sheer difference in concentration (and total number of As molecules present) makes this analysis, based on RTCA screening alone, difficult. Furthermore, a higher concentration range of o-SWCNT was screened with roxarsone. Nevertheless, the findings in Figure 6.4 are very promising for future research, as it appears that the presence of o-SWCNT significantly increases the cytotoxicity of this pentavalent

arsenic species. The examination of total intracellular arsenic uptake using ICP-MS in the presence and absence of o-SWCNT would be of great benefit to discerning the observed increase in cytotoxicity.

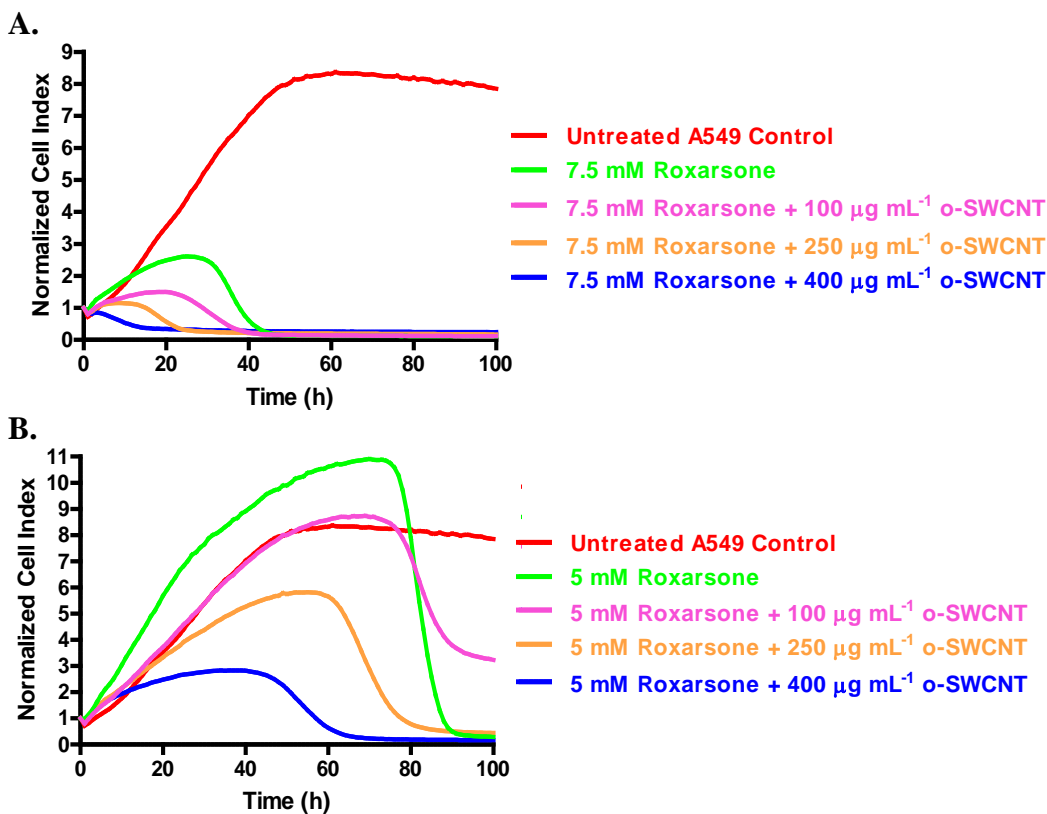


Figure 6.4: RTCA profile of the CI over time for A549 cells treated with A) 7.5mM Roxarsone and 0-400 µg mL⁻¹ o-SWCNT and B) 5mM Roxarsone and 0-400 µg mL⁻¹ o-SWCNT.

To confirm that the observed changes in CI observed in Figure 6.4 were not caused by the o-SWCNT, Figure 6.5A shows the RTCA cytotoxicity profile for A549 cells exposed to o-SWCNT at the same concentrations found in Figure 6.4. This demonstrates that the o-SWCNT alone are not significantly cytotoxic and they do not interfere with RTCA measurements. Figure 6.5B shows the RTCA cytotoxicity profile for A549 cells exposed to the solvent controls for both

concentrations of roxarsone (Fig. 6.4), supporting that the effects observed in Figure 6.4 are mediated by the presence of o-SWCNT and roxarsone.

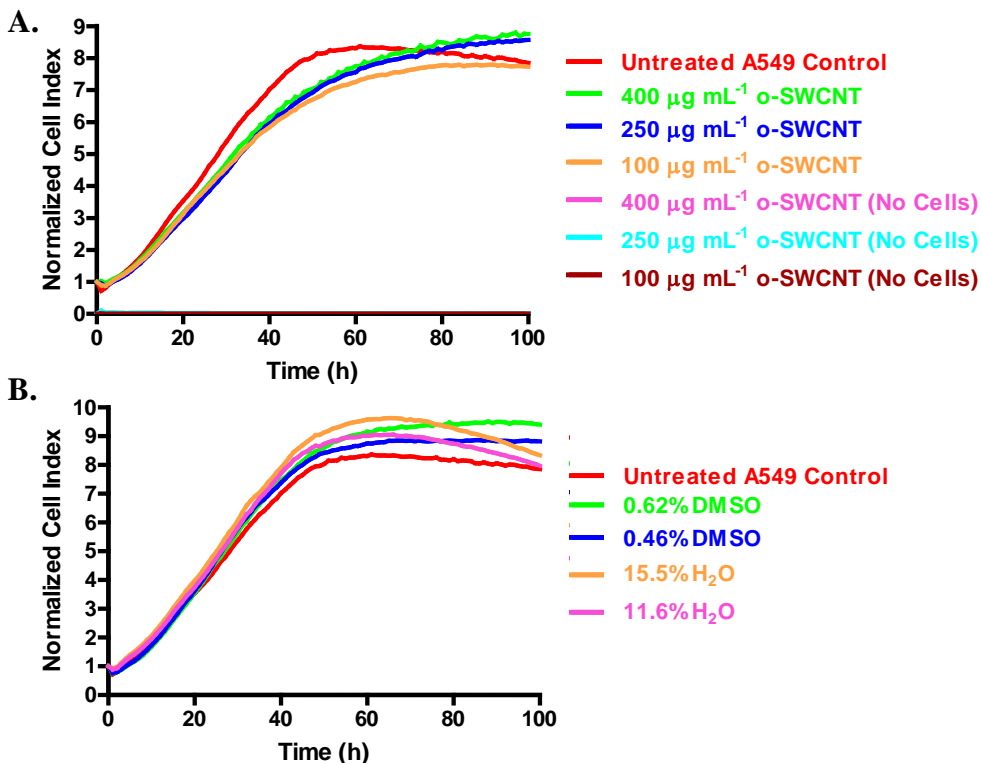


Figure 6.5: A) RTCA profile of the CI over time for A549 cells treated with 0-400 $\mu\text{g mL}^{-1}$ o-SWCNT (as in Fig. 6.4) and the CI over time for wells without cells present to show the effects of o-SWCNT on the RTCA electrodes (CI = 0). B) RTCA profile of the CI over time for A549 cells treated with the solvent controls present in 7.5 mM (0.62% DMSO, 15.5% H₂O) and 5 mM (0.46% DMSO, 11.6% H₂O) roxarsone.

6.4 Conclusions

This chapter demonstrates another application of our developed 96-x RTCA method for analysis of nanoparticles for use in drug discovery and development. Here, our RTCA method was used to examine the potential therapeutic application of three different arsenic species (selected based on RTCA cytotoxicity analysis in Chapter 4) when co-administered with o-SWCNT. These

three species, PAO(III), PAPAO(III), and roxarsone, each demonstrated unique interactions with o-SWCNT, which were easily observed in real-time due to the high-throughput and dye-free analysis provided by our method. A unique o-SWCNT-PAO(III) complex was identified, while both PAPAO(III) and roxarsone warrant further investigation due to the enhanced cytotoxicity of these species when treated with o-SWCNT.

The dye-free aspect of our RTCA method is of particular importance in the analysis of SWCNT toxicity, as several studies have reported interference of SWCNT with traditional dye-based assays for cytotoxicity analysis. Monteiro-Riviere et al. found severe interference of SWCNT with the neutral red (NR) uptake assay, the MTT assay, and the Alamar Blue assay [23]. MTT interference was also reported by Wörle-Knirsch et al. [24]. Furthermore, Davoren et al. reported interference of SWCNT with dyes used in the NR, adenylate kinase (AK), and the interleukin-8 (IL-8) cytokine assays, which they attributed to the adsorbing properties of the nanotubes affecting the dyes [25]. As we observed no interference in any of our RTCA analyses with o-SWCNT, our RTCA method will be of considerable use in future studies of SWCNT drug delivery systems.

6.5 References

- [1] S.S. Suri, H. Fenniri, B. Singh, *J. Occup. Med. Toxicol.* 2 (2007) 16.
- [2] M.F. Beaux 2nd, D.N. McIlroy, K.E. Gustin, *Expert Opin. Drug Deliv.* 5 (2008) 725-735.
- [3] K. Donaldson, R. Aitken, L. Tran, V. Stone, R. Duffin, G. Forrest, A. Alexander, *Toxicol. Sci.* 92 (2006) 5-22.
- [4] Z. Liu, K. Chen, C. Davis, S. Sherlock, Q. Cao, X. Chen, H. Dai, *Cancer Res.* 68 (2008) 6652-6660.
- [5] A. Bianco, K. Kostarelos, C.D. Partidos, M. Prato, *Chem. Commun. (Camb.)* 5 (2005) 571-577.
- [6] K. Kostarelos, L. Lacerda, G. Pastorin, W. Wu, S. Wieckowski, J. Luangsivilay, S. Godefroy, D. Pantarotto, J.P. Briand, S. Muller, M. Prato, A. Bianco, *Nat. Nanotechnol.* 2 (2007) 108-113.
- [7] X. Zhang, L. Meng, Q. Lu, Z. Fei, P.J. Dyson, *Biomaterials* 30 (2009) 6041-6047.
- [8] R.P. Feazell, N. Nakayama-Ratchford, H. Dai, S.J. Lippard, *J. Am. Chem. Soc.* 129 (2007) 8438-8439.
- [9] K.H. Antman, *Oncologist* 6 Suppl 2 (2001) 1-2.
- [10] P.J. Dilda, P.J. Hogg, *Cancer Treat. Rev.* 33 (2007) 542-564.
- [11] Z. Shen, G. Chen, J. Ni, X. Li, S. Xiong, Q. Qiu, J. Zhu, W. Tang, G. Sun, K. Yang, Y. Chen, L. Zhou, Z. Fang, Y. Wang, J. Ma, P. Zhang, T. Zhang, S. Chen, Z. Chen, Z. Wang, *Blood* 89 (1997) 3354-3360.
- [12] S.M. Matulis, A.A. Morales, L. Yehiayan, C. Crutch, D. Gutman, Y. Cai, K.P. Lee, L.H. Boise, *Mol. Cancer Ther.* 8 (2009) 1197-1206.
- [13] S.J. Ralph, *Metal-Based Drugs, Volume 2008* (2008).
- [14] H. Chen, R. Ahn, J. Van den Bossche, D.H. Thompson, T.V. O'Halloran, *Mol. Cancer Ther.* 8 (2009) 1955-1963.
- [15] N. Wong Shi Kam, H. Dai, *Phys. Stat. Sol. (B)* 243 (2006) 3561-3566.
- [16] P.N. Yaron, B.D. Holt, P.A. Short, M. Losche, M.F. Islam, K.N. Dahl, J. *Nanobiotechnology* 9 (2011) 45-3155-9-45.

- [17] F.R. Maxfield, T.E. McGraw, *Nat. Rev. Mol. Cell Biol.* 5 (2004) 121-132.
- [18] H. Jin, D.A. Heller, R. Sharma, M.S. Strano, *ACS Nano* 3 (2009; 2009) 149-158.
- [19] B.D. Holt, K.N. Dahl, M.F. Islam, *ACS Nano* 6 (2012) 3481-3490.
- [20] S. Hirano, X. Cui, S. Li, S. Kanno, Y. Kobayashi, T. Hayakawa, A. Shraim, *Arch. Toxicol.* 77 (2003) 305-312.
- [21] E. Dopp, L.M. Hartmann, A.M. Florea, U. von Recklinghausen, R. Pieper, B. Shokouhi, A.W. Rettenmeier, A.V. Hirner, G. Obe, *Toxicol. Appl. Pharmacol.* 201 (2004) 156-165.
- [22] E. Dopp, U. von Recklinghausen, R. Diaz-Bone, A.V. Hirner, A.W. Rettenmeier, *Environ. Res.* 110 (2010) 435-442.
- [23] N.A. Monteiro-Riviere, A.O. Inman, L.W. Zhang, *Toxicol. Appl. Pharmacol.* 234 (2009) 222-235.
- [24] J.M. Worle-Knirsch, K. Pulskamp, H.F. Krug, *Nano Lett.* 6 (2006) 1261-1268.
- [25] M. Davoren, E. Herzog, A. Casey, B. Cottineau, G. Chambers, H.J. Byrne, F.M. Lyng, *Toxicol. In Vitro* 21 (2007) 438-448.

Chapter 7: Conclusions and Future Prospects

7.1 Introduction

Current methods for assessment of nanoparticle-mediated cytotoxicity are dominated by end-point colorimetric assays, which require the use of labels or dyes to monitor cellular responses [1, 2]. Many nanomaterials have been found to interfere with the dyes or absorbance measurements requisite to these assays [3-7]. Thus, these traditional cytotoxicity assays cannot provide reliable assessment of nanoparticle-mediated cytotoxicity, resulting in the requirement that multiple assays be performed to avoid any erroneous results [8]. This is time-consuming and makes high-throughput assessment difficult to achieve. Therefore, the development of new analytical tools for more efficient, high-throughput, and reliable measurement of nanomaterial-mediated toxicity is needed.

Our group has developed impedance-based real-time cell-electronic sensing techniques for high-throughput testing of chemical toxicity. We have demonstrated the techniques for the profiling of chemical- and microparticle-induced cytotoxicity in real-time [9, 10]. My Ph.D. research aimed to develop this cell-electronic sensing technology for testing nanoparticle-mediated toxicity with applications to environmental studies and drug development. This included the development of RTCA methods for high-throughput testing of engineered nanoparticles (Chapter 2) and environmentally-sampled air particulates (Chapter 3). In Chapter 4, I applied the chemical cytotoxicity testing methods to examine the cytotoxicity of thirteen arsenic species on the same platform, using the same cell lines and experimental conditions, enabling for the first time a comparison of

the relative cytotoxicity of thirteen arsenicals. The unique cytotoxicity of a newly synthesized arsenical, Arsenicin A, identified in Chapter 4 led to further investigation into intracellular accumulation as a key factor contributing to its potent cytotoxicity in Chapter 5. Chapters 2-4 demonstrated the unique capability of RTCA for testing cytotoxicity of nanoparticles and arsenicals to generate multiple data. This provided a basis for further exploration into the potential use of nanoparticle-altered arsenic toxicity for therapeutic use (Chapter 6).

This chapter will summarize the findings of each of these previous chapters and discuss their significance. Future research objectives and studies will also be proposed.

7.2 Chapter Summaries

7.2.1 Chapter 2: Development of a Real-Time Cell-electronic Sensing Method for Analysis of Nanoparticle-Induced Cytotoxicity

The recent increase in production and application of nanomaterials raises concerns of human exposure and health risks. Hence, developing high-throughput *in vitro* testing tools has become one of the priorities for both the safe use and development of nanotechnology [11]. Due to the extensive reports of interference of nanomaterials with traditional dye-based cytotoxicity assays, I hypothesized that an impedance-based cell-electronic sensing technique could overcome these problems to provide accurate measurements of nanoparticle-mediated cytotoxicity. I tested two well-characterized engineered nanoparticles, nTiO₂ and nAg, and selected three human cell lines as sensing probes. Real-time analysis provided both qualitative and quantitative data in the form of cytotoxicity profiles (cell index over time) and unique IC₅₀ histograms (IC₅₀ values over time). I was

able to confirm cytostatic responses on cytotoxicity profiles of CHO-K1 cells (a non-tumor derived mammalian cell line) using flow cytometric analysis to demonstrate S-phase cell cycle arrest due to nTiO₂ exposure. I also confirmed that the IC₅₀ values determined using the RTCA method were acceptable, as IC₅₀ values determined using the neutral red uptake (NRU) assay for nAg were not statistically different. IC₅₀ values for nTiO₂, however, could not be determined due to severe interference with the NRU method. This further confirmed the utility of my developed RTCA method, as it suffered no interferences from either nanoparticle, and provided concentration-, time-, particle-, and cell-dependent toxicological relationships.

7.2.2 Chapter 3: Application of Developed RTCA Method for Environmental Air Quality Monitoring

Nanosized air particulates have been a known by-product of anthropogenic thermo-degradation processes, such as combustion and automobile use, and until recently, have been the only significant source of human exposure to nanosized particles (PM_{0.1}) [12]. With rapid development of nanotechnology leading to incorporation of nanomaterials into thousands of consumer products [13], engineered-nanoparticles in the environment have become a concern [14-16]. Therefore, it is required to develop new techniques and methods for environmental toxicity monitoring of ultrafine particles (PM_{0.1}). I hypothesized that our RTCA method developed in Chapter 2 could be applied to accurately measure nanoparticle-mediated cytotoxicity of environmentally-sampled particulates. Using my RTCA method, I demonstrated its application in air quality monitoring through the evaluation of the cytotoxicity of two forms of particulate

matter (PM) collected from the field. The first set of PM was size-fractionated coal fly ash (CFA) collected from a coal burning power plant in China. The size fractions of CFA were PM₁₀ (>10 μm), PM_{10-2.5} (2.5 μm<x<10 μm), and PM_{2.5} (<2.5 μm). After correcting cell index values due to mild interference of the high doses of PM with RTCA measurements, RTCA analysis provided both qualitative and quantitative analysis of the CFA PM on two human lung carcinoma cell lines, A549 and SK-MES-1. Cytotoxicity was size-dependent (PM₁₀ < PM_{10-2.5} ≈ PM_{2.5}) and cell-dependent (A549 < SK-MES-1). The second set of PM was PM_{2.5} extracted from air quality monitoring filters. After extracting the concentrated air particulates (CAPs) from the filters, CAPs were screened with two particulate standard reference materials (SRMs). RTCA analysis determined that the cytotoxicity of the CAPs was dose-dependent, but was less than that of the two SRMs. Cytotoxicity ranking of the PM samples indicates the utility of the RTCA method for prioritization of environmental samples for further testing for air quality monitoring applications.

7.2.3 Chapter 4: Profiling Cytotoxicity of Thirteen Arsenic Species for Toxicity Ranking

The toxicity of arsenic is dependent upon its chemical species; however, the roles of specific metabolites or intermediates in toxicity mechanisms are poorly understood [17]. The available toxicity data has been obtained using various assays on different cell lines. The species-dependent toxicity and variations in different assays make it difficult to compare the toxicity of different arsenic species. To address this issue, I hypothesized that RTCA methods for chemical cytotoxicity testing developed in our lab can be used for uniform testing

of the cytotoxicity of arsenic species [9]. I examined thirteen different species of arsenic, including inorganic species [As(III), As(V)], methylated metabolites [MMA(III), MAO(III), DMA(III)], thiolated metabolites [DMAG(III), DMMTA(V), MMTTA(V), DMDTA(V)], and non-metabolite organoarsenicals (Arsenicin A, PAO(III), roxarsone, p-arsanilic acid). I selected two human carcinoma cell lines as sensing probes, A549 and T24. Real-time analysis provided both quantitative and qualitative data. Quantitative IC₅₀ values were determined at every hour over the exposure period, indicating cell-dependent and chemical species-dependent cytotoxicity. T24 was more sensitive to all arsenic species than A549. In A549 cells, the toxicity of the species was ranked as PAO(III) > Arsenicin A > MAO(III) ≈ MMA(III) ≈ DMA(III) > DMAG ≈ DMMTA > As(III) > MMTTA > DMDTA ≥ As(V) > Roxarsone > p-Arsanilic Acid. In T24 cells, PAO(III) > MAO(III) > MMA(III) > Arsenicin A > DMAG ≈ DMA(III) ≥ DMMTA ≥ As(III) > MMTTA > As(V) ≥ DMDTA > p-Arsanilic Acid ≈ Roxarsone. Qualitative analysis of the cytotoxicity profiles (cell index over time) demonstrated unique profile shapes for several of the arsenic species. The dimethylated arsenic species, DMA(III), DMAG(III), and DMMTA(V) all presented unique step-wise profile shapes, which were hypothesized to be due to either chemical conversion of arsenic in media over time or due to a common biological response. Hence, RTCA analysis provided important kinetic information about cellular responses and multiple data enabling the toxicity ranking for thirteen species of arsenic and providing a comprehensive study of arsenic toxicity.

7.2.4 Chapter 5: Accumulation of Arsenic Species in Human Cell Lines and Conversion of Arsenic Species in Culture Media

The known cellular interactions of arsenic are extensive [17], making the determination of the causes of observed cytotoxic responses very difficult. However, a key precondition for the induction of any cytotoxic effect by arsenic is cellular uptake. Thus, the examination of intracellular accumulation is an important starting point for understanding arsenic-induced cytotoxic effects. Three interesting findings of arsenic-induced cytotoxic effects in Chapter 4 were the potent cytotoxicity of Arsenicin A, the cell-dependent cytotoxicity of the trivalent arsenicals, and the unique step-wise shape of the cytotoxicity profiles for the dimethylated arsenicals [DMA(III), DMAG(III), DMMTA(V)]. I hypothesized that the higher cytotoxicity of Arsenicin A in comparison to the inorganic arsenical As(III) is in part due to increased intracellular accumulation of Arsenicin A. To confirm this, we treated A549 cells with IC_{50} concentrations of As(III) and Arsenicin A for 24 h and then collected the cell lysate. The cell lysate was analyzed for total arsenic using ICP-MS. ICP-MS analysis revealed that A549 cells exposed to Arsenicin A had four times as many arsenic atoms per cell than the A549 cells treated with As(III), even though the concentration of As(III) used was 76.6 μ M, which was twenty times larger than the concentration of Arsenicin A used (3.5 μ M). These results suggest that intracellular accumulation of arsenic plays a key role in the observed difference in cytotoxicity of Arsenicin A compared to As(III), and the high cytotoxicity of Arsenicin A found in Chapter 4 is likely due to the higher intracellular concentration of arsenic atoms present. Likewise, the cell-dependent cytotoxicity of the trivalent arsenicals, As(III),

MMA(III), and DMA(III), is also influenced by accumulation in A549 and T24 cells. Accumulation of total arsenic in T24 cells treated with As(III) was significantly higher than in A549 cells, consistent with the increased cytotoxicity of As(III) in T24 cells compared to A549 cells observed in Chapter 4.

To understand potential reasons for the step-wise curves in RTCA profiles of some arsenic compounds, my hypothesis was that dimethylated arsenicals, DMA(III) and DMAG(III), convert to the less toxic pentavalent species, DMA(V), in culture media, resulting in the decrease in cytotoxicity of these species over time. The concentrations of As(III), MMA(III), DMA(III), DMAG(III), As(V), DMMTA(V), and DMDTA(V) in cell culture media were analyzed at up to nine timepoints after exposure using HPLC-ICP-MS. This analysis revealed all four trivalent species converted in cell media over time. As(III) had the slowest rate of conversion, with a small peak of As(V) appearing at 24 h. The conversion of MMA(III) to MMA(V) was complete by 56 h, while the conversion of DMAG(III) to DMA(V) was complete by 36 h. DMA(III) had the fastest rate of conversion, with complete conversion to DMA(V) by 9 h. As DMA(V) and MMA(V) are less cytotoxic than their trivalent counterparts in large part due to reduced intracellular uptake, the conversion of the trivalent to pentavalent species supports the reduced cytotoxicity of these arsenicals over time that was observed in Chapter 4. As(V) and DMDTA(V) exhibited no conversion over time in cell culture media at any of the examined timepoints, while arsenicals present in the DMMTA(V) solution did exhibit some conversion over time, although the identity of the arsenicals cannot be confirmed.

7.2.5 Chapter 6: Altered Cytotoxicity of Arsenic Species by Carbon Nanotubes in Human Cancer Cell Lines

A promising application of nanomaterials has been the development of nanoparticle-based drug delivery systems [18, 19]. Of those nanomaterials, one of the most important classes of transporters is single-walled carbon nanotubes (SWCNT) [20, 21]. The US-FDA approval of As_2O_2 as a cancer therapeutic for relapsed or refractory acute promyelocytic leukemia (APL) has led to renewed interest in the development of arsenic-based drugs for cancer treatment. However, As_2O_3 treatment for other types of cancers has had limited efficacy due to its non-selectivity and resulting higher general toxicity and side effects [22]. Thus, with the known limitations of current applications of arsenic-based treatments, I hypothesized that co-treatment of arsenic species with functionalized SWCNT would enhance the observed cytotoxicity of arsenic species in human lung cancer cells. Using the RTCA methods developed in Chapters 2 and 4 for nanoparticle- and arsenic- cytotoxicity testing, I tested low toxicity concentrations of PAO(III), PAPA(III), and roxarsone with a concentration range of o-SWCNT from 0 to $400 \mu\text{g mL}^{-1}$. RTCA analysis of o-SWCNT-PAO(III) demonstrated reduced toxicity as the concentration of o-SWCNT present in the solution of $1 \mu\text{M}$ PAO(III) increased. We used size-exclusion LC-ICP-MS to determine that o-SWCNT-PAO(III) formed a complex, reducing the free PAO(III) in solution, and causing the decrease in cytotoxicity observed with RTCA. RTCA analysis of o-SWCNT-PAPA(III) and o-SWCNT-roxarsone demonstrated a dose-dependent increase in cytotoxicity as the concentration o-SWCNT increased in the arsenic

solution. Further investigation is needed to determine the cause of the enhanced cytotoxicity of these species when treated with o-SWCNT.

7.3 Significance of Thesis Research

The development of the real-time cell-electronic sensing technique, RTCA, for the examination of nanoparticle-mediated cytotoxicity has provided an important tool for use in three distinct areas of research. My work with the engineered nanoparticles, nTiO₂ and nAg, demonstrate the utility of RTCA methods for implementation into high-throughput testing strategies for risk assessment of nanomaterials. *In vitro* cytotoxicity is an important data measure for risk assessment because it can provide the necessary experimental data for prioritizing compounds for further toxicity testing, and helps establish dose-response ranges used in more advanced *in vivo* toxicological testing [23]. My results demonstrate that RTCA analysis can determine concentration-, particle-, time-, and cell-dependent toxicological relationships, providing a wealth of information for the prioritization of nanoparticles for further testing. In addition, real-time analysis provides qualitative data that can be used to predict the mode of action of a nanoparticle, as I demonstrated with the confirmation of a cytostatic response visible in cytotoxicity profiles using cell cycle analysis.

The second area of research in which this RTCA method can be applied is in environmental toxicity testing for air quality monitoring. My work with the two samples of particulate matter (PM), coal fly ash (CFA) and concentrated air particulates (CAPs), demonstrates the potential environmental application of RTCA analysis through the assessment of the cytotoxicity of environmentally-

sampled fractions. This will assist in the prioritization of samples not only for potential toxicity risk, but also for further testing with chemical analysis to determine potential causative agents of the observed toxicity. The data collected from RTCA analysis of these samples can be used to assess human health risks associated with exposure.

The third area of research demonstrates the application of this RTCA method to pharmaceutical research, for example, the examination of nanoparticle-based drug delivery systems. It has been reported that for every one million drugs screened in the pharmaceutical industry, only one of those drugs will become marketable [24]. This suggests the need for better techniques for identifying drug targets and for high-throughput analysis during drug development. My work with RTCA analysis of thirteen arsenicals demonstrates the high-throughput capabilities of this method. I have demonstrated the determination of cytotoxicity of thirteen different species of arsenic in two cell lines to rank their relative toxicity. Hence, chemicals or nanoparticles with desired cytological traits can be more rapidly identified and prioritized for further studies. My research on RTCA studies of nanoparticles demonstrates the advantages of this technique over traditional dye-based assays for testing nanoparticle cytotoxicity. The RTCA testing of nanoparticle toxicity is dye free and overcomes the interference with dyes encountered in traditional assays. This advantage would reduce the false negative and false positive data that can occur because of nanoparticle interference. Therefore, RTCA could provide a considerable benefit in drug discovery as accuracy of the measured response is crucial.

7.4 Future Trends and Studies

7.4.1 Future Trends

A current trend in impedance-based cell-based biosensor research is the multiplexing of impedance arrays with other cell-based assays for simultaneous measurement of several cellular responses. A forerunner in this trend is the Bionas Discovery™ 2500 system. As opposed to the RTCA platform, which only utilizes interdigitated electrodes (IDEs) for sensing, the Bionas 2500 system uses unique microfluidic arrays with three distinct sensing areas. The first is composed of IDEs for impedance detection, the second of Clark-type electrodes to measure O₂ consumption (mitochondrial respiration), and the third is composed of ion-sensitive field-effect transistors (ISFET) to measure pH changes due to extracellular acidification (glycolysis) [25, 26]. Hence, this type of multiplexed system would be of considerable use when examining a set of chemicals as biologically-active and -diverse as arsenic species, as so many factors contribute to the observed cellular responses, including species, cell type, conversion, uptake, etc. From an air quality monitoring perspective, this Bionas system is further distinguished by its ability to screen gas samples, allowing for direct cell exposure to airborne contaminants [27, 28]. Thus, this would be a powerful tool for use in environmental monitoring of airborne nanoparticles or for more accurate *in vitro* dose-response analysis for inhalation studies. Nevertheless, this research promises a bright future for impedance-based detection systems for use in cytotoxicity analysis.

7.4.2 Future Work

To take advantage of the RTCA technique in toxicity-based environmental testing, future work will further apply this technology to air quality monitoring by addressing additional environmental issues; for example, effects of oil sand production on air quality or the effects of coal burning power generation on air quality. The RTCA can examine the cytotoxicity of different sizes of air particulates, ultrafine air particulates (PM_{0.1}), coarse (PM₁₀), and fine (PM_{2.5}) fractions (which contain PM_{0.1}). Another potential research is to further develop the devices/instruments for field application. Such toxicity-based environmental monitoring devices in the field must be portable and stable, providing excellent performance even after potentially long storage periods. Hence, there is a recognized need for this instrumentation to be evaluated for stability and portability, particularly when used for air quality monitoring in the field.

Further work is also needed to better elucidate the cellular responses observed for the thirteen arsenic species we examined. A comparison of cellular accumulation and conversion analysis of the species in media for the remaining untested arsenicals will be key to providing a more complete picture of arsenic toxicity. Also required is the further examination of the unique step-wise profile shape exhibited by the dimethylated arsenicals [DMA(III), DMAG(III), and DMMTA(V)] in the RTCA cytotoxicity profiles. While it was determined that the concentration of DMA(III) present in the DMA(III), DMAG(III), and DMMTA(V) treated culture media decreases over time, the identity and concentration of intracellular arsenic species over time remains unknown.

Because the unique step-wise profile shapes observed are likely due in part to cellular responses to arsenicals present within the cell over time, further studies to examine the influence of these intracellular arsenicals on the cellular mechanisms behind the unique profile shape should be researched.

Finally, future work for the development of o-SWCNT-arsenic delivery systems is needed. As the o-SWCNT-PAO(III) complex was not cytotoxic to the A549 cells, methods to identify how the PAO(III) can be released from the o-SWCNT once delivered inside the cell would be an interesting avenue of pursuit, particularly if the complex can be targeted for delivery into cancer cells.

7.5 References

- [1] N. Lewinski, V. Colvin, R. Drezek, *Small* 4 (2008) 26-49.
- [2] J.M. Hillegass, A. Shukla, S.A. Lathrop, M.B. MacPherson, N.K. Fukagawa, B.T. Mossman, *Wiley Interdiscip. Rev. Nanomed. Nanobiotechnol.* 2 (2010) 219-231.
- [3] L. Braydich-Stolle, S. Hussain, J.J. Schlager, M.C. Hofmann, *Toxicol. Sci.* 88 (2005) 412-419.
- [4] J.M. Worle-Knirsch, K. Pulskamp, H.F. Krug, *Nano Lett.* 6 (2006) 1261-1268.
- [5] N.A. Monteiro-Riviere, A.O. Inman, *Carbon* 44 (2006) 1070-1078.
- [6] M. Davoren, E. Herzog, A. Casey, B. Cottineau, G. Chambers, H.J. Byrne, F.M. Lyng, *Toxicol. In Vitro* 21 (2007) 438-448.
- [7] P.V. AshaRani, G. Low Kah Mun, M.P. Hande, S. Valiyaveetil, *ACS Nano* 3 (2009) 279-290.
- [8] N.A. Monteiro-Riviere, A.O. Inman, L.W. Zhang, *Toxicol. Appl. Pharmacol.* 234 (2009) 222-235.
- [9] J.M. Boyd, L. Huang, L. Xie, B. Moe, S. Gabos, X.F. Li, *Anal. Chim. Acta* 615 (2008) 80-87.
- [10] L. Huang, L. Xie, J.M. Boyd, X.F. Li, *Analyst* 133 (2008) 643-648.
- [11] A.D. Maynard, R.J. Aitken, T. Butz, V. Colvin, K. Donaldson, G. Oberdorster, M.A. Philbert, J. Ryan, A. Seaton, V. Stone, S.S. Tinkle, L. Tran, N.J. Walker, D.B. Warheit, *Nature* 444 (2006) 267-269.
- [12] K. BeruBe, D. Balharry, K. Sexton, L. Koshy, T. Jones, *Clin. Exp. Pharmacol. Physiol.* 34 (2007) 1044-1050.
- [13] Woodrow Wilson International Center for Scholars, Project on Emerging Nanotechnologies, Consumer Product Inventory, www.nanotechproject.org/inventories/consumer (accessed 4.12.2012).
- [14] L. Murr, K. Garza, K. Soto, A. Carrasco, T. Powell, D. Ramirez, P. Guerrero, D. Lopez, J. Venzor, *Int. J. Environ. Res. Public Health* 2 (2005) 31-42.
- [15] M.A. Kiser, P. Westerhoff, T. Benn, Y. Wang, J. Pérez-Rivera, K. Hristovski, *Environ. Sci. Technol.* 43 (2009) 6757-6763.

- [16] E.M. Heithmar, S.A. Pergantis, Characterizing Concentrations and Size Distributions of Metal-containing Nanoparticles in Wastewater, US Environmental Protection Agency, Washington, D.C., 2010, EPA/600/R-10/117.
- [17] M.F. Hughes, B.D. Beck, Y. Chen, A.S. Lewis, D.J. Thomas, *Toxicol. Sci.* 123 (2011) 305-332.
- [18] S.S. Suri, H. Fenniri, B. Singh, *J. Occup. Med. Toxicol.* 2 (2007) 16.
- [19] M.F. Beaux 2nd, D.N. McIlroy, K.E. Gustin, *Expert Opin. Drug Deliv.* 5 (2008) 725-735.
- [20] A. Bianco, K. Kostarelos, C.D. Partidos, M. Prato, *Chem. Commun. (Camb.)* 5 (2005) 571-577.
- [21] K. Kostarelos, L. Lacerda, G. Pastorin, W. Wu, S. Wieckowski, J. Luangsivilay, S. Godefroy, D. Pantarotto, J.P. Briand, S. Muller, M. Prato, A. Bianco, *Nat. Nanotechnol.* 2 (2007) 108-113.
- [22] H. Chen, R. Ahn, J. Van den Bossche, D.H. Thompson, T.V. O'Halloran, *Mol. Cancer Ther.* 8 (2009) 1955-1963.
- [23] National Institute of Environmental Health Sciences, National Institutes of Health, US Public Health Service, Department of Health and Human Services, NIH Publication 01-4500, 2001.
- [24] A. Carnero, *Clin. Transl. Oncol.* 8 (2006) 482-490.
- [25] R. Kubisch, U. Bohrn, M. Fleischer, E. Stutz, *Sensors (Basel)* 12 (2012) 3370-3393.
- [26] U. Bohrn, A. Mucha, C. F. Werner, B. Trattner, M. Bäcker, C. Krumbe, M. Schienle, E. Stütz, D. Schmitt-Landsiedel, M. Fleischer, P. Wagner, and M. J. Schöning, *Sens. Actuators, B: Chem.* 182 (2013) 58-65.
- [27] U. Bohrn, E. Stütz, K. Fuchs, M. Fleischer, M. J. Schöning, and P. Wagner, *Procedia Eng.* 25 (2011) 1421-1424.
- [28] U. Bohrn, E. Stütz, Maximilian Fleischer, M. J. Schöning, and P. Wagner, *Phys. Stat. Sol. A* 208 (2011) 1345-1350.